Flinders UNIVERSITY
ADELAIDE · SOUTH AUSTRALIA

Image Enhancement and its Applications

by

Damian Richard Tohl

Thesis
Submitted to Flinders University
for the degree of

Doctor of Philosophy

College of Science and Engineering

9th March 2019

Certificate of Authorship/Originality

I certify that this thesis:

- *1.* Does not incorporate without acknowledgement any material previously submitted for a degree or diploma in any university.
- *2.* To the best of my knowledge and belief, does not contain any material previously published or written by another person except where due reference is made in the text.

ABSTRACT

IMAGE ENHANCEMENT AND ITS APPLICATIONS

by

Damian Richard Tohl

Images and videos continue to play an important role in daily life, covering a scope that ranges from preserving memories all the way to entertainment and with the advent of technology are becoming more prevalent than ever. Coupled with this, is the desire for better quality, for which image enhancement is a useful tool that can be used to manipulate images and video in order to improve their perceived quality. Likewise, for processes that rely on an image or video source, such as analysis and identification, a good quality input cannot always be guaranteed and so enhancement is used as an important pre-processing step to improve the quality of an input image or video.

Enhancement techniques can improve the perceived quality of images, but many of them introduce other problems which can adversely affect the quality of images. These problems manifest in the form of over- and under-enhancement, a loss of details, halo effects, reduced signal to noise ratio and flickering in video enhancement. The aims of this thesis are to develop enhancement techniques that significantly improve the quality of images and video whilst avoiding the common problems often associated with other enhancement techniques.

One of the techniques we present is a multi-level histogram shape segmentation method that can avoid over and under enhancement by segmenting the histogram in such a way that regions with a similar frequency of occurrence are grouped together and independently equalised.

To achieve brightness preservation for any image independent of the degree of enhancement, we propose a novel method to find a unique S-shaped curve transfer

function for each image using successive approximation. As the S-shaped curve reduces intensities below a certain point and increases intensities above this same point, then for each image there exists a unique location of this point that will maintain the brightness of the image. We also propose a modified gamma curve which approximates the S-shaped curve, but has a wider control over the degree of enhancement and greater computational efficiency.

By making use of recently developed image quality measures, which have improved the correlation between human visual perception and the value they produce, a novel optimisation method is proposed that extends the successive approximation approach to maximise any chosen image quality measure value. Not only does this optimise enhancement, but can be used to assess which features of the image a particular image quality measure targets and how well it correlates with visual perception.

A novel adaptive method for detail enhancement is also proposed in this thesis that can suppress noise in homogeneous regions and avoid halo effects while providing detail enhancement to improve the signal to noise ratio.

Results show that the enhancement techniques presented in this thesis provide a desirable degree of enhancement while outperforming other benchmarking algorithms both quantitatively and visually. These novel image enhancement techniques can also be applied practically in order to improve other processes, such as image expansion, whereby the modified gamma curve is used with an adaptive gamma value based on the difference between two different interpolation methods to regain the sharpness of edges in the expanded image. Another process that can benefit from the use of these image enhancement techniques is enhancement prior to colour filter array demosaicking, which can give better results than the current methods which apply enhancement after demosaicking.

Dedication

To my family, especially my parents Anthony and Dianne Tohl.

Acknowledgements

I would like to thank my PhD supervisor Dr Jimmy Li for his guidance and support during the completion of this thesis. I have learned a great deal from him about research and image processing and have thoroughly enjoyed the time I have spent working with him.

I would also like to thank my late co-supervisor Professor Mike Bull for all of the support he provided as well.

I would like to acknowledge my PhD scolarship the Flinders University, Faculty of Science and Engineering Research Award.

Last, but not least, I would like to thank my parents for their love and support.

Damian Richard Tohl

Adelaide, Australia, 2019.

List of Publications

Journal Papers

J-1. **D. Tohl** and J. S. J. Li, "Contrast Enhancement by Multi-Level Histogram Shape Segmentation with Adaptive Detail Enhancement for Noise Suppression," *Signal Processing: Image Communication*, vol. 71, pp. 45-55, Feb. 2019.

J-2. **D. Tohl** and J. S. J. Li, "Image Enhancement by S-Shaped Curves Using Successive Approximation for Preserving Brightness," *IEEE Signal Processing Letters*, vol. 24, no. 8, pp. 1247-1251, Aug. 2017.

J-3. **D. Tohl** and J. S. J. Li, "Optimizing Image Enhancement Based on an Image Quality Measure," *Pattern Recognition Letters*, (Submitted 2018).

Conference Papers

C-1. **D. Tohl** and J. S. J. Li, "Improved Image Expansion for Preserving Sharpness without Jagged Edges," *Proc. 2018 IEEE Region 10 Conference (IEEE TENCON 2018)*, pp. 1269-1274, Jeju, South Korea, Oct. 2018. (Best Paper Award)

C-2. **D. Tohl**, J. S. J. Li, S. Randhawa and N. Pickering, "Image Enhancement of Color Filter Array Images," *Proc. 2018 IEEE Region 10 Conference (IEEE TENCON 2018)*, pp. 1279-1283, Jeju, South Korea, Oct. 2018.

C-3. **D. Tohl**, J S. J Li, and C. M. Bull, "Pre-Processing Techniques to Improve the Efficiency of Video Identification for the Pygmy Bluetongue Lizard," *Proc. 10th International Conference on Computer Vision Theory and Applications - Volume 1: VISAPP, (VISIGRAPP 2015)*, pp. 623-629, Berlin, Germany, 2015.

C-4. **D. Tohl**, J S. J Li, L. Shamimi, and C. M. Bull, "Image Asymmetry Measurement for the Study of Endangered Pygmy Bluetongue Lizard," *Proc. 28th International Conference on Image and Vision Computing New Zealand (IVCNZ 2013)*, pp 76-81, Wellington, New Zealand, Nov. 2013.

Contents

List of Figures

List of Tables

Abbreviation

ADBE - Absolute meDian Brightness Error

ADEPI - Adaptive Distance-based Edge Preserving Interpolation

ADE-BIQME - proposed Adaptive Detail Enhancement method with background enhancement optimised by BIQME

ADE-QRCM - proposed Adaptive Detail Enhancement method with background enhancement optimised by QRCM

AGCWD - Adaptive Gamma Correction with Weighting Distribution

AMBE - Absolute Mean Brightness Error

BBHE - Brightness preserving Bi-Histogram Equalisation

BIQME - Blind Image Quality Measure of Enhancement images

BOIEM - BIQME-Optimised Image Enhancement Method

BWHE - Bi-Weighted Histogram Equalisation

CFA - Colour Filter Array

CMBM - Contrast and Mean Brightness Measure

DCCI - Directional Cubic Convolution Interpolation

DCT - Discrete Cosine Transform

DSIHE - Dualistic Sub-Image Histogram Equalisation

EGII - Edge-Guided Image Interpolation

EMEG - Expected Measure of Enhancement by Gradient

FPGA - Field-Programmable Gate Array

FSIM - Feature SIMilarity

GIF - Guided Image Filter

HE - Histogram Equalisation

HOI - High-Order Interpolation

INEDI - Improved New Edge Directed Interpolation

IQM - Image Quality Measure

LRSACE - Local Region Stretching Adaptive Contrast Enhancement

MAD - Median of Absolute Deviation from the median

MEDI - Modified Edge Directed Interpolation

MGC - Modified Gamma Curve

MGCSA - Proposed MGC enhancement with brightness preservation by Successive Approximation

MGC-BIQME - proposed MGC enhancement optimised by BIQME

MGC-EMEG - proposed MGC enhancement optimised by EMEG

MGC-QRCM - proposed MGC enhancement optimised by QRCM

MGC-RCIQM - proposed MGC enhancement optimised by RCIQM

MMBEBHE - Minimum Mean Brightness Error Bi-Histogram Equalisation

MSB - Most Significant Bit

NEDI - New Edge Directed Interpolation

NIQMC - No-reference Image Quality Metric for Contrast distortion

NIR - Near-Infra-Red

QRCM - Quality-aware Relative Contrast Measure

RGB - Red, Green and Blue

RICE - Robust Image Contrast Enhancement

RIQMC - Reduced-reference Image Quality Metric for Contrast change

RMSHE - Recursive Mean-Separate Histogram Equalisation

ROHIM - RCIQM-based Optimal HIstogram Mapping

RSECE - Residual Spatial Entropy-based Contrast Enhancement

RSECEDCT - Residual Spatial Entropy-based Contrast Enhancement in DCT

RSIHE - Recursive Sub-Image Histogram Equalisation

RSWHE - Recursively Separated and Weighted Histogram Equalisation

RTIU - Real-Time artifact free Image Upscaling

SECE - Spatial Entropy-based Contrast Enhancement

SECEDCT - Spatial Entropy-based Contrast Enhancement in DCT

SMIRANK - Spatial Mutual Information and pageRANK-based contrast enhancement

SSIM - Structural SIMilarity

SSTF - S-shaped Sigmoid Transfer Function

STBP - s-shaped Sigmoid Transfer function base Brightness Preservation

STSA - proposed s-shaped Sigmoid Transfer function enhancement with brightness preservation by Successive Approximation

TRFI - Trilateral Filter Regression Interpolation

WTHE - Weighted Thresholded Histogram Equalisation

Chapter 1

Introduction

For many people, images and videos play an important role in daily life, from documenting moments and preserving memories, all the way to entertainment. As technology and social media advances, images and videos are becoming more prevalent then ever. With this comes a demand for better quality, which is why enhancement methods are commonly used to improve the perceived quality of images and videos. The same is true for processes that rely on an image or video source, such as analysis and identification, where enhancement is used as an important pre-processing step [3] to ensure a good quality input image or video. Inconsistent quality of input images and video can effect the robustness and accuracy of results, especially when working with images and video captured in trying conditions [4, 5, 6, 7]. Image enhancement performed in the pre-processing stage of these applications will improve the quality of input images and video which in turn, may improve the robustness and accuracy of results.

Image enhancement is a technique that transforms the intensity values of an input image for improving the visual perception of the image [8, 9], but often enhancement produces unwanted effects that can degrade the quality of an image. These unwanted effects are problems such as over- and under-enhancement, halo effects, reduced signal to noise ratio and flickering in video enhancement. In this thesis, the aim

is to develop new enhancement techniques that will avoid those unwanted effects whilst improving the quality of images and video.

When over-enhancement occurs, the result is an unnatural appearance with a loss of details [10], while under-enhancement is the result of not enough improvement to the output image. Over-enhancement is generally introduced by histogram equalisation [11] and while some techniques have reduced this problem by segmenting the histogram and perform equalisation independently on each segment [12, 13, 14, 15, 16, 17], the choice of segmentation locations means that this problem cannot be completely avoided. Furthermore, the inclusion of too many segments may result in under-enhancement. Due to this, a novel method of segmentation is proposed which uses the shape of the histogram to determine the segmentation locations, so that areas of the histogram with a similar frequency of occurrence are grouped together. As over-enhancement typically occurs when peaks in the histogram are redistributed over a wider area, grouping together these regions means peaks can be equalised over a smaller area and over-enhancement can be avoided. In contrast to this, areas with a lower frequency of occurrence can be equalised over a larger area so that a loss of contrast will not occur and under-enhancement can also be avoided.

When applying enhancement techniques to video, if the brightness of each frame is not preserved, then it can cause flickering from frame to frame [16, 18]. Existing enhancement techniques which claim to preserve brightness often do so by introducing limitations on the degree of enhancement or by clipping the dynamic range of the image which can lead to under enhancement. The recently developed S-shaped

sigmoid transfer function (SSTF) [18, 9, 19, 20] is one method where clipping of the intensity values can occur, resulting in a loss of details and contrast. However, as the SSTF reduces intensities below a certain point that intersects with the $y = x$ line and increases intensities above this intersection point, then for each image there exists a unique location of this intersection point that will maintain the brightness of the image. In order to achieve brightness preservation for any image independent of the degree of enhancement, a novel method is proposed to find a unique SSTF for each image by successive approximation. Due to four control parameters in SSTF which must be optimised by minimising an objective function [18], the method is computationally inefficient. Therefore, a number of new equations are proposed to reduce the number of control parameters from four to two to improve computational efficiency. SSTF also has limited control over enhancement when the crossover point is closer to either end of the intensity range, so in order to obtain more control of the degree of enhancement and further improve computational efficiency, a modified gamma curve (MGC) is proposed to produce a curve similar to the shape of SSTF for contrast enhancement.

Recent image quality measures (IQMs) [19, 20, 8, 3, 21, 22, 23, 24, 25, 26, 27] have improved on the correlation between human visual perception and the value which they produce. It follows, that by maximising a chosen IQM in the enhancement process, an optimally enhanced image will be produced according to that IQM. Some recent enhancement methods [9, 19, 20] attempt to optimise enhancement based on a particular IQM. However, the optimisation process in each method is limited, either by some constraints on the control parameters, or by the optimisation

technique itself. This means the output images they produce may not necessarily reflect the maximum IQM value. A novel method is proposed in this thesis that extends the successive approximation approach to optimise image enhancement by maximising any chosen IQM value. Not only does this optimise enhancement, but can be used to assess which features of the image a particular IQM targets and how well it correlates with visual perception.

To prevent a loss of details from occurring in the enhanced output image, detail enhancement can be incorporated into enhancement process. When applying detail enhancement, most techniques are unable to discern between details and noise and will often enhance noise as well as details producing noisy enhanced images and reducing the signal to noise ratio. Furthermore, edges that are included within detail enhancement can sometimes be over enhanced and may produce halo effects giving the image an unnatural appearance. One recent method of detail enhancement [3, 24] increases the weightings to the high frequency components in the frequency domain after global contrast enhancement has been performed. However, this method of detail enhancement will have minimal effect if the details are already lost in the initial global contrast enhancement. Moreover, as both details and noise contain high frequency components, the noise level will also be raised and halo effects may be produced, resulting in output images with worse signal-to-noise ratio and halo effects at edges. A novel median of absolute deviation from the median (MAD) [28] adaptive method for detail enhancement is proposed in this thesis which can suppress noise in homogeneous regions while providing detail enhancement to improve the signal to noise ratio. Halo effects at edges are also avoided by separating

image details from the background and edges so that only the details are enhanced by the proposed method.

The novel image enhancement techniques proposed in this thesis can be applied practically in order to improve other processes which include image enhancement as a step within their execution. Two of those process which are explored include image expansion and enhancement prior to colour filter array demosaicking. The proposed MGC presented in this thesis can be applied to image expansion where it is used with an adaptive gamma value, based on the difference between two different interpolation methods, to regain the sharpness of edges in the expanded image. The image enhancement techniques presented in this thesis can be applied prior to colour filter array demosaicking which can help reduce interpolation errors.

The results in each chapter show that the enhancement techniques presented in this thesis provide a desirable degree of enhancement while outperforming other benchmarking algorithms both quantitatively and visually.

1.1 Thesis Organisation

This thesis is organised as follows:

- *Chapter 2*: The multi-level histogram shape segmentation method is described in this chapter.
- *Chapter 3*: Image and video enhancement with brightness preservation by successive approximation with the S-shaped sigmoid transfer function and the modified gamma curve are given in this chapter.

- *Chapter 4*: This chapter describes how images can be optimised by using a binary search in conjunction with the modified gamma curve to maximise an image quality assessment method.

- *Chapter 5*: A novel adaptive detail enhancement method is proposed in this chapter.

- *Chapter 6*: In this chapter, two novel applications for the proposed enhancement methods are presented.

- *Chapter 7*: A brief summary of the thesis contents and its contributions are given in the this chapter.

- *Chapter 8*: Future extensions to the proposed enhancement methods are outlined in the final chapter.

Chapter 2

Multi-Level Histogram Shape Segmentation

2.1 Introduction

Histograms give an overview of image grey level distribution and density, average luminance, contrast and other characteristics of images [29]. Histogram equalisation (HE) flattens and stretches the dynamic range of a histogram for image contrast enhancement [16] to improve visual perception [30, 11, 31]. However, there are two main problems associated with standard histogram equalisation, namely, over-enhancement and a loss of details in different regions of an image. Over-enhancement results in an unnatural appearance and is often associated with a loss of details [10]. Fig. 2.1(b) shows an example of the HE output where the peak in the far left side of the histogram has been shifted right, resulting in the back regions in the foreground of the image to appear grey. The smaller peaks in the histogram have been spread out as well, resulting in over-enhancement with a loss of details in the sky and water.

To overcome these problems, one approach [16, 32, 15, 14, 12, 13] is by segmentation of the histogram based on its mean or median value to form sub-images and performing histogram equalisation on each sub-image independently. Other approaches [17, 33, 34] include the application of a different weight to each sub-image, as an approach to reduce over- and under-enhancement. However, none of those methods can completely avoid over-enhancement because histograms are segmented

in a manner such that they may include intensity values with a wide range of frequency of occurrence. Furthermore, introducing too many segments may also cause the undesirable effect of under-enhancement where the image retains its initial poor contrast.

Weighted thresholded histogram equalisation (WTHE) [10] applies a weight to the probability density function before histogram equalisation. A smaller weight is given to intensity values with a high frequency of occurrence and a larger weight is given to intensity values with a low frequency of occurrence. However, adjusting the weights will not totally eliminate over- and under-enhancement and this method still inherits similar problems to histogram equalisation. Fig. 2.1(h) shows that the smaller peaks in the histogram of the WTHE output are still spread out, resulting in a loss of details in the sky and water. To preserve brightness, WTHE adds the difference between the mean brightness of the original and equalised image to the final image output, but this may cause clipping of the intensity values and reduce the dynamic range of the image. This is obvious in the histogram of the WTHE output, shown in Fig. 2.1(h), by the large peak in centre of the histogram and the reduced range of intensity values.

For the methods which only segment the histogram into two sub-histograms, namely, brightness preserving bi-histogram equalisation (BBHE) [12], dualistic sub-image histogram equalisation (DSIHE) [13], bi-weighted histogram equalisation (BWHE) [34], and minimum mean brightness error bi-histogram equalisation (MMBEBHE) [14], they may perform well for images with a well-defined bimodal distribution of the intensity values. However, most images will not have the characteristics of such a

histogram and these methods will not generally produce favourable outcomes. Fig. 2.1(c) - Fig. 2.1(e) shows the output of BBHE, DSIHE and MMBEBHE respectively, the red dotted line gives the location of the single segmentation point which was inappropriately located and unable to stop the shift of the large peak associated with the black region of the image or the spreading out of the smaller peaks, resulting in over-enhancement and a loss of details in the sky. Additional segmentation thresholds are needed to segment the histogram to reduce the over-enhancement problem.

For methods using multiple sub-histograms, namely, local region stretching adaptive contrast enhancement (LRSACE) [35], recursive mean-separate histogram equalisation (RMSHE) [16], recursive sub-image histogram equalisation (RSIHE) [15], and recursively separated and weighted histogram equalisation (RSWHE) [17], over-enhancement still cannot be avoided completely as the histograms are not always segmented at appropriate thresholds. In the LRSACE method, the segmentation points are fixed and therefore not adaptable to various types of images. The recursive methods provide multi-level segmentation, but histograms may be segmented at points that will still cause over-enhancement. Moreover, recursive methods are known to be computationally inefficient. Fig. 2.1(f) - Fig. 2.1(g) shows the outputs for RMSHE and RSIHE respectively, the segmentation points, shown by the red dotted lines, are at inappropriate locations and still result in over-enhancement of the sky.

Recursively separated and weighted histogram equalisation (RSWHE) [17] combines recursive mean segmentation with adaptive weights to avoid over enhancement.

The weightings are applied in this method with the intention of preserving brightness and as such, constrain the overall enhancement, resulting in output images with minimal inadequate enhancement for inputs with poor contrast.

The problem with existing histogram segmentation equalisation techniques is that some segments may include intensity values with a wide range of frequency of occurrence, resulting in over-enhancement and a loss of details. This motivates the proposal of the multi-level histogram shape segmentation (MLHSS) method which can avoid these problems by segmenting the histogram in such a way that regions with a similar frequency of occurrence are grouped together. Equalisation is then performed independently on each segment and over-enhancement can be avoided as intensity values can only be remapped within the same segment.

2.2 Method

Applying enhancement to the luminance component of an image with a limited colour dynamic range will produce an output with good contrast, but dull colour due to no improvement of the colour dynamic range. Therefore, contrast expansion is applied to the input image as an initial step of the proposed enhancement method to achieve more vivid colour enhancement [36, 37, 38]. In order to avoid any clipping of pixel values, each colour pixel is initially scaled based on the global maximum and minimum intensity values among all the colours. Let $\boldsymbol{X}$ be an original image in RGB colour space with an intensity range of [0,255] where $\boldsymbol{X} = \{\boldsymbol{R}, \boldsymbol{G}, \boldsymbol{B}\}$, $r(i,j) \in \boldsymbol{R}$, $g(i,j) \in \boldsymbol{G}$, $b(i,j) \in \boldsymbol{B}$ and i, j are the location indices of each pixel and $x_c(i,j) = \{r_c(i,j), g_c(i,j), b_c(i,j)\}$ be a colour pixel of the contrast expanded

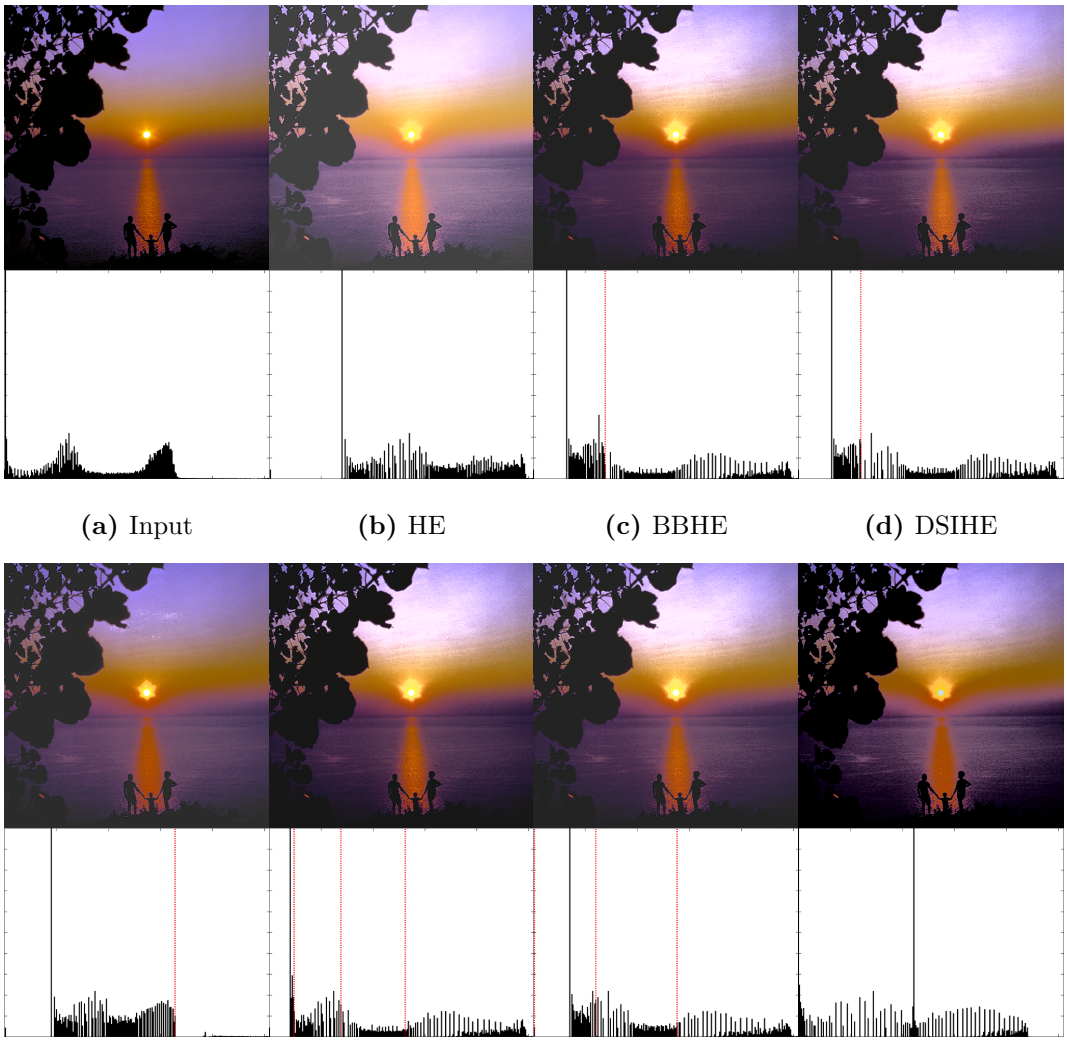

(a) Input **(b)** HE **(c)** BBHE **(d)** DSIHE

(e) MMBEBHE **(f)** RMSHE **(g)** RSIHE **(h)** WTHE

Figure 2.1 : An example of existing histogram equalisation techniques. (a) The *family* input image. Enhancement by (b) HE, (c) BBHE, (d) DSIHE (e) MMBEBHE, (f) RMSHE, (g) RSIHE and (h) WTHE. The red dotted lines in the histogram indicate segmentation locations.

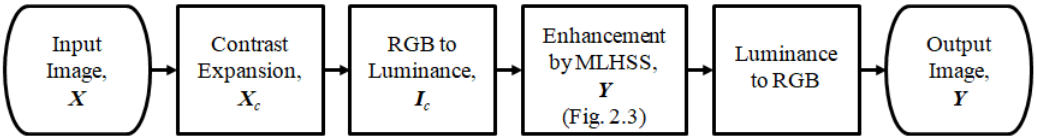

Figure 2.2 : Flowchart for the overall image enhancement method featuring the proposed multi-level histogram shape segmentation.

image, $\boldsymbol{X}_c$. The global maximum and minimum intensities of $\boldsymbol{X}$ among all colours are determined first as follows:

$$I_{max} = max\{max\{\boldsymbol{R}\}, max\{\boldsymbol{G}\}, max\{\boldsymbol{B}\}\}, \tag{2.1}$$

$$I_{min} = min\{min\{\boldsymbol{R}\}, min\{\boldsymbol{G}\}, min\{\boldsymbol{B}\}\}. \tag{2.2}$$

Each pixel in the RGB colour space is then scaled by the following equations:

$$r_c(i,j) = 255\left(\frac{r(i,j) - I_{min}}{I_{max} - I_{min}}\right), \tag{2.3}$$

$$g_c(i,j) = 255\left(\frac{g(i,j) - I_{min}}{I_{max} - I_{min}}\right), \tag{2.4}$$

$$b_c(i,j) = 255\left(\frac{b(i,j) - I_{min}}{I_{max} - I_{min}}\right). \tag{2.5}$$

As global maximum and minimum intensity values among all the colours, I_{max} and I_{min}, are used to scale the three colours, the ratio between them will be maintained and there is no chance of altering the original balance of colour. If any one of the three colours already uses the full dynamic range, then this step will have no effect on the overall enhancement of the image. Alternatively, if the input dynamic range of all three colours is limited, this step will ensure that the full dynamic range is utilised and the output will have full vivid colour.

In the proposed method, a novel multi-level histogram shape segmentation method is developed for enhancement of the contrast expanded image, $\boldsymbol{X}_c$. In order to avoid over-enhancement, regions of intensity values with a similar frequency of occurrence have to be separated for individual equalisation. This can be detected by observing a sudden change in the magnitude of neighbouring values in the histogram of the luminance component, I_c, of the contrast expanded image.

Throughout this thesis, the luminance of the image is obtained by transforming the RGB colour space to the device independent CIELAB colour space as defined by the International Commission of Illumination [39]. The "lightness" values from the CIELAB colour space are then taken as the luminance of the image.

To prevent small fluctuations and to remove outliers in the histogram from producing an excessive number of segmentation points which will reduce the degree of enhancement, the histogram, H, is smoothed by an alpha-trimmed mean filter [40] which is known to be able to effectively remove outliers while smoothing the input to produce the output, H_s. The alpha-trimmed mean filter output is obtained by ranking a set of samples in order, removing (trimming) a fixed fraction, alpha ($0 \leq \alpha \leq 0.5$), from the high and low ends of the sorted set of samples and computing the mean of the remaining samples. When $\alpha = 0$, the range of summation is over the entire set of samples and the filter output is the sample mean. When $\alpha = 0.5$ the filter output is the sample median.

For the detection of abrupt changes at position, q, of the smoothed histogram, H_s, a window on each side of q of width N is formed and the sum of the histogram values inside each window is evaluated, where ${K_q}^l$ and ${K_q}^r$ are the sum of the

histogram values inside the windows to the left and right hand side of q respectively as follows:

$$K_q{}^l = \sum_{k=1}^{N} H_s(q-k), \tag{2.6}$$

$$K_q{}^r = \sum_{k=1}^{N} H_s(q+k). \tag{2.7}$$

This process is repeated for the full range of the histogram to produce a ratio curve, c, which is based on the ratio of the maximum and minimum of $K_q{}^l$ and $K_q{}^r$ as given as follows:

$$c(q) = \begin{cases} \frac{K_{max}}{K_{min}} & (K_{min} > 0)\&(K_{max} > d|\boldsymbol{I}_c|) \\ 1 & otherwise \end{cases}, \tag{2.8}$$

where $K_{min} = min\left\{K_q{}^l, K_q{}^r\right\}$, $K_{max} = max\left\{K_q{}^l, K_q{}^r\right\}$, $|\boldsymbol{I}_c|$ is the total number of pixels of the contrast expanded image luminance, $\boldsymbol{I}_c$, d is a percentage of $|\boldsymbol{I}_c|$ and '&' is a logical 'and' operator.

When $K_{min} = 0$, the ratio of K_{max} to K_{min} is undefined at that point and it will be replaced by unity, assuming that it is a flat region in the histogram (i.e. $K_{max} = K_{min}$) at which no abrupt change has occurred. When the number of pixels within the window is too small, i.e. when the number is smaller than a percentage, d, of the size of the image, they are the minority and its ratio should also be ignored and set to unity. The peaks of the ratio curve give the location at which abrupt changes of the histogram have occurred and therefore are the locations at which the histogram should be segmented to produce the sub-images. In other words, peaks in the ratio curve are located at turning points in the histogram where the frequency of occurrence is changing from small to large, or from large to small. The window

width, N, can be used to control the number of peaks in the ratio curve. Increasing N will reduce the number of peaks detected and in turn reduce the number of segmentation thresholds and vice versa. Therefore, the degree of enhancement can be controlled by adjusting the value of N.

To detect the location of the peaks, the first derivative, c', of the ratio curve is evaluated and the zero-crossings of this derivative give all the peak and trough locations. As only the peak locations are required, only zero-crossings where the sign changes from positive to negative are taken as segmentation thresholds. Let $\boldsymbol{S}$ be the set of the segmentation thresholds located at the peaks of the ratio curve where $n = 1, 2, \ldots, |\boldsymbol{S}|$ and $|\boldsymbol{S}|$ is the cardinal number of $\boldsymbol{S}$ as follows:

$$\boldsymbol{S} = \{q : (c'(q) > 0)\&(c'(q+1) \leq 0)\&(c(q) > C)\}, \tag{2.9}$$

where C is a threshold for the slope of the histogram and $N \leq q < L - N$. The range for q is equal to $[N, L - N)$ so that both (2.6) and (2.7) are valid.

The ratio curve, $c(q)$ at location q must be greater than the threshold C for an abrupt change of the histogram to have had occurred. In a flat region of the histogram, $c(q) = 1$ (as K_{max} and K_{min} in (2.8) are equal), hence, C must be greater than unity to detect any abrupt changes.

In order to cover the full range of intensity values for an intensity range of $[0, L-1]$, the lower and upper bounds of the intensity range should be included to be the lower and upper segmentation boundaries. Therefore, $S(1) = 0$, $S(|\boldsymbol{S}|) = L$ are added to the set $\boldsymbol{S}$ and all the q values in (2.9) are re-assigned to $[S(2), \ldots, S(|\boldsymbol{S}|-1)]$ in the ranked-order of magnitude of q. The interval for each sub-image is given by

$[S(n), S(n+1)-1]$ where $n = 1, 2, \ldots, (|\boldsymbol{S}| - 1)$.

Let $\boldsymbol{V}_n$ be the n^{th} sub-image with intensity values within the intensity interval of $[S(n), S(n+1)-1]$ from the contrast expanded luminance, $\boldsymbol{I}_c$ as follows:

$$\boldsymbol{V}_n = \{I_c(i,j) \in \boldsymbol{I}_c : S(n) \leq I_c(i,j) \leq S(n+1) - 1\}, \tag{2.10}$$

where $n = 1, 2, \ldots, (|\boldsymbol{S}| - 1)$.

Let $\boldsymbol{F}_n$ be the n^{th} equalised sub-image output of $\boldsymbol{V}_n$ using standard histogram equalisation [11]. Each $\boldsymbol{F}_n$ is an equalised sub-image over a section of the full intensity range and the concatenation of all $\boldsymbol{F}_n$ will give an overall equalised image, $\boldsymbol{Y}$, with the full intensity range as follows:

$$\boldsymbol{Y} = \sum_{n=1}^{|\boldsymbol{S}|-1} \boldsymbol{F}_n, \tag{2.11}$$

where

$$\boldsymbol{F}_n = \{Y(i,j) \in \boldsymbol{Y} : S(n) \leq Y(i,j) \leq S(n+1) - 1\}. \tag{2.12}$$

Fig. 2.2 gives the block diagram for the overall image enhancement process and Fig. 2.3 gives the detailed block diagram for our proposed multi-level histogram shape segmentation method. Fig. 2.4 shows the outputs at each step of the proposed multi-level histogram shape segmentation method for the *cactus* image. The solid red line indicates the alpha-trimmed mean filter output, which removes outliers to give a smoothed histogram which still preserves the underlying structure of the original histogram. The ratio curve is represented by the solid blue line and the ratio curve threshold, C, is represented by the dotted blue line. Peaks in the ratio curve which exceed the ratio curve threshold are used to determine the segmentation

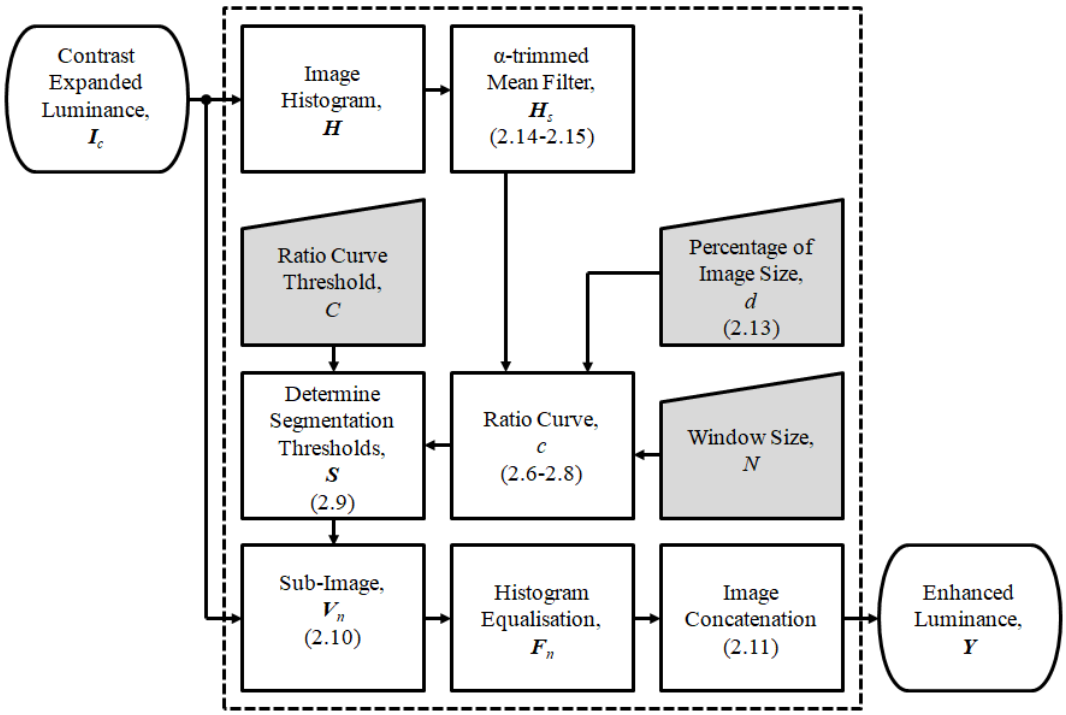

Figure 2.3 : Flowchart for image enhancement by the proposed multi-level histogram shape segmentation method.

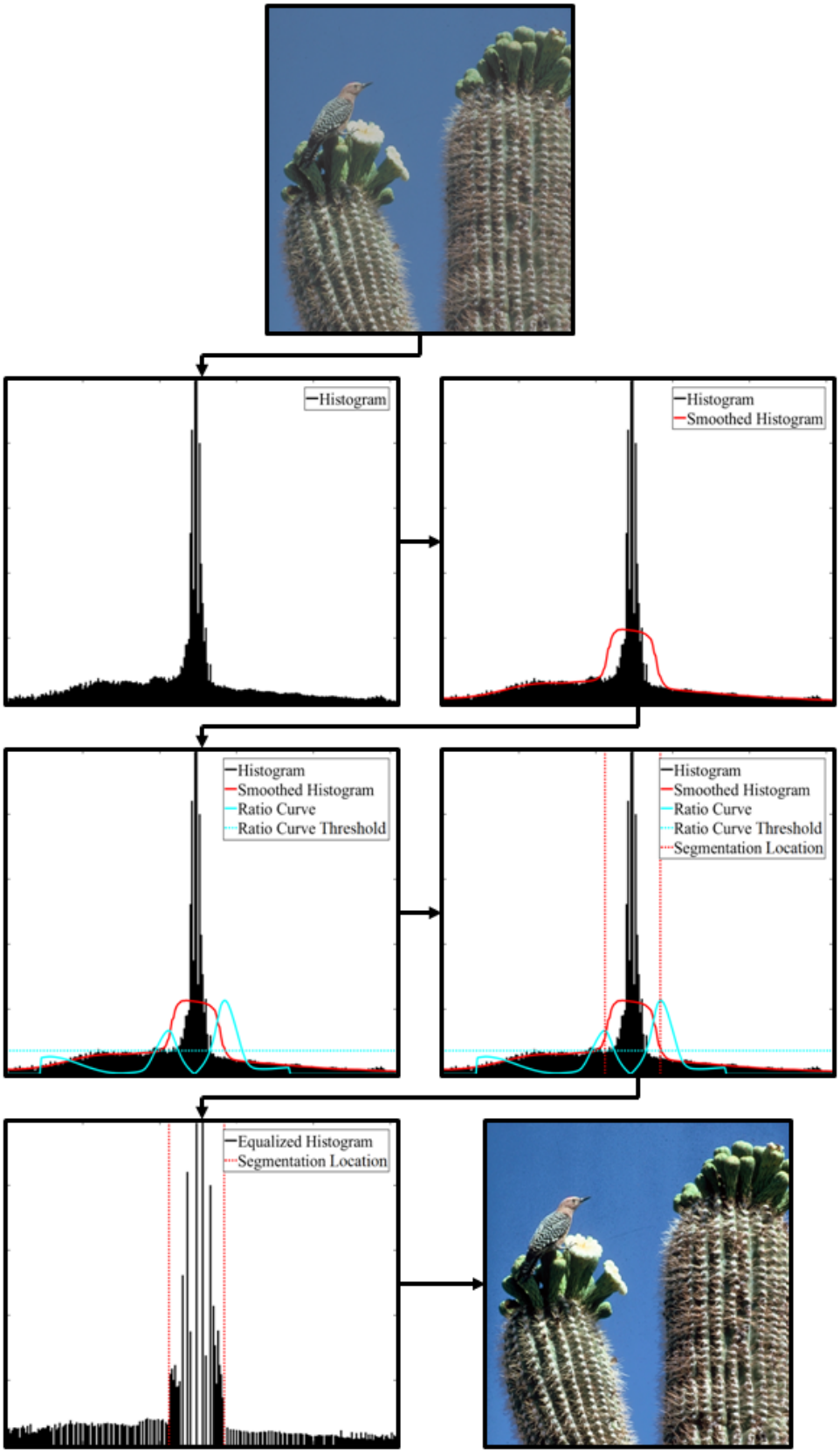

Figure 2.4 : Diagram to show the outputs at each step of the proposed multi-level histogram shape segmentation method for the *cactus* image.

locations, which are indicated by the dotted red lines. Equalisation is then performed independently on each segment to give the enhanced image output.

2.3 Control Parameters

There are five different variables that can be used to control the performance of the proposed multi-level histogram shape segmentation method and they are all related to the definition of the ratio curve. Three of the variables, namely, the ratio curve window width, N, the percentage of total image pixels, d, and the ratio curve threshold, C, directly control the formation of the ratio curve and in turn the number of segments included in the histogram equalisation process. The other two, namely, the window width, M, and the alpha value, α, control the smoothing properties of the alpha-trimmed mean filter, which is applied to the histogram of the image so that local variances in the histogram do not produce an excessive number of segments. These variables give great control over the enhancement of an image, but they are also highly interactive with each other such that changing a single variable in isolation may not necessarily lead to the expected change in the output image.

2.3.1 Ratio Curve Window Width

The ratio curve window width, N, is used to control the sensitivity of the ratio curve to the image histogram. A smaller window width will be more sensitive to local variations in the histogram and as a result will lead to more segmentations. This will give less overall enhancement to image as histogram equalisation is being applied over a larger number of smaller segments. A larger window width will be

less sensitive to local variations in the histogram so that the ratio curve will reflect the overall shape of the histogram resulting in fewer segmentations and also stronger enhancement.

All of the images used for testing are 8-bit, i.e. they have 2^8 or 256 intensity values and as such, the histograms produced by these images will have 256 bins. Therefore, although the ratio curve window can be any width, values which are powers of two have been used in this thesis so that the effect changing the window size has on the ratio curve is clear to see. Ratio curve window widths which are powers of two also have a symbiotic relationship with the histogram in that for $N = 32$, the ratio curve is evaluated over a quarter of the histogram, for $N = 16$, the ratio curve is evaluated over an eighth of the histogram, for $N = 8$, the ratio curve is evaluated over a sixteenth of the histogram and so on. Fig. 2.5 shows the ratio curves and corresponding segmentation points for an image histogram for the window widths $N = 4, 8, 16$ and 32. The ratio curve has been normalised to the same scale as the histogram so they can be displayed together in a legible manner and the relationship between the two can be observed. A small window width (i.e. $N = 4$), is more sensitive to the jaggedness of the histogram and a lot of ratio curve peaks will be produced as a result, as shown in Fig. 2.5(b). As the window width increases it becomes less sensitive to the jaggedness of the histogram and less ratio curve peaks will be produced as a result. For very large window widths (i.e. $N = 32$), only a few ratio curve peaks will be produced, as shown in Fig. 2.5(e).

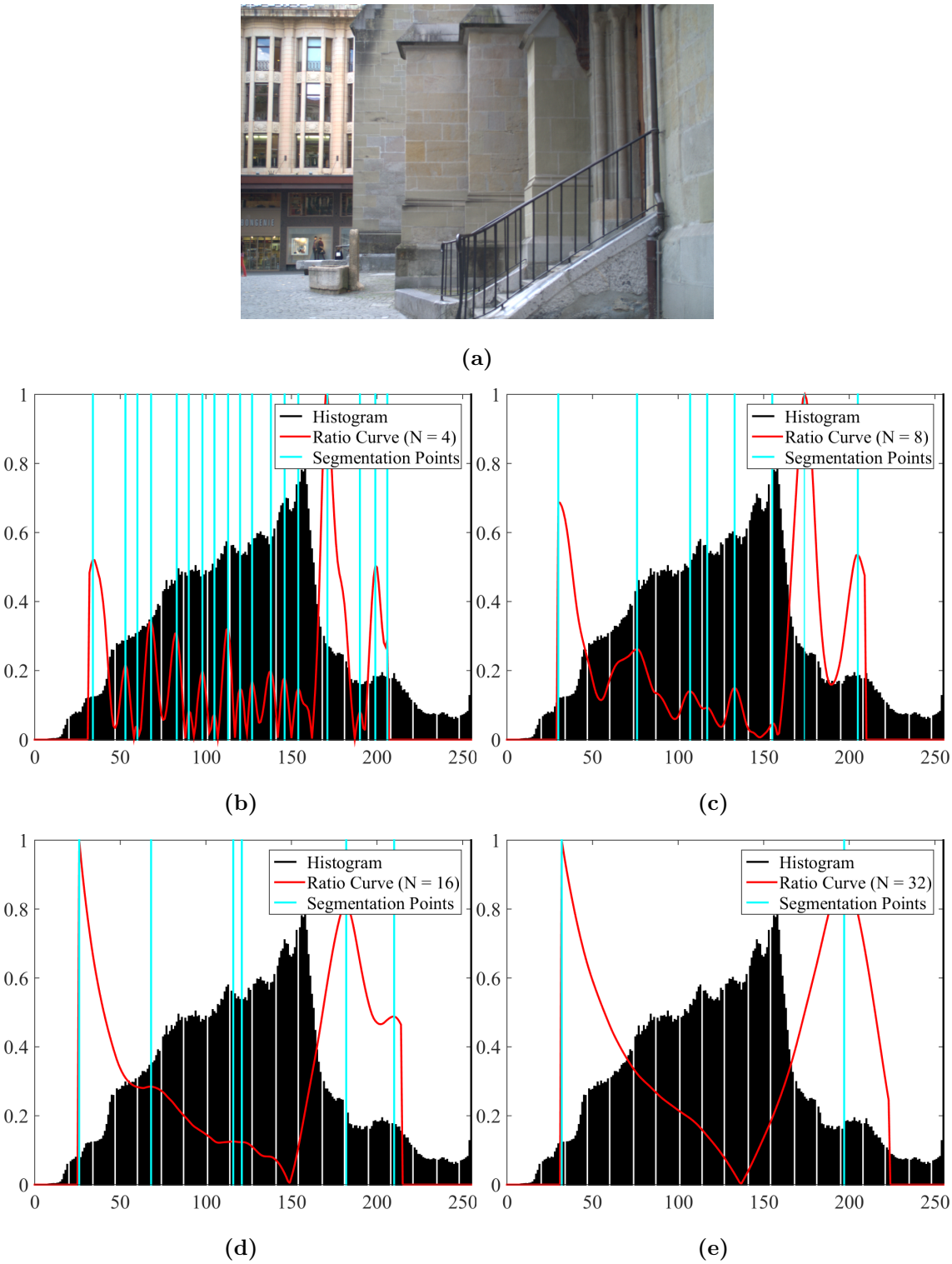

Figure 2.5 : The histogram for (a) the *building* image with the ratio curve and segmentation points for (b) $N = 4$, (c) $N = 8$, (d) $N = 16$ and (e) $N = 32$.

2.3.2 Percentage of Total Image Pixels

The percentage, d, of the total number of pixels in the luminance image, I_c, is used reduce the number of segmentations in areas of the histogram with a low frequency of occurrence. A smaller percentage will allow the evaluation of the ratio curve over areas of the histogram with a low frequency of occurrence, leading to more segmentations in those areas. This will result in less enhancement in those areas, possibly leading to the under-enhancement of the image. A larger percentage will stop the evaluation of the ratio curve in those areas of the histogram with a low frequency of occurrence, eliminating segmentations in those areas and giving stronger enhancement. If very large percentages are used, then the evaluation of the ratio curve will be stopped in areas of the histogram with a higher frequency of occurrence, potentially leading to over-enhancement.

As the window width, N, for defining the ratio curve is variable, larger window widths will include more bins of the histogram and hence more pixels and smaller window widths will include less. Therefore the percentage of total pixels, d, should vary with the window width, N, for a consistent result. As an example, for an image with an even distribution of intensities, 100% of the image pixels would be located across the entire histogram, 50% of the image pixels would be located across half of the histogram, 25% of the image pixels would be located across a quarter of the histogram and so on. Considering the above and the fact we want to ignore areas of the histogram where the number of pixels are in the minority when defining the ratio curve, we can assume that when the percentage of total pixels is less than half that of the expected percentage for an image with an even distribution over the

window width, N, then it should be ignored. Therefore the ratio curve, d, is defined as follows:

$$d = \left(\frac{1}{2}\right)\left(\frac{N \times 100}{256}\right). \tag{2.13}$$

Fig. 2.6 shows the ratio curves and the corresponding segmentation points for the *water* image for the window widths $N = 8$ and $N = 16$ with and without the percentage of total pixels, d, applied. The histogram has a large area, from intensity value 0 to 128, with a low frequency of occurrence. Without the percentage of total pixels, d, applied in Fig. 2.6(b) and Fig. 2.6(c), there are a large number of segmentations which will reduce the amount of enhancement produced in this region.

2.3.3 Ratio Curve Threshold

The ratio curve threshold, C, is used to determine which peaks in the ratio curve will form segmentation points for the histogram equalisation process. Only when the height of a peak exceeds the ratio curve threshold, C, will it be used to form a segmentation point. For larger values of the ratio curve threshold, a smaller number of segments will be included and when the ratio curve threshold becomes very large, no segments will be included at all and standard histogram equalisation will be performed.

The height of peaks in the ratio curve varies significantly depending on the histogram and the width of the ratio curve window, N. Often, the height of the peaks correspond to the ratio curve window width, as shown in Fig. 2.7(a). There are also images for which the peak heights will not necessarily correspond to the

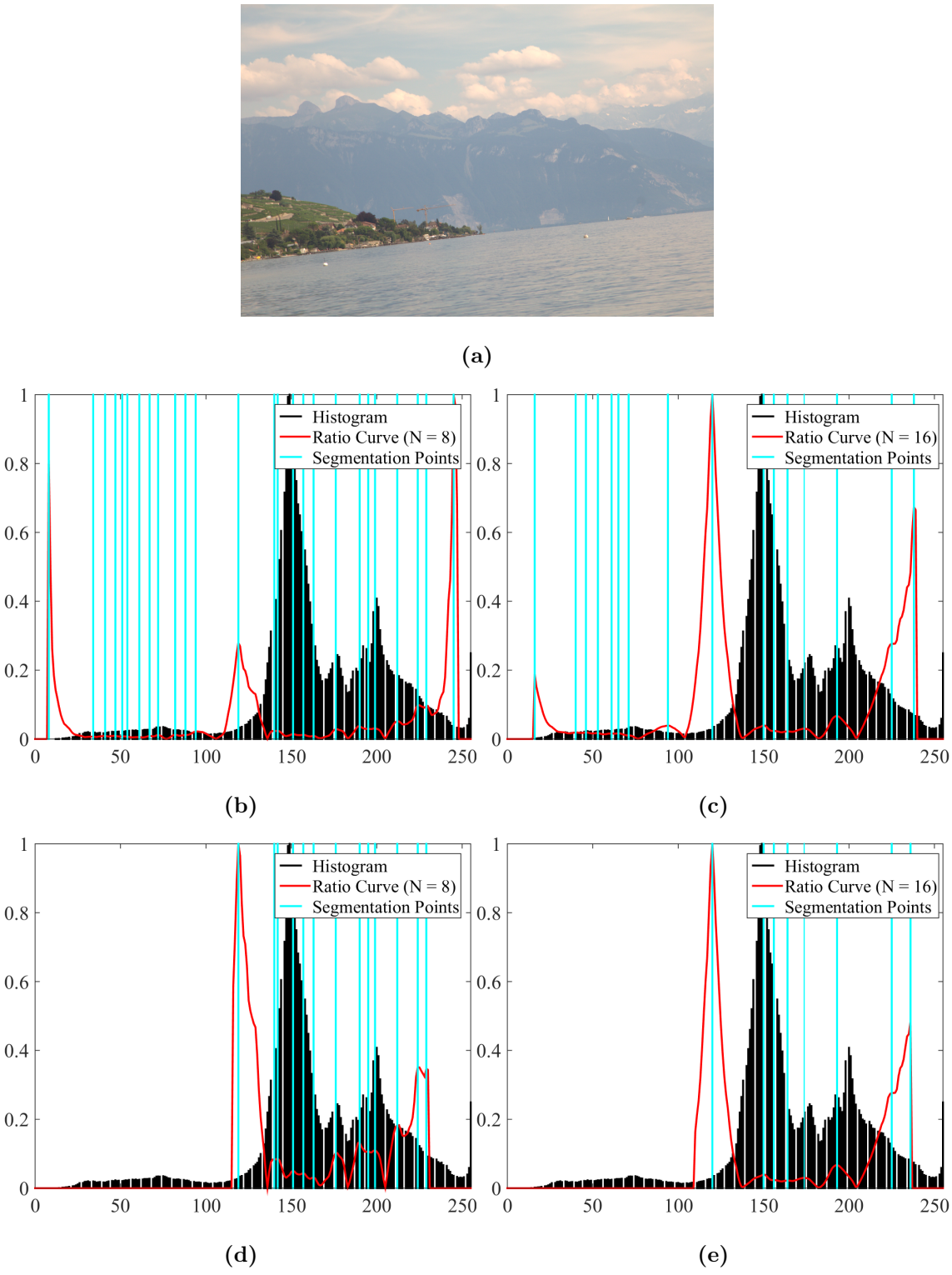

Figure 2.6 : The histogram for (a) the *water* image with the ratio curve and segmentation points for (b) $N = 8$ and $d = 0$, (c) $N = 16$ and $d = 0$, (d) $N = 8$ and $d = 1.563\%$ and (e) $N = 16$ and $d = 3.125\%$.

ratio curve window width, as shown in Fig. 2.7(b) where the largest ratio curve window width produces some of the smallest peaks. Therefore, the best ratio curve threshold value depends on the image and the user is able to adjust the value to suit each image. However, for comparison with the other benchmarking algorithms a ratio curve threshold of $C = 2$ is set for every test image. This reason this value is chosen for testing will be discussed in the quantitative results section 2.4.1.

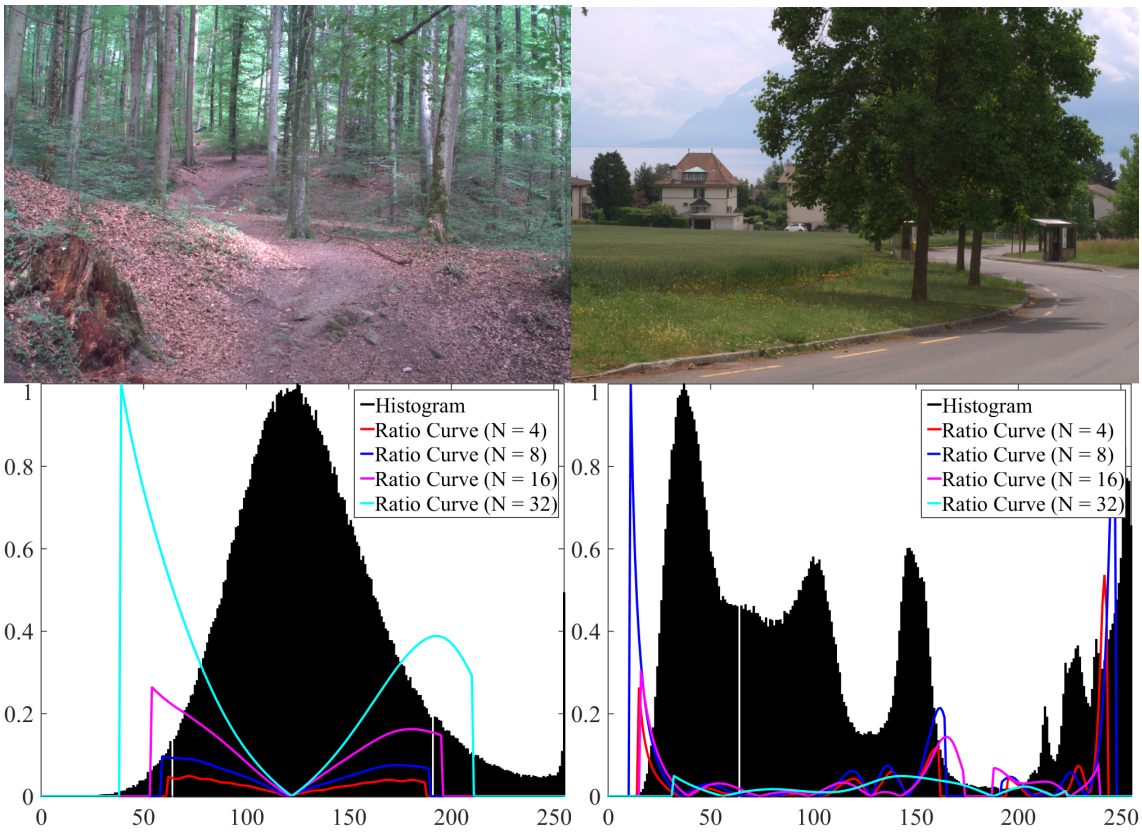

Figure 2.7 : The original image and the corresponding histogram and ratio curves for (a) the *forest* image and (b) the *country* image.

2.3.4 Alpha-Trimmed Mean Filter

Image histograms can often have both empty bins and spikes which can affect the evaluation of the ratio curve, producing unwanted peaks which do not necessarily reflect the general shape of the histogram. By applying an alpha-trimmed mean filter, the histogram can be smoothed before evaluating the ratio curve so that it better reflects the shape of the histogram.

The window width of the alpha-trimmed mean filter, M, should be the equivalent to the total width of the ratio curve window so that the position of peaks in the ratio curve is not shifted due to miss-matched window widths. As the ratio curve is evaluated on the left and right side of a centre position, its total span of the window is $2N + 1$, therefore M is defined as follows:

$$M = 2N + 1. \tag{2.14}$$

The alpha value, α, should be set to remove the smallest and largest values as follows:

$$\alpha = \frac{M - 2}{M}. \tag{2.15}$$

A smoothed histogram can also be estimated from the image using the kernel method [41]. The smoothness of the estimated histogram can be controlled by adjusting the bandwidth parameter. However, the bandwidth parameter has a strong influence on the histogram and can over-smooth it, distorting the underlying structure. As the proposed multi-level histogram shape segmentation method is based on the shape of the histogram, distorting the underlying structure of the histogram will affect the performance of the proposed method. Therefore, the alpha-trimmed

mean filter is preferred as it will effectively remove outliers without distorting the underlying structure of the histogram

2.4 Results

A range of different images are used for testing throughout this thesis, they consist of a large variety of both natural images and images which have had their contrast reduced. The test images used for quantitative evaluations and visual assessment are comprised of the RGBNIR [2], CSIQ [1] and TID2013 [42] datasets. The RGBNIR dataset [2] consists of 477 RGB natural and near-infra-red (NIR) images. The CSIQ dataset [1] has 30 reference images to which the contrast is incrementally reduced where "level 1" is the smallest amount of contrast reduction and "level 5" is the largest amount of contrast reduction. The TID2013 dataset [42] consists of 25 reference images for which the contrast is increased and reduced to 5 different levels: "level 1" corresponds to a small contrast reduction; "level 2" corresponds to a small contrast increase; "level 3" corresponds to a larger contrast reduction; "level 4" corresponds to a larger contrast increase; and "level 5" corresponds to the largest contrast reduction. All the images from the three datasets, excluding those NIR images in the RGBNIR dataset, were used for quantitative assessment, giving a total of 807 test images and a selection of these images are used throughout the thesis for visual assessment.

The proposed method is compared with eight other histogram equalisation based benchmarking algorithms, namely, HE [11], BBHE, [12], DSIHE [13], MMBEBHE [14], RMSHE [16], RSIHE [15], RSWHE [17] and WTHE [10]. Default parameter

settings for all algorithms are used.

2.4.1 Quantitative Results

Recently a number of image quality measures (IQMs) have been developed [19, 20, 8, 3, 21, 22, 23, 24, 25, 26, 27], to measure the quality of enhancement. One of the main objectives of the IQMs is to provide better correlation between the measured value and visual quality of enhancement. Therefore, several of these recently developed IQMs are used to quantitatively assess the performance of the proposed method when compared with the other benchmarking algorithms. The expected measure of enhancement by gradient (EMEG) [3], the quality-aware relative contrast measure (QRCM) [8] and the blind image quality measure of enhanced images (BIQME) [19] were used for our quantitative comparison. EMEG is based on the gradient to assess the strength of enhancement in the output image, QRCM is a combination of the relative contrast enhancement between the input and output image, and any distortions that result from enhancement and BIQME combines contrast, sharpness, brightness, colourfulness and naturalness into one quality score using a regression module.

Statistical analysis is used throughout the thesis to determine quantitatively which method provides the best enhancement. To do this, p-values [3] are employed which represent the proportion of output images by an enhancement method that have a higher IQM value when compared with the output images of another enhancement method. In Table 2.1-2.3, the p-values [3] for each of the benchmarking algorithms, namely, HE (i.e. M1), BBHE (i.e. M2), DSIHE (i.e. M3), MMBEBHE

(i.e. M4), RMSHE (i.e. M5), RSIHE (i.e. M6), RSWHE (i.e. M7), WTHE (i.e. M8) and the proposed MLHSS method where $N = 8$ (i.e. M9) and $N = 16$ (i.e. M10) were found for all 807 test images to statistically determine which algorithm provided the best enhancement. Table 2.1-2.3 should be read by row, whereby each entry in a row is the proportion of one methods output images, with a higher IQM value, with respect to every other method represented by each column. The p-values [3] based on EMEG in Table 2.1, represent the proportion of enhanced test images when $\{EMEG_A > EMEG_B\}$ where $EMEG_A$ and $EMEG_B$ are values produced by algorithms A and B, for a test image respectively. Table 2.2 and 2.3 contains the p-values which are based on QRCM and BIQME respectively. In Table 2.1-2.3, the rows correspond to algorithm A and the columns correspond to algorithm B.

In Table 2.1 based on EMEG, the proposed method, MLHSS ($N = 8$), produced p-values higher than 0.57 for all of the 807 test images when compared with the majority of the benchmarking algorithms. The proposed method was unable to outscore the HE, BBHE and DSIHE methods, this is due the fact that the proposed method includes more segments which reduces the overall strength of enhancement, but improves the quality of the output images. As the height of peaks in the ratio curve generally corresponds to the width of the ratio curve window, N and because the ratio curve threshold was fixed at $C = 2$, more segments were included when $N = 16$. This has resulted in slightly less overall enhancement for the proposed method when $N = 16$ as opposed to $N = 8$ which is reflected in the slightly lower p-values in Table 2.1-2.3.

In Table 2.2 based on QRCM, the proposed method, MLHSS ($N = 8$), gave a

Table 2.1 : The p-values for $EMEG_A > EMEG_B$ where M1:HE, M2:BBHE, M3:DSIHE, M4:MMBEBHE, M5:RMSHE, M6:RSIHE, M7:RSWHE, M8:WTHE, M9:MLHSS ($N = 8$) and M10:MLHSS ($N = 16$).

	M1	M2	M3	M4	M5	M6	M7	M8	M9	M10
M1	-	0.747	0.672	0.922	0.918	0.890	0.959	0.885	0.793	0.865
M2	0.252	-	0.155	0.605	0.844	0.848	0.865	0.623	0.564	0.658
M3	0.326	0.789	-	0.691	0.881	0.876	0.884	0.675	0.620	0.700
M4	0.078	0.390	0.301	-	0.730	0.618	0.851	0.439	0.424	0.548
M5	0.082	0.156	0.118	0.268	-	0.254	0.773	0.234	0.278	0.421
M6	0.110	0.151	0.124	0.382	0.739	-	0.814	0.379	0.356	0.483
M7	0.041	0.135	0.116	0.146	0.224	0.185	-	0.037	0.097	0.129
M8	0.115	0.377	0.323	0.561	0.763	0.620	0.963	-	0.426	0.621
M9	0.172	0.434	0.378	0.575	0.722	0.644	0.903	0.572	-	0.623
M10	0.107	0.342	0.300	0.452	0.579	0.517	0.871	0.379	0.323	-

similar result as in Table 2.1, outscoring five of the eight benchmarking algorithms for all of the 807 test images.

In Table 2.3 based on BIQME, the proposed method, MLHSS ($N = 8$) performed better then in Table 2.1 and 2.2, outperforming all of the other benchmarking algorithms with p-values higher than 0.50 for all of the 807 test images when compared with all the other benchmarking algorithms except HE and DSIHE.

Currently, no IQMs perfectly correlate with visual assessment and active research is still ongoing in the area of image quality assessment to produce a stronger correlation between quantitative and qualitative measurements. For this reason, visual assessment is included along with the quantitative results, so that methods can be assessed both on the quantitative values they produce as well as the visual quality of their outputs. Although the proposed method does not outperform a few bench-

Table 2.2 : The p-values for $QRCM_A > QRCM_B$ where M1:HE, M2:BBHE, M3:DSIHE, M4:MMBEBHE, M5:RMSHE, M6:RSIHE, M7:RSWHE, M8:WTHE, M9:MLHSS ($N = 8$) and M10:MLHSS ($N = 16$).

	M1	M2	M3	M4	M5	M6	M7	M8	M9	M10
M1	-	0.595	0.540	0.724	0.784	0.756	0.841	0.658	0.594	0.721
M2	0.405	-	0.300	0.612	0.786	0.792	0.784	0.568	0.520	0.603
M3	0.460	0.643	-	0.674	0.827	0.812	0.799	0.617	0.561	0.625
M4	0.276	0.385	0.317	-	0.680	0.579	0.778	0.367	0.424	0.528
M5	0.216	0.212	0.173	0.320	-	0.266	0.710	0.201	0.321	0.446
M6	0.243	0.208	0.186	0.421	0.729	-	0.730	0.322	0.394	0.502
M7	0.159	0.216	0.201	0.222	0.290	0.270	-	0.102	0.191	0.230
M8	0.342	0.432	0.382	0.633	0.799	0.675	0.898	-	0.508	0.647
M9	0.404	0.480	0.439	0.575	0.678	0.605	0.809	0.492	-	0.570
M10	0.278	0.397	0.375	0.472	0.551	0.498	0.768	0.353	0.378	-

marking algorithms, as given in Table 2.1-2.3, the visual assessment results in the next section 2.4.2, show that the proposed method produces better image quality enhancement than those other benchmarking algorithms, free from over-enhancement and clipping.

Table 2.4 gives the average processing time in seconds for enhancing an image in one of the three datasets for the benchmarking and proposed methods. All processing was done in MATLAB using an 8th generation Intel® Core™ i7 Q840 processor at 1.87GHz. The MATLAB code for all of the benchmarking algorithms in this chapter were implemented by the author of this thesis. The table shows that the proposed MLHSS method has a comparable average processing time when compared with the other methods, especially for the CSIQ and TID2013 datasets.

Fig. 2.8 shows the ratio curve threshold value verses the average p-value for

Table 2.3 : The p-values for $BIQME_A > BIQME_B$ where M1:HE, M2:BBHE, M3:DSIHE, M4:MMBEBHE, M5:RMSHE, M6:RSIHE, M7:RSWHE, M8:WTHE, M9:MLHSS ($N = 8$) and M10:MLHSS ($N = 16$).

	M1	M2	M3	M4	M5	M6	M7	M8	M9	M10
M1	-	0.897	0.864	0.955	0.950	0.943	0.962	0.908	0.753	0.838
M2	0.103	-	0.254	0.647	0.870	0.841	0.815	0.582	0.494	0.596
M3	0.134	0.683	-	0.740	0.895	0.876	0.849	0.660	0.543	0.646
M4	0.045	0.349	0.252	-	0.715	0.612	0.810	0.373	0.411	0.486
M5	0.048	0.130	0.105	0.284	-	0.258	0.710	0.161	0.255	0.354
M6	0.057	0.159	0.124	0.387	0.732	-	0.748	0.283	0.318	0.440
M7	0.037	0.185	0.151	0.187	0.287	0.252	-	0.055	0.152	0.150
M8	0.092	0.416	0.338	0.623	0.839	0.717	0.945	-	0.455	0.618
M9	0.216	0.503	0.456	0.589	0.745	0.680	0.848	0.545	-	0.553
M10	0.136	0.404	0.354	0.512	0.644	0.559	0.848	0.380	0.393	-

Table 2.4 : The average processing time in seconds for an image in each of the three datasets for the proposed multi-level histogram shape segmentation method and the other benchmarking algorithms.

Method	Average Processing Time (s)		
	RGBNIR	CSIQ	TID2013
HE	0.79	0.34	0.31
BBHE	0.81	0.34	0.27
DSIHE	0.82	0.34	0.26
MMBEBHE	0.79	0.33	0.26
RMSHE	1.89	0.77	0.58
RSIHE	0.78	0.34	0.31
WTHE	0.89	0.40	0.37
MLHSS ($N = 8$)	1.20	0.40	0.31
MLHSS ($N = 16$)	1.19	0.40	0.31

different datasets. In this case, the p-values were only found for the proposed method for $N = 8$ and $N = 16$ with different ratio curve threshold values for QRCM and BIQME to determine which ratio curve threshold value gave the best enhancement. It follows, that the maximum degree of enhancement will be obtained when there are no segments and standard histogram equalisation is performed, but to avoid the problem of over-enhancement, segments must be included. In every case, the CSIQ dataset showed a spike in the average p-value for the ratio curve threshold value, $C = 2$ and in some cases the TID2013 dataset also showed a spike for the same value. Therefore, the ratio curve threshold, $C = 2$, was used for all experimental results.

2.4.2 Visual Assessment

For visual assessment, to compare our proposed method with eight other benchmarking algorithms, a range of different types of images, namely, Fig. 2.9(b) the *cactus* image, Fig. 2.10(b) the *painted face* image and Fig. 2.11(a) the *mountain* image from the three datasets, were used.

The contrast reduced *cactus* image, shown in Fig. 2.9(b), was selected as the sky background is challenging for many equalisation algorithms. The image produced by HE, shown in Fig. 2.9(c), was over-enhanced and exhibited an unnatural appearance as a result of the peak in the histogram being spread out too far. The images produced by BBHE, DSIHE and MMBEBHE, shown in Fig. 2.9(d) - Fig. 2.9(f) respectively, were also over-enhanced, as the single segmentation was inadequate to prevent the peak in the histogram from being spread out. The RMSHE, RSIHE and

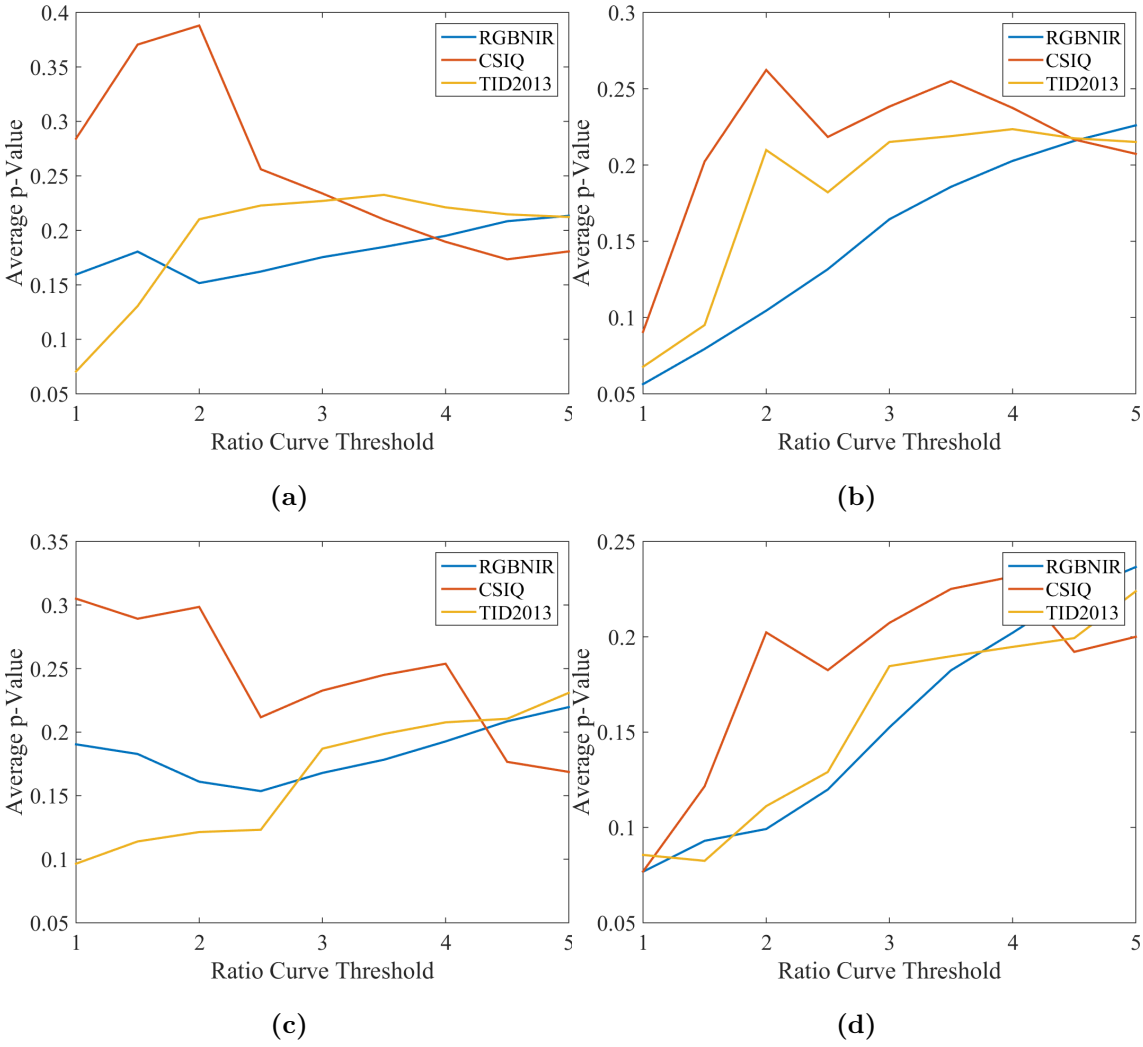

Figure 2.8 : The ratio curve threshold, C vs the average p-value for the proposed method with (a) QRCM and $N = 8$, (b) BIQME and $N = 8$, (c) QRCM and $N = 16$ and (d) BIQME and $N = 16$.

RSWHE output images, shown in Fig. 2.9(g) - Fig. 2.9(i) respectively, were under-enhanced with contrast that remained poor like the input image. This was due to an extra un-required segmentations which reduce the overall strength of enhancement. The image produced by WTHE, shown in Fig. 2.9(j), was over-enhanced, while not as severe as HE, the sky still has an unnatural grainy appearance. The proposed MLHSS method, with $N = 8$ and $N = 16$, each produced similarly visually pleasing outputs, shown in Fig. 2.9(k) and Fig. 2.9(l) respectively, with vivid colour and appropriate enhancement over the entire image. The histogram was segmented appropriately, so that the peak was not spread out too wide avoiding over-enhancement.

The contrast reduced *painted face* image, shown in Fig. 2.10(b), was chosen as it is difficult for enhancement algorithms to produce natural enhancement in the human face. Like the previous example, the image produced by HE, shown in Fig. 2.10(c), was over-enhanced with a loss of details in the girl's right cheek. The images produced by BBHE, DSIHE and MMBEBHE, shown in Fig. 2.10(d) - Fig. 2.10(f) respectively, had various degrees of over-enhancement with a loss of details in the girl's right cheek and a unnatural appearance in the light background behind the girl. This was because these methods having only a single inappropriately located segment in the histogram. The RMSHE and RSIHE output images, shown in Fig. 2.10(g) and Fig. 2.10(h) respectively, were also over-enhanced in the light background behind the girl due to inappropriately located segments. The RSWHE output, shown in Fig 2.10(i), was dull with poor contrast like the input. The image produced by WTHE, shown in Fig. 2.10(j), was clipped, with a reduced dynamic

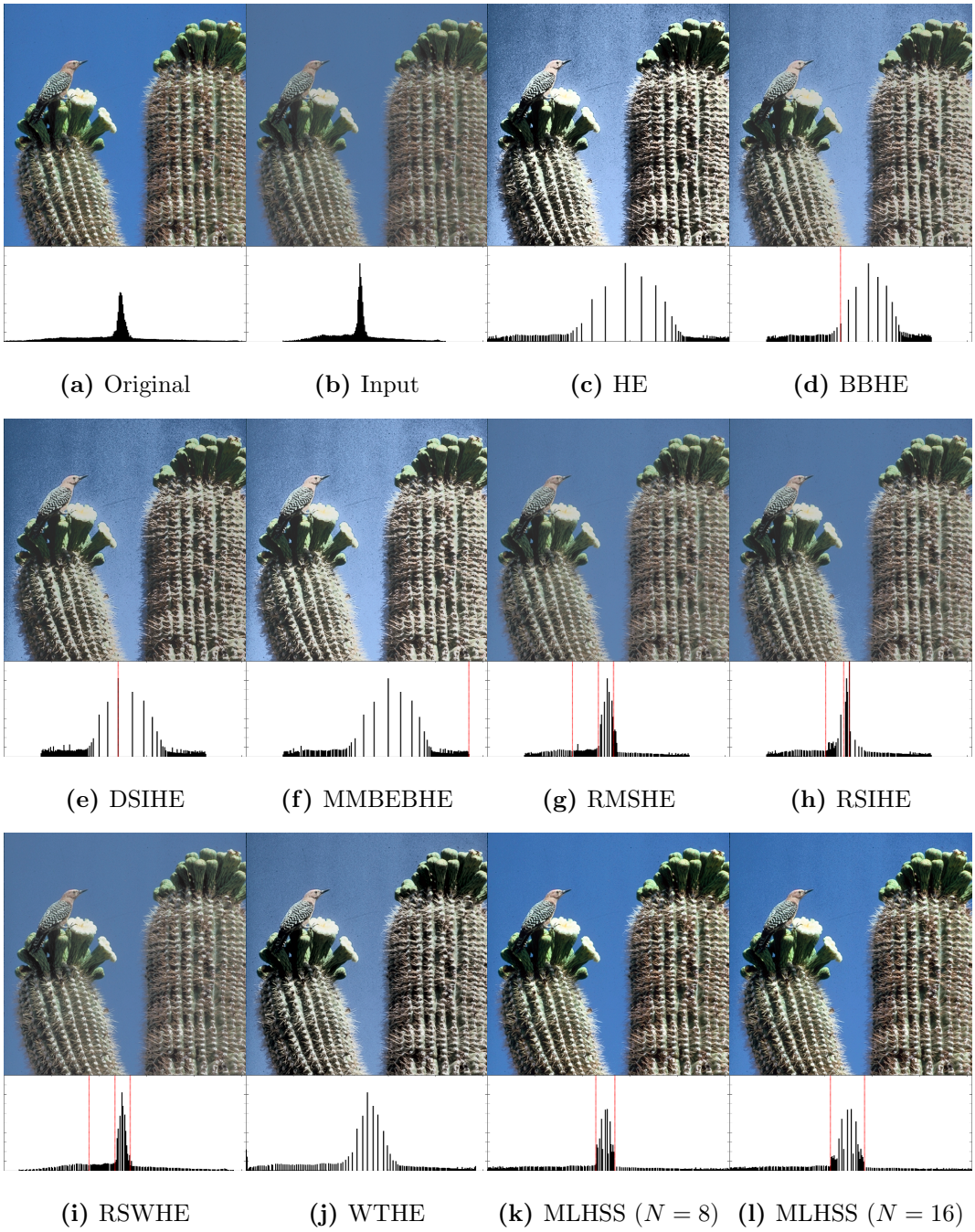

(a) Original **(b)** Input **(c)** HE **(d)** BBHE

(e) DSIHE **(f)** MMBEBHE **(g)** RMSHE **(h)** RSIHE

(i) RSWHE **(j)** WTHE **(k)** MLHSS ($N = 8$) **(l)** MLHSS ($N = 16$)

Figure 2.9 : The enhancement results for the proposed multi-level histogram shape segmentation method and the other benchmarking algorithms using the *cactus* image from the CSIQ dataset. (a) The original image. (b) The contrast reduced input image. The enhanced output by (c) HE, (d) BBHE, (e) DSIHE (f) MMBEBHE, (g) RMSHE, (h) RSIHE, (i) RSWHE, (j) WTHE and the proposed (k) MLHSS ($N = 8$) and (l) MLHSS ($N = 16$). The red dotted lines in the histogram indicate segmentation locations.

range seen in the histogram. The output produced by the proposed method with $N = 8$, shown in Fig. 2.10(k), was also over-enhanced, as the ratio curve threshold of $C = 2$ was too high in this case. However, the image produced by the proposed MLHSS method, with $N = 16$, displayed adequate and naturally appearing enhancement, as shown in Fig. 2.10(l), due to the appropriately segmented histogram.

The *mountain* image, shown in Fig. 2.11(a), was used to see how the enhancement algorithms performed on natural scenery. The image produced by HE, shown in Fig. 2.11(b) was over-enhanced with a loss of details in the mountain peak and an unnatural appearance in the sky. The images produced by BBHE, DSIHE, MMBEBHE, RMSHE, RSIHE and RSWHE, shown in Fig. 2.11(c) - Fig. 2.11(h) respectively, all exhibited of loss of details in the mountain peak due to inappropriate segmentation locations. The WTHE output, shown in Fig. 2.11(i), also produced an image with a loss of details, not only in the mountain peak, but in the clouds above the mountain as well. The proposed MLHSS method, with both $N = 8$ and $N = 16$, produced visually pleasing images without any loss of details in the mountain ranges or clouds, as shown in Fig. 2.11(j) and Fig. 2.11(k) respectively.

Idividual EMEG values for the figures included in visual assessment.

For many images, the trade off for improving the quality of enhancement by increasing the number of segmentations is a reduced strength in the degree of enhancement using the proposed method. Table 2.5-2.7 give the individual EMEG, QRCM and BIQME values respectively for the proposed multi-level histogram shape segmentation method and the other benchmarking algorithms for Fig. 2.9, Fig. 2.10 and Fig. 2.11, values highlighted in bold indicate the highest scores. Each table

(a) Original **(b)** Input **(c)** HE **(d)** BBHE

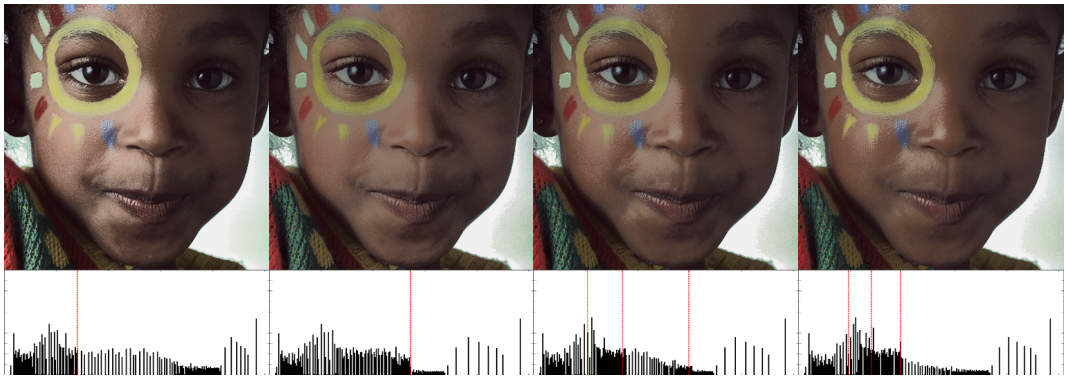

(e) DSIHE **(f)** MMBEBHE **(g)** RMSHE **(h)** RSIHE

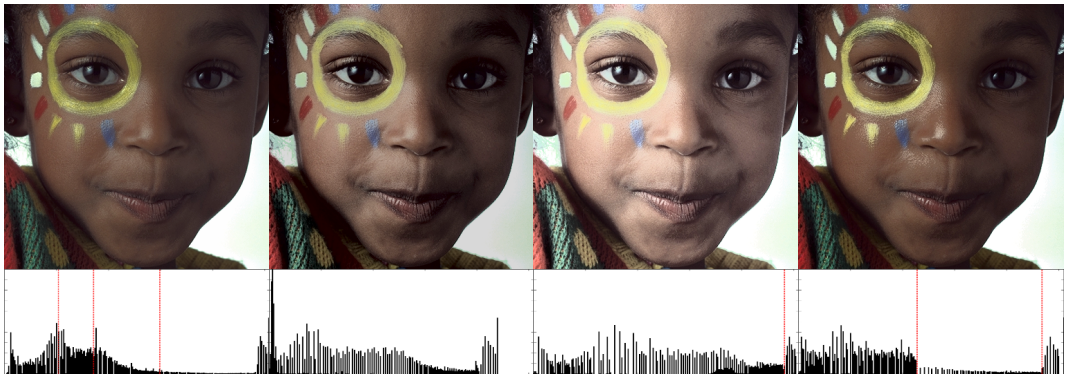

(i) RSWHE **(j)** WTHE **(k)** MLHSS ($N = 8$) **(l)** MLHSS ($N = 16$)

Figure 2.10 : The enhancement results for the proposed multi-level histogram shape segmentation method and the other benchmarking algorithms using the *painted face* image from the TID2013 dataset. (a) The original image. (b) The contrast reduced input image. The enhanced output by (c) HE, (d) BBHE, (e) DSIHE (f) MMBEBHE, (g) RMSHE, (h) RSIHE, (i) RSWHE, (j) WTHE and the proposed (k) MLHSS ($N = 8$) and (l) MLHSS ($N = 16$). The red dotted lines in the histogram indicate segmentation locations.

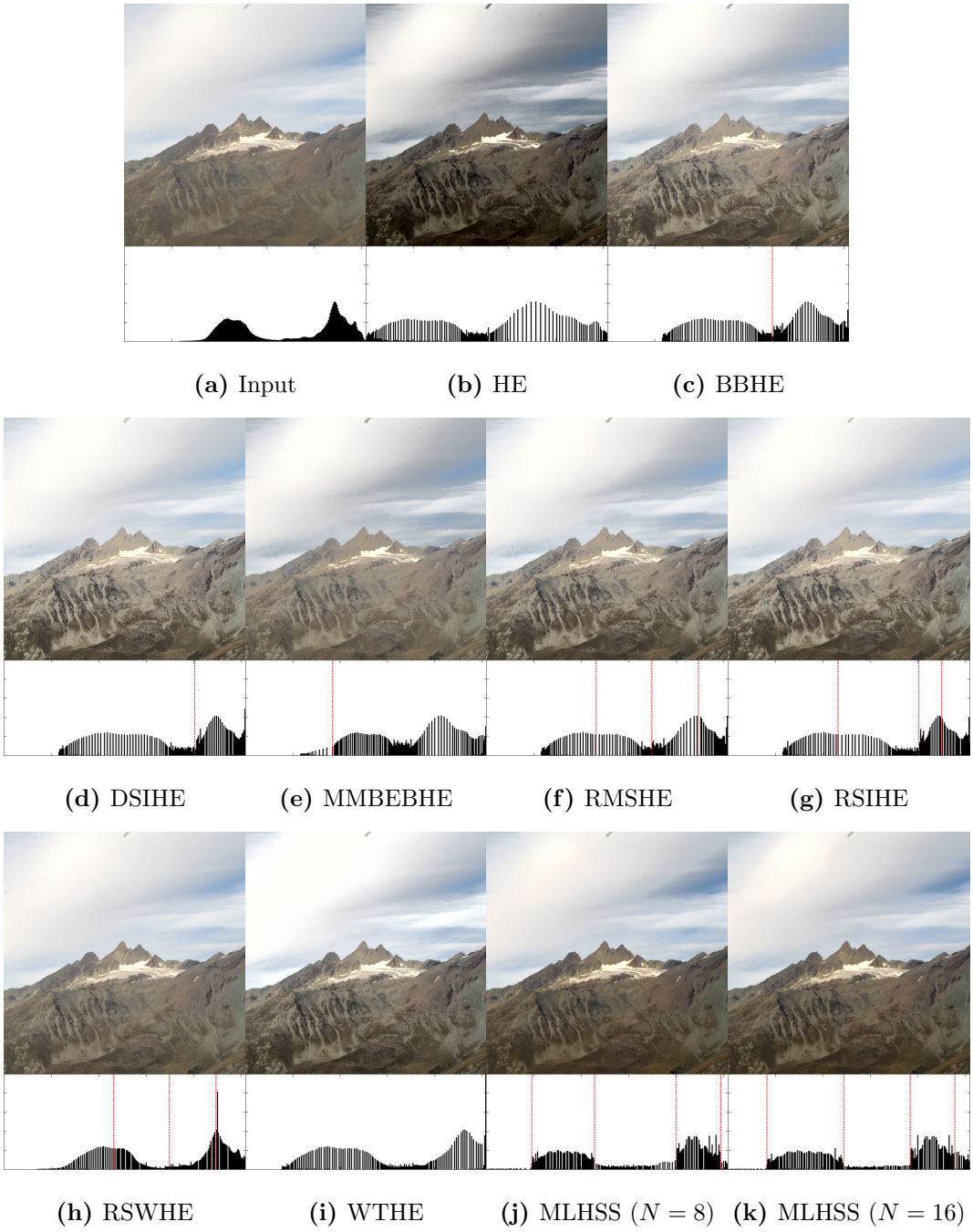

(a) Input **(b)** HE **(c)** BBHE

(d) DSIHE **(e)** MMBEBHE **(f)** RMSHE **(g)** RSIHE

(h) RSWHE **(i)** WTHE **(j)** MLHSS ($N = 8$) **(k)** MLHSS ($N = 16$)

Figure 2.11 : The enhancement results for the proposed multi-level histogram shape segmentation method and the other benchmarking algorithms using the *mountain* image from the RGBNIR dataset. (a) The input image. The enhanced output by (b) HE, (c) BBHE, (d) DSIHE (e) MMBEBHE, (f) RMSHE, (g) RSIHE, (h) RSWHE, (i) WTHE and the proposed (j) MLHSS ($N = 8$) and (k) MLHSS ($N = 16$). The red dotted lines in the histogram indicate segmentation locations.

Table 2.5 : The individual EMEG values for the proposed multi-level histogram shape segmentation method and the other benchmarking algorithms for the *cactus*, *painted face* and *mountain* images shown for visual assessment in Fig. 2.9, Fig. 2.10 and Fig. 2.11 respectively.

Method	*cactus*	*painted face*	*mountain*
HE	**0.581**	0.330	**0.170**
BBHE	0.385	0.299	0.140
DSIHE	0.397	0.325	0.146
MMBEBHE	0.447	0.224	0.120
RMSHE	0.245	0.239	0.147
RSIHE	0.268	0.241	0.149
RSWHE	0.260	0.252	0.112
WTHE	0.431	0.299	0.142
MLHSS ($N = 8$)	0.388	**0.343**	0.129
MLHSS ($N = 16$)	0.378	0.304	0.131

Table 2.6 : The individual QRCM values for the proposed multi-level histogram shape segmentation method and the other benchmarking algorithms for the *cactus*, *painted face* and *mountain* images shown for visual assessment in Fig. 2.9, Fig. 2.10 and Fig. 2.11 respectively.

Method	*cactus*	*painted face*	*mountain*
HE	**0.310**	0.124	0.083
BBHE	0.157	0.061	0.130
DSIHE	0.157	0.096	**0.149**
MMBEBHE	0.214	-0.008	0.068
RMSHE	0.087	0.006	0.139
RSIHE	0.115	0.009	0.148
RSWHE	0.106	0.034	0.076
WTHE	0.280	0.090	0.097
MLHSS ($N = 8$)	0.278	**0.139**	0.100
MLHSS ($N = 16$)	0.271	0.085	0.113

Table 2.7 : The individual BIQME values for the proposed multi-level histogram shape segmentation method and the other benchmarking algorithms for the *cactus*, *painted face* and *mountain* images shown for visual assessment in Fig. 2.9, Fig. 2.10 and Fig. 2.11 respectively.

Method	*cactus*	*painted face*	*mountain*
HE	**0.674**	0.662	**0.637**
BBHE	0.572	0.617	0.511
DSIHE	0.595	0.638	0.499
MMBEBHE	0.603	0.595	0.473
RMSHE	0.518	0.603	0.509
RSIHE	0.532	0.606	0.506
RSWHE	0.530	0.613	0.472
WTHE	0.646	0.623	0.534
MLHSS ($N = 8$)	0.623	**0.669**	0.552
MLHSS ($N = 16$)	0.626	0.617	0.566

shows that the respective IQM value for the proposed method is greater then, or comparable to many of the other benchmarking algorithms. However, as the IQM values are based on a combination of both the degree and quality of enhancement, the reduced strength of enhancement of the proposed method restricts it from achieving the highest scores for all of the images. For this reason, the enhancement methods presented in the following chapters are design to improve the quality of enhancement while still maintaining an adequate degree of enhancement.

2.5 Conclusion

It has been shown that the proposed multi-level histogram shape segmentation method is able to enhance an image without over-enhancement by appropriately segmenting the image histogram. By detecting abrupt changes in the histogram,

intensity values with a similar frequency of occurrence are grouped together for independent equalisation. Furthermore, the proposed initial contrast expansion step produces more vivid colour enhancement of an image, without altering the original balance of colour. The proposed method outperformed the other benchmarking algorithms visually, without the usual adverse problems of over-enhancement and a loss of details that other enhancement methods posses.

The proposed method is highly adaptable to different types of images, allowing a user to adjust both the ratio curve window width and the ratio curve threshold to control the number of segmentation points and hence, the quality of enhancement. However, including more segments to improve the quality of enhancement will in turn reduce the overall strength of enhancement. Therefore, in the following chapters, alternative enhancement methods are explored which allow a user more control over the degree of enhancement without sacrificing the output image quality.

Chapter 3

Image and Video Enhancement with Brightness Preservation by Successive Approximation

3.1 Introduction

Brightness preservation is not essential when enhancing a single image, but it is an important aspect when enhancing video, as changes in the brightness transition from frame to frame can cause flickering [18, 17, 10]. Histogram equalisation enhances an image by equalising the number of pixels per intensity, this results in the mean brightness of an output image always being shifted to the middle intensity value [16]. The methods discussed in the previous chapter, namely, BBHE [12], DSIHE [13], MMBEBHE [14], RMSHE [16], RSIHE [15] and RSWHE [17], attempt to preserve image brightness by segmenting the histogram and performing equalisation on each segment independently. Intensity values with a large frequency of occurrence can only be re-distributed within the same segment, they cannot be re-distributed to other segments, so the brightness is maintained to a certain extent, but it will not be preserved. By introducing more segments the brightness of an image can be better maintained, to the point where if there are 255 segments for an 8-bit image the brightness will be perfectly maintained. However, enhancement is limited within each segment, so including more segments will reduce the overall enhancement of the output image, resulting in under-enhancement. Other brightness

preserving methods, such as WTHE [10], reduce the dynamic range of the output to maintain the same brightness of the input, but this causes clipping and can also result in under-enhancement. In other words, these methods attempt to preserve brightness by limiting the degree of enhancement, but in each case brightness can only be preserved when the enhancement is limited to such a degree that it is no longer visible.

There are a group of methods [3, 24, 8], which instead of using the histogram to perform enhancement, use the spatial locations of intensity values of an image. The spatial entropy-based contrast enhancement (SECE) method was the first to perform enhancement by mapping input intensities to output intensities using the spatial entropy of intensity values. However, the output produced by this method is usually a simple linear mapping. Furthermore, this method has no control over the degree of enhancement. The spatial mutual information and PageRank-based contrast enhancement (SMIRANK) [8] and residual spatial entropy-based contrast enhancement (RSECE) [24] methods improved on SECE by including the spatial relationships of intensities as well as their distribution and including control over the degree of enhancement. The RSECE method also further extends on SECE by attempting to preserve image brightness. However, brightness preservation is performed in the discrete cosine transform (DCT) domain which means the entire dynamic range may not be used, resulting in under-enhancement of the output image.

Another group of recently developed methods are based on S-shaped curves [18, 9, 43] and can improve image contrast to give a better correlation with the

human visual system. To preserve the median brightness of each image, a median brightness subtraction and addition method was developed for the S-shaped sigmoid transfer function (SSTF) and is known as the SSTF based brightness preserving (STBP) [18] method. STBP shifts the intensity range of the image such that the image median is at 127.5 for an intensity range of [0,255]. However, the range of the SSTF is limited to the same range of [0,255] and any values above or below this range after intensity shifting will be clipped, resulting in a loss of details and contrast. The automatic robust image contrast enhancement (RICE) [9] method with saliency preservation combines the original image with the histogram equalised output and the STBP output to produce an enhanced image. Saliency preservation is used to optimise the parameters of this method to give optimum outputs, however due to the constraint of saliency preservation, the output images RICE produces are often under enhanced.

As as S-shaped curve will increase and decrease intensities above and below an intersection point respectively, we propose to preserve either the mean or median image brightness by shifting the intersection point along the $y = x$ line by using the corresponding mean or median value in the feedback loop at each iteration of successive approximation [38]. In this way, an intersection point is found that allows for an increase in the dynamic range of intensities of an output image, while retaining the same mean or median brightness as the input image. This ability to simultaneously increase contrast while preserving brightness makes the proposed method ideal for video enhancement.

Furthermore, the brightness of an image can be adjusted by adding a signed

offset to the mean or median within the process of successive approximation. This allows a user to change the brightness of an image or video, without causing any clipping of the intensity range. Moreover, when enhancing video, the brightness can be increased or decreased while preserving the transition from frame to frame to avoid flickering. Alternatively, the proposed method can be used to preserve the brightness of a video by pre-setting the designated brightness and then all of the processed images will have their brightness shifted to match that same value.

Gamma correction is another method that has good correlation with the human visual system [44] One recent method to make use of gamma correction is the adaptive gamma correction with weighting distribution (AGCWD) [33] algorithm which uses gamma correction to enhance an image with an adaptive gamma value based on the histogram weightings proposed in WTHE. However, the output images are often over-enhanced resulting in a loss of details in the bright regions of an image. Furthermore, to preserve the brightness of images, this method limits the dynamic range of the output so that it is the same as the input, giving limited contrast enhancement in the output image.

By modifying gamma correction, an S-shaped curve can be produced that approximates the SSTF, but with greater computational efficiency and a wider range of control over the degree of enhancement [45]. In this chapter, the proposed method for brightness preservation using successive approximation with both the SSTF and modified gamma curve (MGC) will be described and their quantitative and visual results will be compared.

3.2 Method

The contrast expansion method [38, 36, 37] detailed in Chapter 2 is applied to the image in the RGB colour space as an initial step of this proposed enhancement method to improve the dynamic range of colours and achieve more vivid colour enhancement.

3.2.1 The S-Shaped Sigmoid Transfer Function

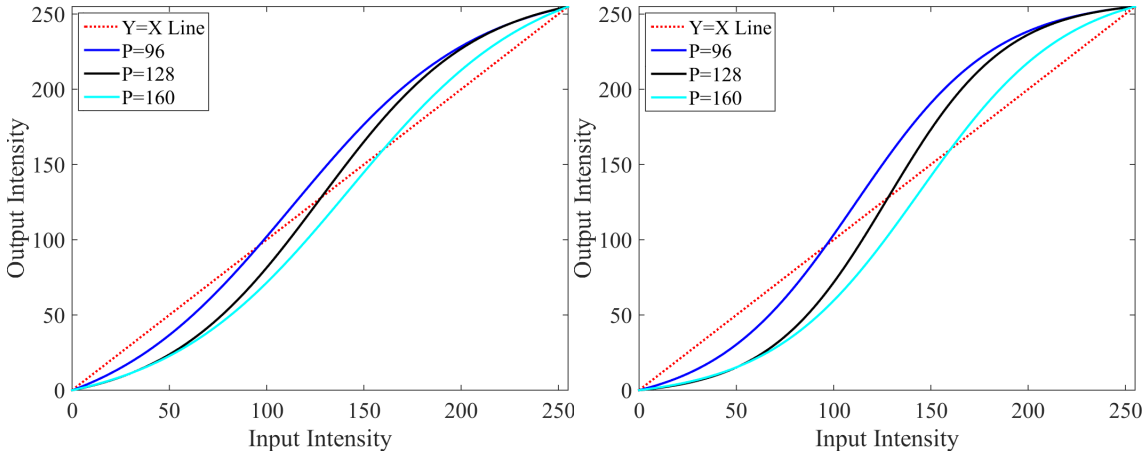

Figure 3.1 : The SSTF with different intersection points, P, for (a) $\alpha = 9$ and (b) $\alpha = 5$.

The SSTF is given by the following equation [9]:

$$y = \frac{\pi_1 - \pi_2}{1 + e^{-\frac{x-\pi_3}{\pi_4}}} + \pi_2, \tag{3.1}$$

with the constraints that the above curve must intersect with the line $y = x$ at both end points, $(x_1,\ y_1) = (0,\ 0)$ and $(x_2,\ y_2) = (255,\ 255)$ and the intersection point,

$(x_3, y_3) = (P, P)$. The fourth point (x_4, y_4) is defined as follows:

$$(x_4, y_4) = \begin{cases} (25, \alpha), & P \geq 127.5 \\ (230, 255 - \alpha), & P < 127.5 \end{cases}, \tag{3.2}$$

where α is a parameter to set the degree of contrast enhancement by altering the degree of curvature of the SSTF curve and $0 < \alpha < 25$.

The enhancement control point, (x_4, y_4), is defined at equal but opposite distances from both ends of the curve, depending on whether the intersection point is above or below the centre point. This will maximise the interval between the intersection and enhancement control points to obtain the optimum solution when optimising the SSTF curve. When α is small, the degree of enhancement is large and vice versa.

The optimal control parameters $\pi = \{\pi_1, \pi_2, \pi_3, \pi_4\}$ are obtained by minimising the following objective function [18]:

$$\pi_{opt} = argmin \sum_{i=1}^{4} \left| y_i - \left(\frac{\pi_1 - \pi_2}{1 + e^{-\frac{x_i - \pi_3}{\pi_4}}} + \pi_2 \right) \right|. \tag{3.3}$$

To improve computational efficiency, we propose to reduce the number of optimum control parameters from four to two by partly solving the equations. By substituting the end point $(x_1, y_1) = (0, 0)$ into (3.1), we have:

$$\frac{\pi_3}{\pi_4} = log \left(\frac{-\pi_1}{\pi_2} \right). \tag{3.4}$$

By the substitution of both end points, $(x_1, y_1) = (0, 0)$ and $(x_2, y_2) = (255, 255)$, into (3.1), we have:

$$\pi_4 = \frac{-255}{log \left(\frac{\frac{255}{\pi_1} - 1}{\frac{255}{\pi_2} - 1} \right)} = f(\pi_1, \pi_2). \tag{3.5}$$

By substituting π_4 in (3.5) into (3.4), we have:

$$\pi_3 = \frac{-255}{log\left(\frac{\frac{255}{\pi_1}-1}{\frac{255}{\pi_2}-1}\right)} log\left(\frac{-\pi_1}{\pi_2}\right) = g(\pi_1, \pi_2). \tag{3.6}$$

Since π_3 and π_4 are now a function of π_1 and π_2, (3.5) and (3.6) can be substituted into (3.1) so that the SSTF curve is a function of π_1 and π_2 only. The remaining optimum control parameters are $\pi = \{\pi_1, \pi_2\}$ and can be obtained by minimising the following objective function.

$$\pi_{opt} = argmin \sum_{i=3}^{4} \left| y_i - \left(\frac{\pi_1 - \pi_2}{1 + e^{-\frac{x_i - g(\pi_1,\pi_2)}{f(\pi_1,\pi_2)}}} + \pi_2 \right) \right|. \tag{3.7}$$

Let $\boldsymbol{X}$ be an image in RGB colour space with an intensity range of [0, L-1] where L is 256 for an 8-bit image. Let $\boldsymbol{X}_c$ be the output processed by the contrast expansion method in Chapter 2 and $\boldsymbol{I}_c$ be the luminance component of $\boldsymbol{X}_c$. Enhancement by the SSTF using the optimised parameters, π_{opt}, is given by the following:

$$Y(i,j) = \frac{\pi_1 - \pi_2}{1 + e^{-\frac{I_c(i,j) - \pi_3}{\pi_4}}} + \pi_2, \tag{3.8}$$

where $Y(i, j)$ is the luminance component of the enhanced image.

Refer to Fig. 3.1 for an example of the SSTF curve with various intersection points and α values.

3.2.2 The Modified Gamma Curve

Although the efficiency of the SSTF curve can be greatly increased by halving the number of control parameters, there still remains two control parameters that need to be optimised during each iteration of successive approximation to preserve brightness. Furthermore, the control over the degree of enhancement is limited

between $0 < \alpha < 25$. For computation efficiency, with a wider control of the degree of enhancement, a novel modified gamma curve (MGC) [45], approximating the shape of the SSTF is proposed.

Standard gamma correction for image enhancement, is given by the following [11]:

$$Y(i,j) = (L-1)\left(\frac{I_c(i,j)}{L-1}\right)^{\gamma}, \tag{3.9}$$

where $Y(i,j)$ is the luminance component of the enhanced image and γ is the control parameter for the degree of contrast enhancement which can be any value greater than unity for enhancement. Let (P, P) be an intersection point on the modified gamma curve (MGC) at which the input and output image intensities both equal P. This intersection point is the point on the MGC at which the MGC changes from reducing to increasing intensity values. The proposed MGC consists of the standard gamma curve from the minimum intensity value, 0, to the intersection point and an inverse reflection of the gamma curve from the intersection point to the maximum intensity value, $L-1$, producing a curve with the required shape as follows:

$$Y(i,j) = \begin{cases} \frac{I_c(i,j)^{\gamma}}{P^{\gamma-1}}, & I_c(i,j) < P \\ (L-1) - \frac{((L-1)-I_c(i,j))^{\gamma}}{((L-1)-P)^{(\gamma-1)}}, & I_c(i,j) > P \\ I_c(i,j), & otherwise \end{cases}. \tag{3.10}$$

To show that the MGC is continuous about the intersection point, $I_c(i,j) = P$ is substituted into $Y(i,j) = \frac{I_c(i,j)^{\gamma}}{P^{\gamma-1}}$ as follows:

$$\begin{aligned} Y(i,j) &= \tfrac{P^{\gamma}}{P^{\gamma-1}}, \\ \therefore Y(i,j) &= P^{\gamma-(\gamma-1)}, \\ \therefore Y(i,j) &= P. \end{aligned} \tag{3.11}$$

$I_c(i,j) = P$ is also substituted into $Y(i,j) = (L-1) - \frac{((L-1)-I_c(i,j))^\gamma}{((L-1)-P)^{\gamma-1}}$ as follows:

$$\begin{aligned} Y(i,j) &= (L-1) - \tfrac{((L-1)-P)^\gamma}{((L-1)-P)^{\gamma-1}}, \\ \therefore Y(i,j) &= (L-1) - ((L-1)-P)^{\gamma-(\gamma-1)}, \\ \therefore Y(i,j) &= (L-1) - (L-1) + P, \\ \therefore Y(i,j) &= P. \end{aligned} \tag{3.12}$$

As both equations resolve to $Y(i,j) = P$, the MGC is continuous about the intersection point, P.

Fig. 3.2(a) and Fig. 3.2(b) give the shape of our proposed MGC with different γ values at different locations of the intersection point. When equivalent degrees of

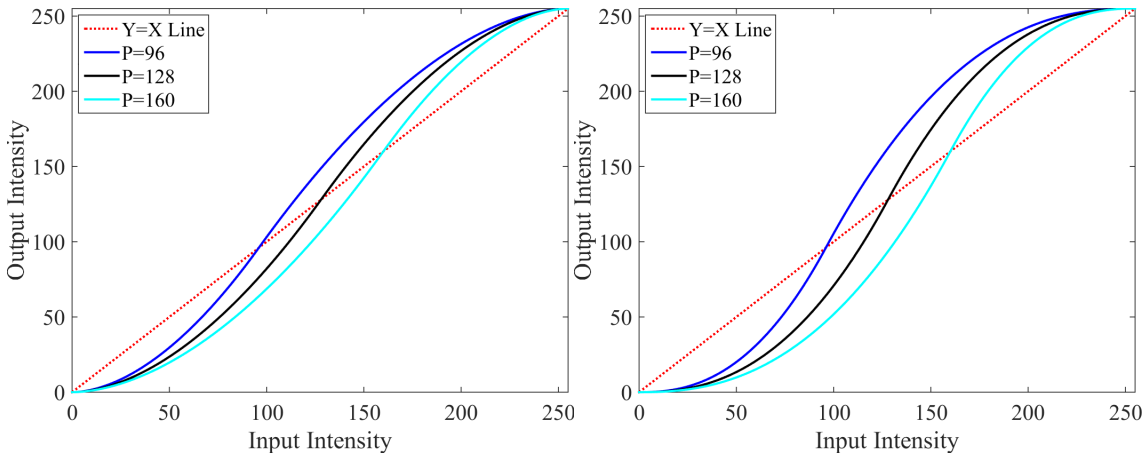

Figure 3.2 : The MGC with different P for (a) $\gamma = 1.8$ and (b) $\gamma = 2.4$.

enhancement are set for both the SSTF and the MGC, Fig. 3.3 shows that at different intersection points, P, the curves produced by the different methods maintain approximately the same shape. The MGC provides slightly stronger enhancement for the very small and very large intensity values.

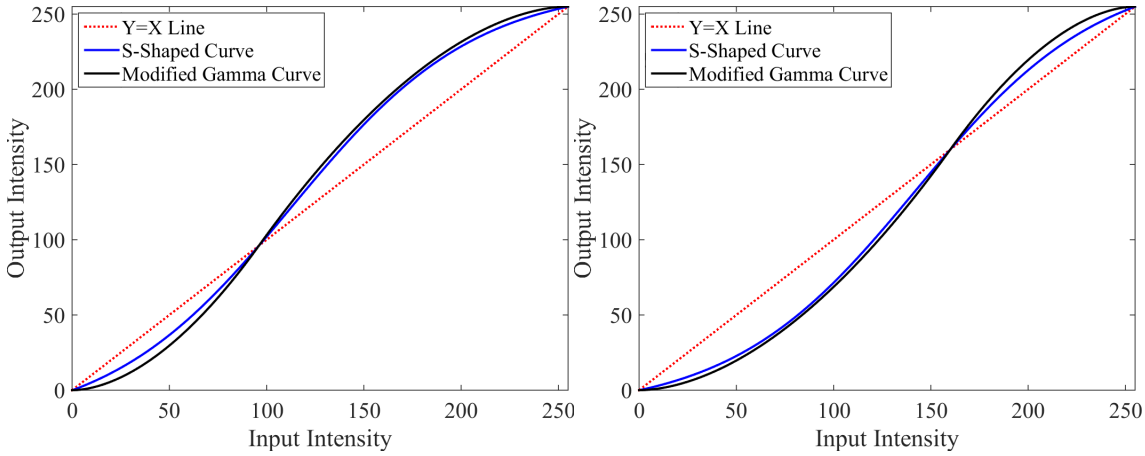

Figure 3.3 : The SSTF vs the MGC for equivalent degrees of enhancement at (a) $P = 96$ and (c) $P = 160$.

3.2.3 Brightness Preservation by Successive Approximation

Enhancement is applied to the luminance of the contrast expanded image, $\boldsymbol{I}_c$, while preserving the mean or median of the luminance of the original image, $\boldsymbol{I}$.

Let P be represented by an N-bit binary number initialised to zero. At the start of successive approximation, the most significant bit (MSB) of P is set to '1'. Suppose the mean brightness is to be preserved, i.e. $I' = \bar{I}$ and switch $S1$ is at position A. At the end of each iteration, the mean, $\bar{Y}$, of the enhanced image is re-calculated, and $Y' = \bar{Y}$. If $I' \leq Y'$, the '1' value of that bit is kept, it is reset to '0' otherwise. This process is repeated until all the N-bits are determined. It is computationally efficient as only N iterations are required. When $\alpha \geq 25$ for enhancement using the SSTF and when $\gamma \leq 1$ for enhancement using the MGC, no further contrast enhancement is possible and the process will terminate. To preserve

median brightness, the only difference is to switch $S1$ to position B. Refer to Fig. 3.4 for our proposed contrast enhancement algorithm by successive approximation.

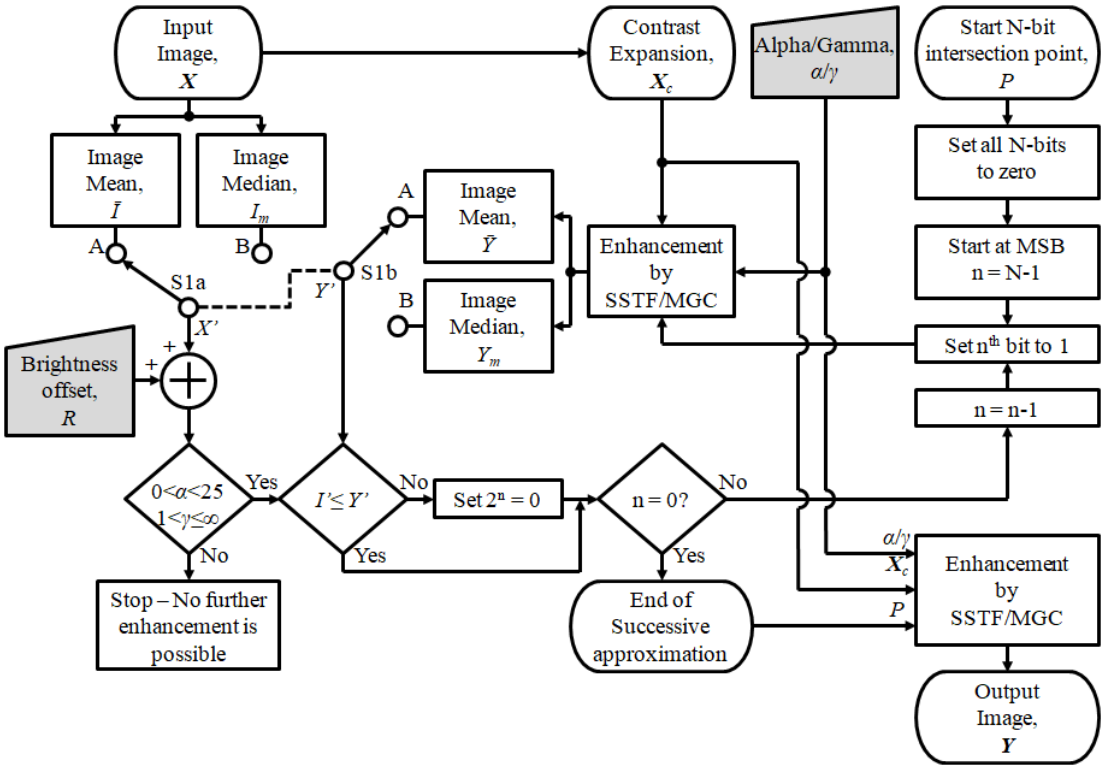

Figure 3.4 : Flowchart for image enhancement with brightness preservation by successive approximation.

3.3 Results

A total of 807 test images from the NIRRGB [2], CSIQ [1] and TID2013 [42] datasets were used for quantitative evaluations and some were selected for visual assessment. The outputs of the proposed method, namely STSA and MGCSA, which are the SSTF and MGC based enhancement methods with brightness preservation

by successive approximation respectively, were compared with eight benchmarking algorithms, namely, RSWHE [17], WTHE [10], AGCWD [33], STBP [18], RICE [9], SECE [3], RSECE [24] and SMIRANK [8]. Default parameter settings for all benchmarking algorithms were used. The equivalent α and γ values of 6 and 2.2 were set as the default values for the proposed STSA and MGCSA methods respectively, for all the quantitative and visual assessment results. To preserve mean brightness, $S1$ is set at A as the default for all the quantitative and visual assessment results of the proposed method, except for Table 3.4 where $S1$ is set at B to preserve median brightness.

3.3.1 Quantitative Results

Table 3.1 gives the average processing time in seconds for enhancing an image in one of the three datasets using the proposed STSA method with the original number of four optimum control parameters, the STSA method with the reduced number of two optimum control parameters and the MGCSA method. The objective function in (3.3) was solved by the numeric solver function, "vpasolve", in MATLAB using an 8th generation Intel® Core™ i7 Q840 processor at 1.87GHz. The MATLAB code for RSWHE, WTHE, AGCWD and STBP was implemented by the author of this thesis and the MATLAB code for RICE, SECE, RSECE and SMIRANK was provided by the respective authors of those algorithms. It shows that the newly derived equations to reduce the number of optimum control parameters greatly improved computational efficiency using the SSTF. However, the MGC is significantly more computationally efficient than the SSTF and as shown in Table 3.2 is comparable

and in some cases more efficient than the other benchmarking algorithms.

Table 3.1 : The average processing time in seconds for an image in each of the three datasets for the proposed STSA method with four control parameters, the proposed STSA method with two control parameters and the proposed MGCSA method.

Dataset	STSA (4 Control Parameters)	STSA (2 Control Parameters)	MGCSA
RGBNIR	66.66	26.77	1.81
CSIQ	94.63	13.56	0.53
TID2013	91.72	12.58	0.40

Table 3.2 : The average processing time in seconds for an image in each of the three datasets for the proposed image enhancement with brightness preservation method and the other benchmarking algorithms.

Method	Average Processing Time (s)		
	RGBNIR	CSIQ	TID2013
RSWHE	0.78	0.34	0.31
WTHE	0.89	0.40	0.37
AGCWD	0.88	0.38	0.34
STBP	2.89	2.51	3.13
RICE	0.95	0.43	0.40
SECE	2.69	0.93	0.76
RSECE	1.69	0.61	0.57
SMIRANK	2.07	0.79	1.05
STSA	26.77	13.56	12.58
MGCSA	1.81	0.53	0.40

For brightness preservation assessment, the absolute mean brightness error (AMBE) [17, 33], the absolute median brightness error (ADBE) and the contrast and mean brightness measure (CMBM) [24] were used. AMBE measures the absolute difference in mean brightness between the input and output images, likewise ADBE

measures the absolute difference in median brightness between the input and output images and CMBM is a measure that combines mean brightness preservation with relative contrast enhancement. Table 3.3 gives the AMBE average, maximum and standard deviation values of the 807 test image by the respective algorithms. Table 3.3 shows that the proposed STSA and MGCSA methods both gave excellent mean brightness preservation with a standard deviation less than unity and an average AMBE value of 0, the smallest values amongst all of the tested methods. Furthermore, the proposed MGCSA method was also able to preserve brightness to within ± 2 for all of the 807 test images.

Table 3.3 : The AMBE average, maximum and standard deviation values for the proposed image enhancement with brightness preservation method and the other benchmarking algorithms.

Method	Average AMBE	Maximum	Standard Deviation
RSWHE	2	6	1.04
WTHE	1	7	1.89
AGCWD	35	56	10.39
STBP	2	28	2.97
RICE	3	6	1.70
SECE	6	25	8.27
RSECE	1	4	1.22
SMIRANK	8	26	10.19
STSA ($S1$ at A)	0	7	0.36
MGCSA ($S1$ at A)	0	2	0.28

Table 3.4 gives the ADBE average, maximum and standard deviation values of the 807 test image by the respective algorithms. The proposed STSA and MGCSA methods were set to preserve median brightness (i.e. $S1$ is at B) and Table 3.4 shows that both methods had an average ADBE value of 0, better than all of the other

benchmarking algorithms. Moreover, the proposed MGCSA method once more had a standard deviation less than unity and preserved brightness to within ± 2 for all of the 807 test images. The proposed MGCSA method gives better brightness preservation when compared to the proposed STSA method, due to it having slightly stronger enhancement when the intersection point is further away from the centre value, as shown in Fig. 3.3. A greater number of algorithms focus on preserving the mean brightness of an image, as the median is only a robust estimation of the image brightness. Therefore, even though the proposed method can preserve either the mean or median image brightness, only the mean is preserved for the rest of the experimental results (i.e. $S1$ is set at A).

Table 3.4 : The ADBE average, maximum and standard deviation values for the proposed image enhancement with brightness preservation method and the other benchmarking algorithms.

Method	Average ADBE	Maximum	Standard Deviation
RSWHE	3	16	1.42
WTHE	7	151	12.37
AGCWD	44	73	12.47
STBP	1	2	0.06
RICE	4	11	2.26
SECE	10	57	9.06
RSECE	3	16	1.42
SMIRANK	17	66	12.48
STSA ($S1$ at B)	0	30	1.47
MGCSA ($S1$ at B)	0	2	0.24

In Table 3.5, the p-values [8] for each of the benchmarking algorithms were found for all 807 test images to statistically determine which algorithm provided the best combination of enhancement and brightness preservation as measured by CMBM.

The p-values [8] based on CMBM in Table 3.5, represent the proportion of enhanced test images when $\{CMBM_A > CMBM_B\}$ where $CMBM_A$ and $CMBM_B$ are values produced by algorithms A and B, for a test image respectively. In Table 3.5, both of the proposed methods, STSA and MGCSA (i.e. Row M9 and row M10 respectively), gave a p-value greater than 0.52 when compared with the other benchmarking algorithms for all 807 test images. In other words, both of the proposed methods outperformed all the other benchmarking algorithms based on the CMBM image quality measure.

Table 3.5 : The p-values for $CMBM_A > CMBM_B$ where M1:RSWHE, M2:WTHE, M3:AGCWD, M4:STBP, M5:RICE, M6:SECE, M7:RSECE, M8:SMIRANK, M9:STSA and M10:MGCSA.

	M1	M2	M3	M4	M5	M6	M7	M8	M9	M10
M1	-	0.077	0.239	0.193	0.326	0.030	0.014	0.003	0.020	0.010
M2	0.921	-	0.530	0.685	0.812	0.693	0.410	0.093	0.198	0.118
M3	0.761	0.468	-	0.539	0.736	0.581	0.466	0.181	0.269	0.162
M4	0.804	0.314	0.461	-	0.737	0.473	0.264	0.093	0.060	0.021
M5	0.672	0.186	0.262	0.262	-	0.259	0.136	0.027	0.043	0.016
M6	0.970	0.306	0.419	0.527	0.740	-	0.126	0.019	0.064	0.035
M7	0.985	0.589	0.533	0.732	0.864	0.874	-	0.006	0.187	0.074
M8	0.998	0.907	0.819	0.905	0.973	0.981	0.994	-	0.473	0.310
M9	0.980	0.802	0.731	0.941	0.957	0.936	0.810	0.525	-	0.016
M10	0.990	0.882	0.838	0.979	0.984	0.965	0.926	0.690	0.984	-

To measure the quality of enhancement, both the quality-aware relative contrast measure (QRCM) [8] and the blind image quality measure of enhanced images (BIQME) [19] were used. QRCM is a reference based measure combining the relative contrast enhancement between the input and output image and penalises any distortions that result from enhancement and BIQME is a no-reference based measure

that combines contrast, sharpness, brightness, colourfulness and naturalness into one quality score using a regression module. In Table 3.6 based on QRCM, both the proposed methods, STSA and MGCSA (i.e. Row M9 and row M10 respectively), produced p-values higher than 0.66 for all of the 807 test images when compared with all the other benchmarking algorithms except SMIRANK, however, SMIRANK is unable to preserve the brightness of images with an average AMBE of 8 ± 26 as shown in Table 3.3. In Table 3.7 based on BIQME, both of the proposed methods (i.e. Row M9 and row M10), outperformed all of the other benchmarking algorithms with p-values higher than 0.54 for all of the 807 test images. In both Table 3.6 and 3.7, the proposed MGCSA method outperformed the proposed STSA method because the MGC produces slightly stronger enhancement when the intersection point is further away from the centre value, as shown in Fig. 3.3.

Table 3.6 : The p-values for $QRCM_A > QRCM_B$ where M1:RSWHE, M2:WTHE, M3:AGCWD, M4:STBP, M5:RICE, M6:SECE, M7:RSECE, M8:SMIRANK, M9:STSA and M10:MGCSA.

	M1	M2	M3	M4	M5	M6	M7	M8	M9	M10
M1	-	0.102	0.302	0.193	0.380	0.047	0.016	0.001	0.063	0.060
M2	0.898	-	0.606	0.788	0.855	0.695	0.496	0.029	0.312	0.201
M3	0.698	0.394	-	0.520	0.682	0.517	0.372	0.083	0.337	0.260
M4	0.807	0.211	0.480	-	0.756	0.468	0.195	0.031	0.105	0.047
M5	0.617	0.145	0.319	0.243	-	0.240	0.091	0.010	0.087	0.068
M6	0.953	0.302	0.482	0.532	0.760	-	0.183	0.019	0.197	0.160
M7	0.984	0.503	0.628	0.806	0.908	0.817	-	0.004	0.330	0.202
M8	0.999	0.970	0.916	0.969	0.990	0.981	0.996	-	0.782	0.663
M9	0.937	0.688	0.663	0.893	0.913	0.802	0.669	0.218	-	0.152
M10	0.941	0.799	0.739	0.953	0.932	0.840	0.798	0.335	0.843	-

Table 3.7 : The p-values for $BIQME_A > BIQME_B$ where M1:RSWHE, M2:WTHE, M3:AGCWD, M4:STBP, M5:RICE, M6:SECE, M7:RSECE, M8:SMIRANK, M9:STSA and M10:MGCSA.

	M1	M2	M3	M4	M5	M6	M7	M8	M9	M10
M1	-	0.055	0.602	0.348	0.336	0.311	0.278	0.120	0.174	0.130
M2	0.946	-	0.749	0.906	0.915	0.835	0.913	0.543	0.504	0.379
M3	0.397	0.250	-	0.376	0.361	0.377	0.348	0.268	0.275	0.259
M4	0.652	0.091	0.623	-	0.591	0.481	0.413	0.196	0.063	0.036
M5	0.663	0.083	0.639	0.406	-	0.447	0.374	0.192	0.161	0.126
M6	0.687	0.165	0.623	0.517	0.553	-	0.378	0.064	0.191	0.145
M7	0.721	0.087	0.652	0.585	0.626	0.615	-	0.099	0.177	0.114
M8	0.879	0.454	0.731	0.804	0.808	0.936	0.898	-	0.454	0.368
M9	0.825	0.492	0.724	0.936	0.836	0.809	0.822	0.542	-	0.115
M10	0.870	0.618	0.741	0.963	0.874	0.855	0.885	0.631	0.882	-

3.3.2 Visual Assessment

Fig. 3.5 shows the results when the brightness was increased by an offset of 60 so that both the conventional method and the proposed methods have the same increased mean brightness. The conventional method of adding a constant offset to the image caused intensity clipping in the bright cloud area resulting in a loss of details, this can also be seen by the large spike in the far right of the histogram shown in Fig. 3.5(b). Both of the proposed STSA and MGCSA methods, shown in Fig. 3.5(c) and Fig. 3.5(d) respectively, were able to better preserve the details in the cloud without any clipping, this can also be seen in the corresponding histograms where there are no large spikes. Moreover, the proposed MGCSA method was the only method which increased the brightness by the exact offset of 60, the conventional method increased the brightness by 57 and the proposed STSA method

increased the brightness by 52, as given by the mean values in the corresponding histograms in Fig. 3.5.

The results for enhancement on a video are shown in Fig. 3.6 for the methods which claim to be brightness preserving and their corresponding AMBE values are given in Table 3.8. The output images of the RSWHE method, shown in Fig. 3.6(b) are very similar to the inputs giving virtually no enhancement. The WTHE method over enhanced the last few images in the sequence, as shown in Fig. 3.6(c), resulting in an unnatural appearance and also failing to preserve brightness with the largest AMBE values given in Table 3.8. Similarly, the RICE method over enhanced the 4th image in the sequence, as shown in Fig. 3.6(e). The outputs of the STBP method, shown in Fig. 3.6(d), display an intensity range clipping problem as the sun in all the images appears greyer with reduced contrast. The RSECE method was unable to preserve the brightness of the images, as shown in Fig. 3.6(f), with a constant increase in the AMBE values of the last 3 images in the sequence, as given in Table 3.8. The proposed STSA and MGCSA methods, as shown in Fig. 3.6(g) and Fig. 3.6(h) respectively, produced adequately enhanced images without over-enhancement or intensity clipping and no flickering as the brightness was well preserved with a maximum AMBE value of 1, as given by Table 3.8.

The "Level 5" *foxy* image from the CSIQ dataset [1], shown in Fig. 3.7(b), was used for visual assessment. None of the benchmarking methods, shown in Fig. 3.7(c) - Fig. 3.7(j) were able to recover the vivid colour of the original foxy image. The proposed STSA and MGCSA methods, shown in Fig. 3.7(k) and Fig. 3.7(l) respectively, were able to enhance the contrast while recovering the original vivid

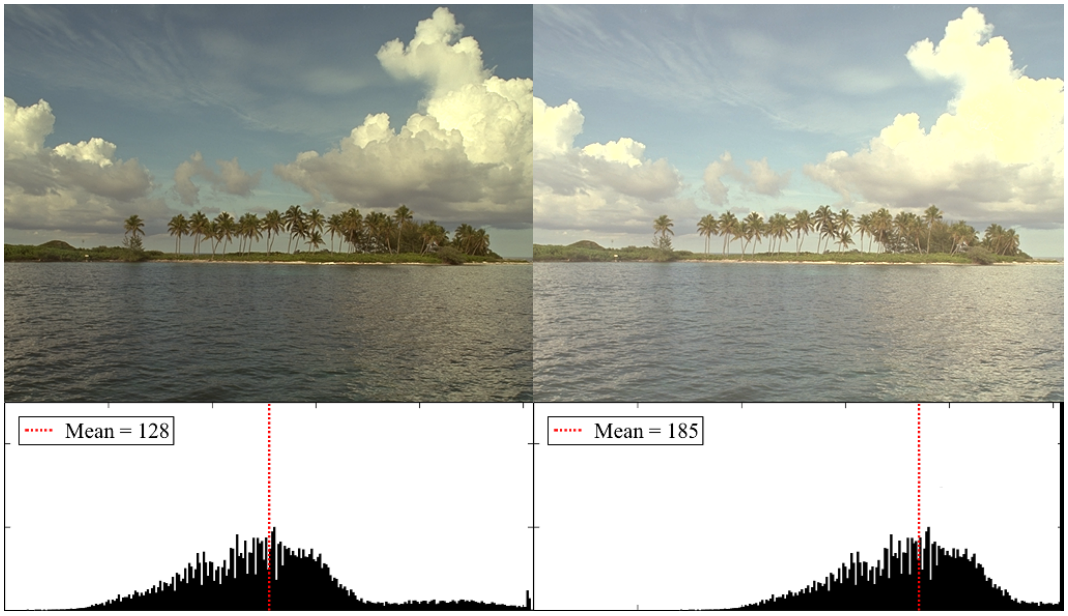

(a) Input **(b)** Standard Increase

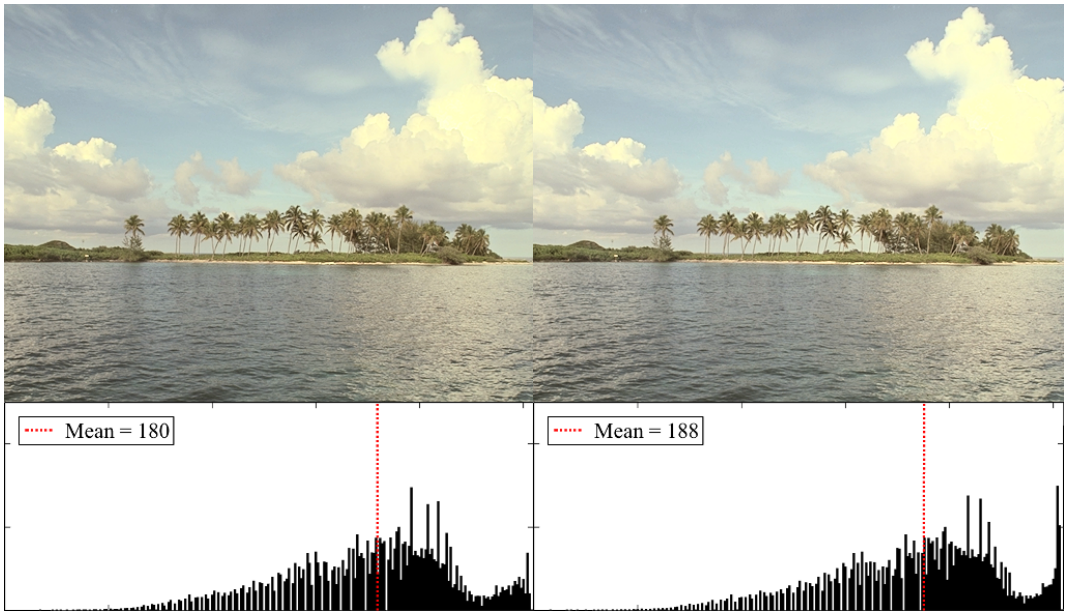

(c) STSA **(d)** MGCSA

Figure 3.5 : The results of increasing the brightness of (a) the original *cloud* image from the TID2013 dataset by (b) adding a constant of 60, (c) the proposed STSA method (S1 at A), $\alpha = 6$, $R = 60$ and (d) the proposed MGCSA method ($S1$ at A), $\gamma = 2.2$, $R = 60$.

(a) Input

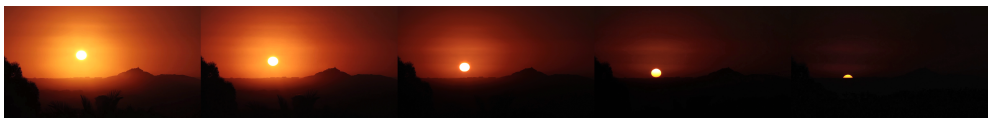

(b) RSWHE

(c) WTHE

(d) STBP

(e) RICE

(f) RSECE

(g) STSA

(h) MGCSA

Figure 3.6 : The enhancement results for the proposed image enhancement with brightness preservation method and the other benchmarking algorithms using the *sunset* image sequence. (a) The input image sequence. The enhanced output by (b) RSWHE (c) WTHE, (d) STBP, (e) RICE, (f) RSECE and the proposed (g) STSA and (h) MGCSA.

Table 3.8 : The AMBE values for each image in the *sunset* sequence as shown in Fig. 3.6.

Method	Sunset Sequence Image				
	Frame 1	Frame 2	Frame 3	Frame 4	Frame 5
RSWHE	4	4	4	3	3
WTHE	3	8	18	25	29
STBP	5	6	7	4	1
RICE	3	0	0	2	2
RSECE	0	0	3	6	7
STSA	1	1	0	0	0
MGCSA	0	0	1	0	0

colour of the fox and preserving image brightness.

The *plane* image from the TID2013 dataset [42], shown in Fig. 3.8(b), was also used for visual assessment. The RSWHE, AGCWD, STBP and RICE outputs, shown in Fig. 3.8(c), and Fig. 3.8(e) - Fig. 3.8(g) respectively, were all under enhanced, with little difference from the input image. The WTHE output, shown in Fig. 3.8(d), was over enhanced as seen in the unnatural appearance of the sky behind the plane. The WTHE output also showed signs of clipping, with a loss of details in the plane itself. The SECE, RSECE and SMIRANK outputs, shown in Fig. 3.8(h) - Fig. 3.8(j) respectively, were unable to recover the vivid colour of the original. The outputs of the proposed STSA and MGCSA methods, shown in Fig. 3.8(k) and Fig. 3.8(l) respectively, displayed an adequate degree of contrast enhancement without signs of over-enhancement or clipping. It should also be noted that in all of the visual assessment results, the amount of enhancement between the proposed STSA and MGCSA methods were very similar. This supports the fact that

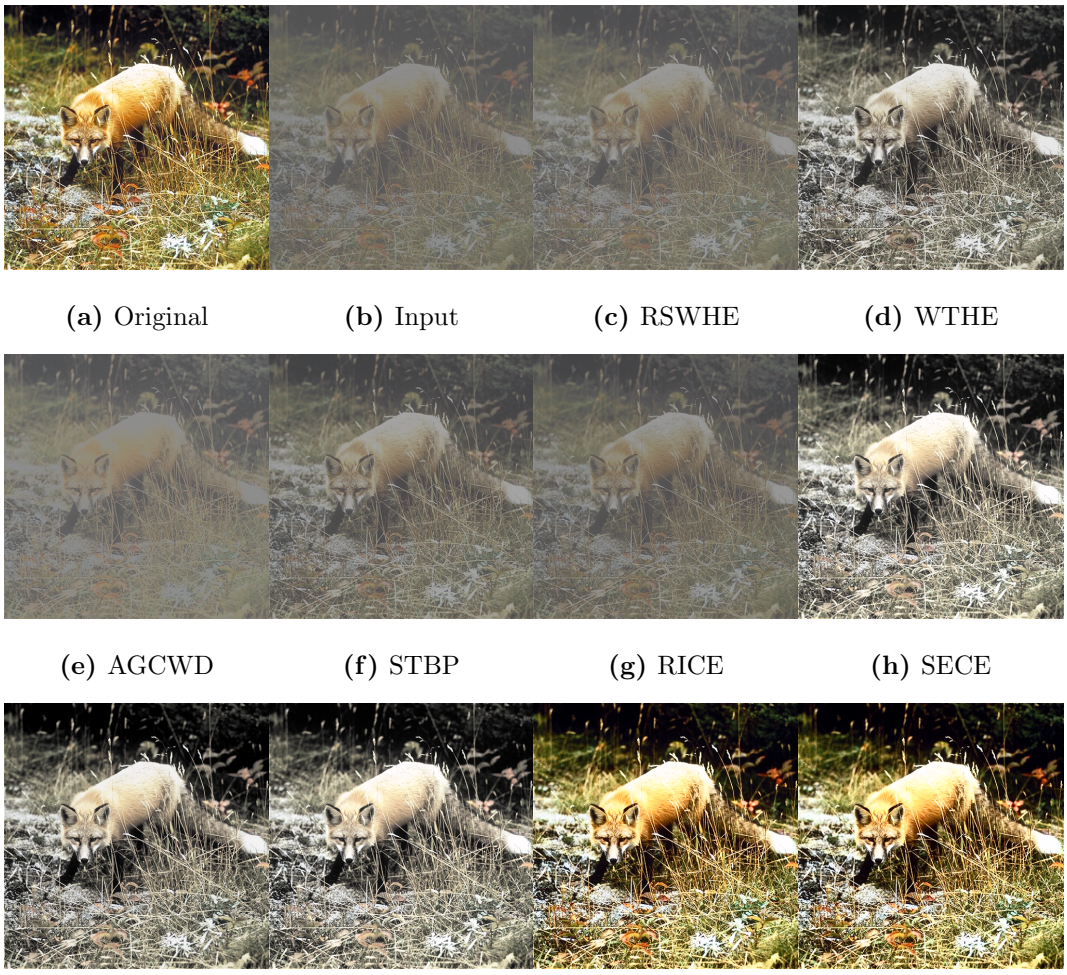

(a) Original **(b)** Input **(c)** RSWHE **(d)** WTHE

(e) AGCWD **(f)** STBP **(g)** RICE **(h)** SECE

(i) RSECE **(j)** SMIRANK **(k)** STSA **(l)** MGCSA

Figure 3.7 : The enhancement results for the proposed image enhancement with brightness preservation method and the other benchmarking algorithms using the *foxy* image from the CSIQ dataset. (a) The original image. (b) The contrast reduced input. The enhanced output by (c) RSWHE, (d) WTHE, (e) AGCWD, (f) STBP, (g) RICE, (h) SECE, (i) RSECE, (j) SMIRANK and the proposed (k) STSA ($S1$ at A, $\alpha = 6$) and (l) MGCSA ($S1$ at A, $\gamma = 2.2$).

the MGC is a good approximation of the SSTF whilst providing better brightness preservation and greater computational efficiency.

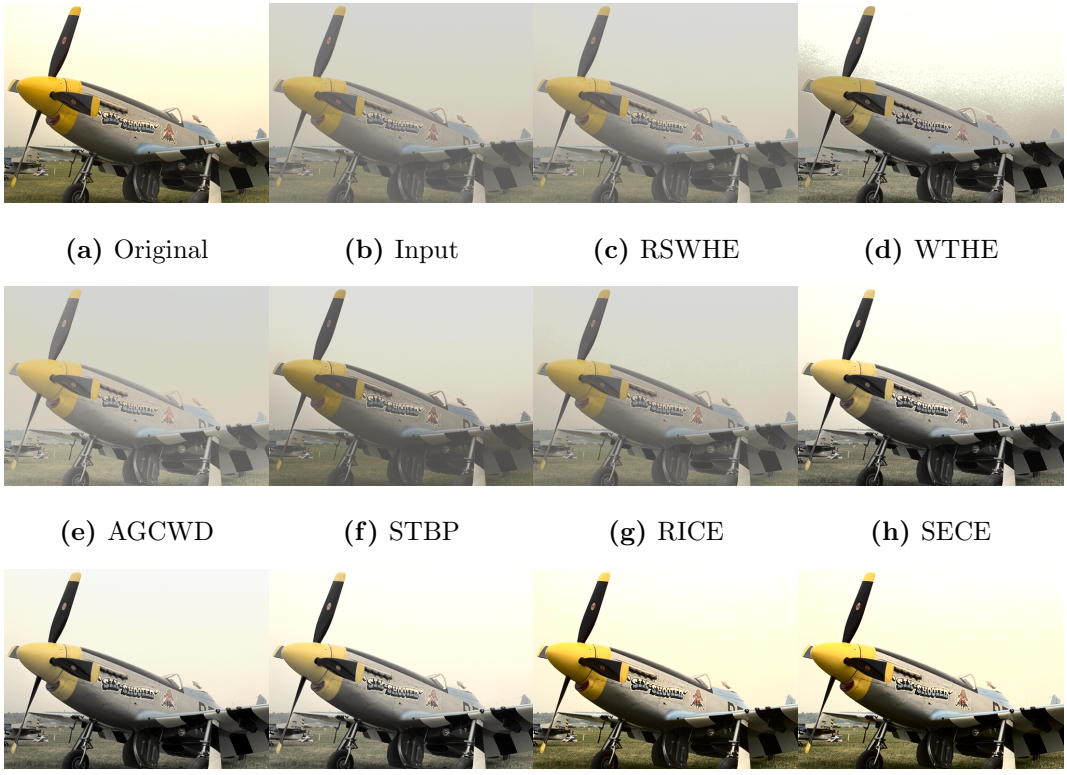

(a) Original **(b)** Input **(c)** RSWHE **(d)** WTHE

(e) AGCWD **(f)** STBP **(g)** RICE **(h)** SECE

(i) RSECE **(j)** SMIRANK **(k)** STSA **(l)** MGCSA

Figure 3.8 : The enhancement results for the proposed image enhancement with brightness preservation method and the other benchmarking algorithms using the *plane* image from the TID2013 dataset. (a) The original image. (b) The contrast reduced input image. The enhanced output by (c) RSWHE, (d) WTHE, (e) AGCWD, (f) STBP, (g) RICE, (h) SECE, (i) RSECE, (j) SMIRANK and the proposed (k) STSA ($S1$ at A, $\alpha = 6$) and (l) MGCSA ($S1$ at A, $\gamma = 2.2$).

3.4 Conclusion

By applying successive approximation to both the SSTF and the MGC in the proposed method, the brightness of an image can be preserved whilst providing various degrees of contrast enhancement with no over-enhancement or intensity clipping. The two newly derived equations to reduce the number of optimum control parameters from four to two for solving the SSTF significantly increased the speed of the method. However, the computational efficiency of the MGC makes the speed of the proposed method comparable and in some cases faster than the other benchmarking algorithms. The MGC also provides the best and most consistent brightness preservation among all of the methods tested and gave the strongest quantitative results for image enhancement. Furthermore, the proposed method allows a user to change the brightness of an image without clipping at either ends of the intensity range. This makes the proposed method perfect for video enhancement as it can enhance a video while preserving or changing its brightness without causing any intensity clipping or flickering.

Chapter 4

Optimised Image Enhancement

4.1 Introduction

In order to assess the quality of enhanced images, a number of image quality measures (IQMs) have been developed [19, 20, 8, 3, 21, 22, 23, 24, 25, 26, 27]. The purpose of these IQMs is to provide a value that not only correlates to the strength of enhancement, but also its visual quality. It is therefore desirable to optimise the visual quality of image enhancement by maximising the value produced by a chosen IQM.

One method that optimises enhancement based on an IQM is robust image contrast enhancement (RICE) [9]. In this method, an objective function is defined that combines three histograms, namely, the input histogram, the HE output histogram and the SSTF output histogram. The function is then minimised based on an IQM that measures saliency preservation. By combining the three histograms, the RICE method aims to produce enhancement while retaining a histogram close to that of the input, but this requirement constrains enhancement for input images with poor contrast, resulting in under-enhancement.

The BIQME-optimised image enhancement method (BOIEM) [19] builds on RICE by cascading it with the adaptive gamma correction with weighting distribution (AGCWD) method [33], so that stronger enhancement can be produced for

input images with poor contrast. This method optimises enhancement by maximising the BIQME value with parameters chosen from a fixed set of values. However, the choice of parameter values is limited and may not be adequate to optimise enhancement for a wide variety of images.

There is another enhancement optimising method similar to BOIEM, which maximises the reduced-reference image quality metric for contrast change (RIQMC) [20] and is known as RIQMC based optimal histogram mapping (ROHIM) [20]. ROHIM applies a mean shift to the image and then obtains the four optimum control parameters for enhancement by the SSTF that will maximise the RIQME value. To make the optimisation process practical, only two parameters are optimised, the one that controls the degree of enhancement of the SSTF and the one that controls the mean shift. However, as the mean shift is cascaded with the SSTF, it can result in clipping of the intensity values before the SSTF is applied, leading to over-enhancement and a loss of details in the output images.

None of these enhancement methods truly produce the most optimally enhanced image according to their chosen IQM because either the optimisation process, or the enhancement method is limited in the described ways. Therefore, to overcome the limitations of other methods, we propose to optimise image enhancement by using the successive approximation approach to maximising any chosen IQM.

If brightness preservation is not a requirement for enhancement, then instead of locating the intersection point of the MGC at a position that will preserve brightness, an optimum intersection point can be found that will maximise any IQM so that enhancement is optimised according to that IQM. To enhance the contrast of an

image, intensities above and below an intersection point, at which the input and output intensities are equal, must be stretched monotonically. As a result, regions of the image with intensities above the intersection point will be brighter and the other regions will be darker. Analogously, if an IQM increases with image gradient, then increasing the strength of edges in an image will increase the image gradient and hence, the value of the IQM. As a result, the location of the optimum intersection point will be the intensity value which intersects with the maximum number of edges. In this way, the maximum number of edges will be stretched and therefore enhanced, producing a maximum value for that particular IQM. In this chapter, we apply a binary search algorithm in conjunction with the MGC proposed in the Chapter 3, to locate an optimum intersection point such that the output of an IQM is maximised.

4.2 Method

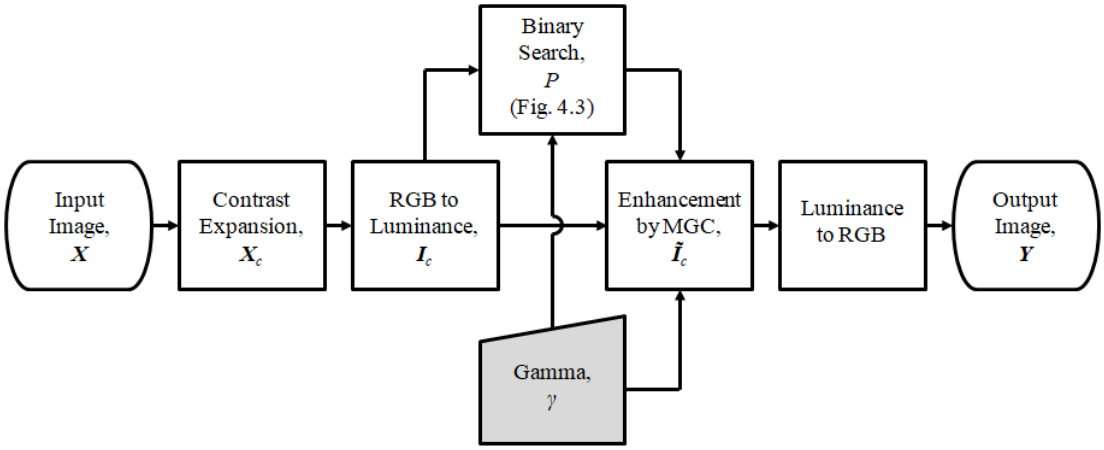

Figure 4.1 : Flowchart for the overall image enhancement method featuring the proposed optimisation technique.

The contrast expansion method [38, 36, 37] described in Chapter 2 is again applied initially to the image in the RGB colour space to improve the dynamic range of colours and achieve more vivid colour enhancement.

4.2.1 The Optimum Intersection Point

EMEG [3], QRCM [8], BIQME [19] and RIQMC [20], were chosen to showcase our method because they are some of the more recently developed IQMs for the evaluation of image enhancement and are known to correlate well with visual assessment. In particular, results will show that the proposed method can produce higher BIQME and RIQMC values than the other benchmarking algroithms, namely, BOIEM and ROHIM, which optimise these two IQMs respectively.

Fig. 4.2(a) - 4.2(d) give the 3D plots of 55 reference images from the CSIQ [1] and TID2013 [42] datasets for the EMEG, QRCM, BQIME and RIQMC values versus every location of the intersection point respectively. Each bell-shaped curve represents a single image and this shows that every image of the datasets has a unique global maximum value for each IQM. Therefore, by using the IQM value as the feedback in a binary search, an intersection point can be found which will maximise the IQM value for the output image, thus optimising the output according to that particular IQM.

4.2.2 The Optimisation Algorithm

The optimal intersection point, P_{opt}, is located by a binary search algorithm and its flow chart is shown in Fig. 4.3. Consider an N-bit luminance component where the minimum and maximum intensity values are 0 and $2^N - 1$ respectively. The

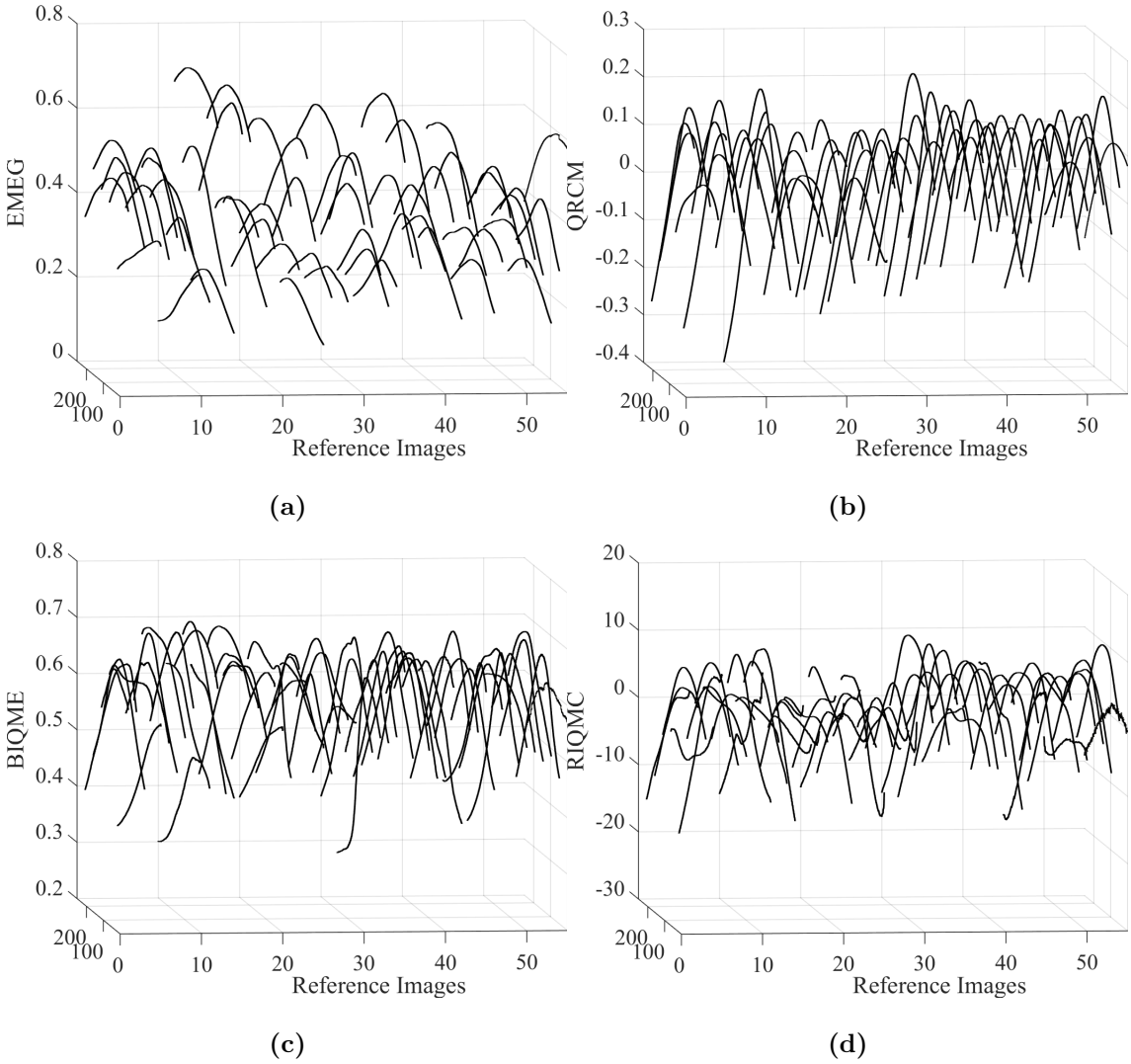

Figure 4.2 : The IQM value Vs the intersection point, P, location for (a) EMEG, (b) QRCM, (c) BIQME and (d) RIQMC.

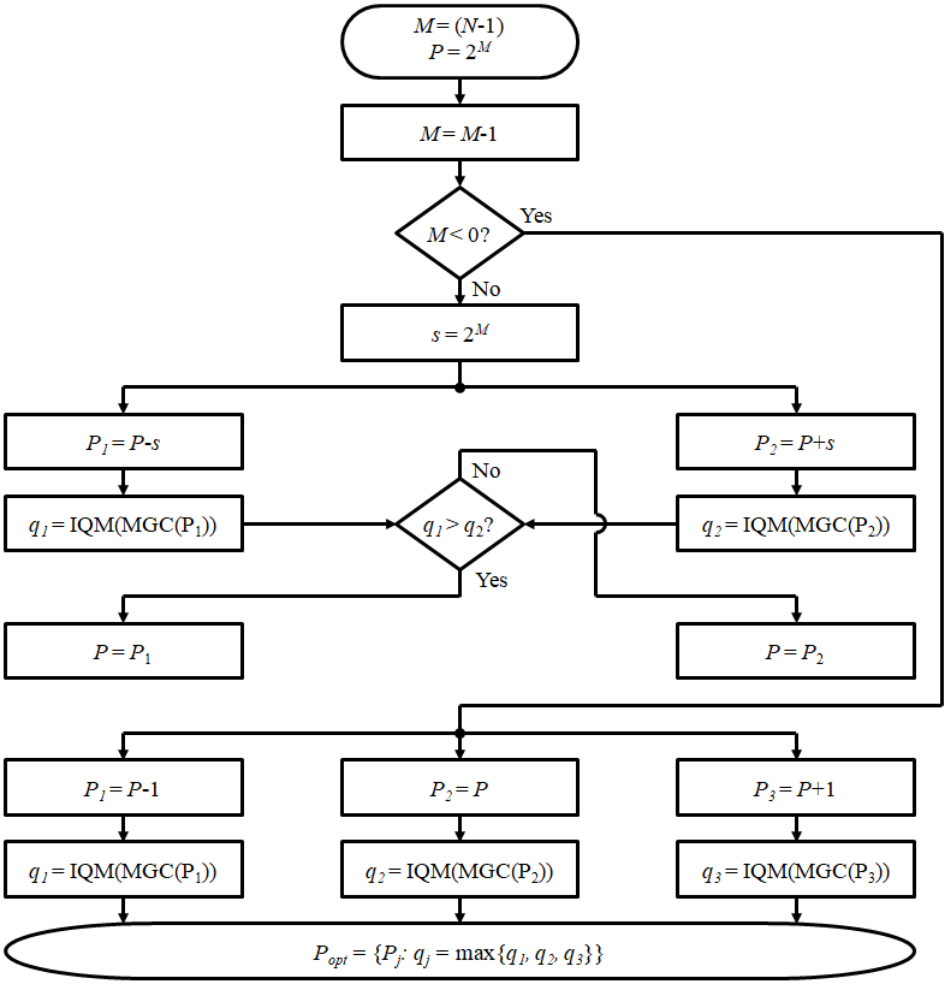

Figure 4.3 : Flowchart for the proposed binary search algorithm to find the optimum intersection point for image enhancement.

intersection point, P, is initialised at the mid intensity value of 2^{N-1}. A step size, s, which is equal to 2^{N-2} is evaluated. Two IQM values, namely, q_1 and q_2 of the enhanced images at two intermediate intersection points of $(P - s)$ and $(P + s)$, are then determined respectively. If q_1 is greater than q_2, P will be replaced by $(P - s)$, otherwise P will be replaced by $(P + s)$. The step size, s, is then halved and the process is repeated until it is reduced to unity. Finally, P_{opt}, is set to one of the three intersection points, namely, $(P - 1)$, P or $(P + 1)$, whichever produces an enhanced image with the largest IQM value. The number of searches is equal to $(N - 1)$. As each search requires two IQM calculations, plus the final step of three IQM calculations, minus one result already calculated from the previous step, the total number of IQM values that need to be re-calculated is equal to $(2(N - 1) + 3 - 1) = 2N$. The overall complexity depends on the IQM, but it is generally computationally efficient due to the small number of searches.

It should be noted, that in the case of a smaller IQM value being better, then instead of searching for the largest IQM value we can search for the smallest IQM value by checking whether or not q_1 is *smaller* than q_2.

4.3 Results

A total of 807 test images from the NIRRGB [2], CSIQ [1] and TID2013 [42] datasets were used for quantitative evaluations and some were selected for visual assessment. The outputs of the proposed method, namely MGC-EMEG, MGC-QRCM, MGC-BIQME and MGC-RIQMC, which were optimised by EMEG [3], QRCM [8], BIQME [19] and RIQMC [20] respectively, were compared with six

benchmarking algorithms, namely, SECE [3], RSECE [24], SMIRANK [8], RICE [9], ROHIM [20] and BOIEM [19]. Default parameter settings for all benchmarking algorithms were used and a γ value of 2.2 was set as the default value for all the quantitative and visual assessment results of the proposed method.

4.3.1 Quantitative Results

Four IQMs, namely, the expected measure of enhancement by gradient (EMEG) [3], the quality-aware relative contrast measure (QRCM) [8], the blind image quality measure of enhanced images (BIQME) [19] and the reduced-reference image quality metric for contrast change (RIQMC) [20] were used for the quantitative comparison. EMEG is based on the gradient to assess the strength of enhancement in the output image, QRCM is a combination of the relative contrast enhancement between the input and output image, and any distortions that result from enhancement, BIQME combines contrast, sharpness, brightness, colourfulness and naturalness into one quality score using a regression module and RIQMC combines phase congruency and statistics information of the image histogram into a single metric to measure image quality.

In Table 4.1-4.4, the p-values [8] for each of the benchmarking algorithms, namely, SECE (i.e. M1), RSECE (i.e. M2), SMIRANK (i.e. M3), RICE (i.e. M4), BOIEM (i.e. M5) and ROHIM (i.e. M6) and the proposed methods MGC-EMEG (i.e. M7), MGC-QRCM (i.e. M8), MGC-BIQME (i.e. M9) and MGC-RIQMC (i.e. M10) were found for all 807 test images to statistically determine which algorithm provided the best enhancement. Table 4.1-4.4 give the p-values [8] derived from

the results of different IQMs. In Table 4.1, the p-values [8] are based on EMEG and represent the proportion of enhanced test images when $\{EMEG_A > EMEG_B\}$ where $EMEG_A$ and $EMEG_B$ are values produced by algorithms A and B, for a test image respectively. Table 4.2, 4.3 and 4.4 contains the p-values which are based on QRCM, BIQME and RIQMC respectively.

In Table 4.1, when the proposed method, MGC-EMEG (i.e. Row M7), was optimised by EMEG, p-values higher than 0.62 were obtained for all of the 807 test images when compared with the other benchmarking algorithms. In particular, the proposed method outperformed the RICE and BOIEM methods with a perfect score of unity for the p-values. Moreover, when the proposed method was optimised by other IQMs, namely, QRCM, BIQME and RIQMC, p-values higher than 0.50 were obtained for all of the 807 test images when compared with the other benchmarking algorithms.

Table 4.1 : The p-values for $EMEG_A > EMEG_B$ where M1:SECE, M2:RSECE, M3:SMIRANK, M4:RICE, M5:BOIEM, M6:ROHIM, M7:MGC-EMEG, M8:MGC-QRCM, M9:MGC-BIQME and M10:MGC-RIQMC.

	M1	M2	M3	M4	M5	M6	M7	M8	M9	M10
M1	-	0.113	0.035	0.608	0.455	0.181	0.001	0.012	0.012	0.016
M2	0.887	-	0.009	0.776	0.680	0.242	0.004	0.011	0.025	0.048
M3	0.964	0.991	-	0.898	0.838	0.340	0.124	0.195	0.201	0.248
M4	0.390	0.223	0.102	-	0.029	0.143	0.000	0.010	0.026	0.032
M5	0.545	0.318	0.161	0.971	-	0.165	0.000	0.014	0.030	0.038
M6	0.819	0.758	0.658	0.857	0.835	-	0.379	0.445	0.463	0.491
M7	0.999	0.996	0.875	1.000	1.000	0.621	-	0.968	0.965	0.990
M8	0.988	0.989	0.805	0.990	0.986	0.555	0.016	-	0.563	0.822
M9	0.988	0.974	0.798	0.974	0.969	0.535	0.011	0.418	-	0.673
M10	0.984	0.952	0.751	0.968	0.962	0.508	0.006	0.155	0.307	-

When the proposed method, MGC-QRCM (i.e. Row M8), was optimised by QRCM as shown in Table 4.2, it produced p-values higher than 0.62 for all of the 807 test images when compared with the other benchmarking algorithms. In other words, it outperformed all the other benchmarking algorithms.

Table 4.2 : The p-values for $QRCM_A > QRCM_B$ where M1:SECE, M2:RSECE, M3:SMIRANK, M4:RICE, M5:BOIEM, M6:ROHIM, M7:MGC-EMEG, M8:MGC-QRCM, M9:MGC-BIQME and M10:MGC-RIQMC.

	M1	M2	M3	M4	M5	M6	M7	M8	M9	M10
M1	-	0.183	0.019	0.760	0.642	0.373	0.152	0.033	0.136	0.100
M2	0.817	-	0.004	0.908	0.822	0.485	0.258	0.050	0.204	0.141
M3	0.981	0.996	-	0.990	0.967	0.813	0.663	0.372	0.605	0.579
M4	0.240	0.090	0.010	-	0.051	0.229	0.084	0.012	0.064	0.063
M5	0.357	0.177	0.033	0.949	-	0.285	0.110	0.025	0.087	0.078
M6	0.626	0.515	0.186	0.771	0.715	-	0.346	0.162	0.279	0.266
M7	0.848	0.742	0.336	0.916	0.890	0.654	-	0.009	0.384	0.366
M8	0.967	0.950	0.627	0.988	0.975	0.836	0.971	-	0.963	0.967
M9	0.864	0.796	0.395	0.936	0.913	0.719	0.601	0.007	-	0.475
M10	0.900	0.859	0.420	0.937	0.922	0.732	0.631	0.005	0.503	-

In Table 4.3, the proposed method, MGC-BIQME (i.e. Row M9), which was optimised by BIQME, produced p-values higher than 0.72 for all of the 807 test images when compared with the other benchmarking algorithms. This shows the proposed MGC-BIQME method outperformed all the other benchmarking algorithms. Furthermore, when the proposed method was compared with BOIEM (i.e. Column M5), a method that is also optimised by BIQME, a p-value of 0.957 was produced, showing that the proposed method was better at optimising enhancement by maximising the BIQME value than the BOIEM method.

Table 4.3 : The p-values for $BIQME_A > BIQME_B$ where M1:SECE, M2:RSECE, M3:SMIRANK, M4:RICE, M5:BOIEM, M6:ROHIM, M7:MGC-EMEG, M8:MGC-QRCM, M9:MGC-BIQME and M10:MGC-RIQMC.

	M1	M2	M3	M4	M5	M6	M7	M8	M9	M10
M1	-	0.378	0.064	0.553	0.477	0.209	0.208	0.095	0.038	0.154
M2	0.615	-	0.099	0.626	0.535	0.218	0.222	0.112	0.036	0.176
M3	0.936	0.898	-	0.808	0.753	0.369	0.409	0.259	0.104	0.335
M4	0.447	0.374	0.192	-	0.203	0.202	0.230	0.093	0.030	0.157
M5	0.523	0.463	0.244	0.794	-	0.243	0.261	0.124	0.043	0.190
M6	0.791	0.781	0.631	0.792	0.755	-	0.519	0.437	0.275	0.514
M7	0.791	0.778	0.591	0.768	0.739	0.481	-	0.400	0.014	0.502
M8	0.905	0.887	0.741	0.906	0.875	0.563	0.586	-	0.022	0.600
M9	0.962	0.963	0.895	0.970	0.957	0.725	0.973	0.957	-	0.958
M10	0.846	0.824	0.665	0.843	0.810	0.483	0.491	0.378	0.015	-

When the proposed method, MGC-RIQMC (i.e. Row M10), was optimised by RIQMC as shown in Table 4.4, it produced p-values higher than 0.57 for all of the 807 test images when compared with the other benchmarking algorithms. Moreover, when the proposed method is compared with ROHIM (i.e. Column M6) optimised by RIQMC, a p-value of 0.686 was produced. This indicates that the proposed method was better at optimising enhancement by maximising the RIQMC value than ROHIM.

Among the four IQMs, namely, EMEG, QRCM, BIQME and RIQMC, used in the proposed method, the quantitative results produced by the proposed method optimised by one IQM still performed very well when measured by the other three IQMs as shown by the p-values in Tables 4.1-4.4.

Table 4.5 gives the average processing time per test image in seconds for the

Table 4.4 : The p-values for $RIQMC_A > RIQMC_B$ where M1:SECE, M2:RSECE, M3:SMIRANK, M4:RICE, M5:BOIEM, M6:ROHIM, M7:MGC-EMEG, M8:MGC-QRCM, M9:MGC-BIQME and M10:MGC-RIQMC.

	M1	M2	M3	M4	M5	M6	M7	M8	M9	M10
M1	-	0.307	0.012	0.778	0.642	0.413	0.302	0.149	0.204	0.107
M2	0.693	-	0.021	0.865	0.804	0.440	0.352	0.162	0.234	0.107
M3	0.988	0.979	-	0.988	0.965	0.649	0.772	0.564	0.631	0.425
M4	0.222	0.135	0.012	-	0.197	0.258	0.197	0.092	0.113	0.041
M5	0.358	0.196	0.035	0.803	-	0.287	0.224	0.092	0.130	0.056
M6	0.587	0.560	0.351	0.742	0.713	-	0.519	0.374	0.431	0.314
M7	0.698	0.648	0.228	0.803	0.776	0.481	-	0.160	0.295	0.005
M8	0.851	0.838	0.436	0.908	0.908	0.626	0.830	-	0.592	0.033
M9	0.796	0.766	0.369	0.887	0.870	0.569	0.691	0.393	-	0.022
M10	0.893	0.893	0.575	0.959	0.944	0.686	0.993	0.944	0.959	-

benchmarking algorithms and the proposed method when optimised by the four different IQM's, namely, EMEG, QRCM, BIQME and RIQMC. All experiments were performed in MATLAB using an 8th generation Intel® Core™ i7 Q840 processor at 1.87GHz. The MATLAB code for the benchmarking algorithms in this chapter were provided by their respective authors. It shows that the processing time of the proposed methods depends on the complexity of an IQM and when optimisation is based on EMEG and QRCM, it performs better then the benchmarking BOIEM and ROHIM optimisation methods.

4.3.2 Visual Assessment

For visual assessment, to compare our proposed method with the six other benchmarking algorithms, a vast range of different types of images, namely, Fig. 4.4(b) the *family* image, Fig. 4.5(b) the *girl in red* image, Fig. 4.6(b) the *painted face*

Table 4.5 : The average processing time in seconds for an image in each of the three datasets for the proposed optimised enhancement method and the other benchmarking algorithms.

Method	Average Processing Time (s)		
	RGBNIR	CSIQ	TID2013
SECE	2.69	0.93	0.76
RSECE	1.69	0.61	0.57
SMIRANK	2.07	0.79	1.05
RICE	0.95	0.43	0.40
BOIEM	4.23	2.77	2.88
ROHIM	24.36	9.37	7.09
MGC-EMEG	3.23	1.47	1.36
MGC-QRCM	3.74	1.50	1.27
MGC-BIQME	29.44	17.27	17.03
MGC-RIQMC	36.49	22.00	16.80

image and Fig. 4.7(a) the *pyramid* image from the three datasets, were used.

The contrast reduced *family* image, from the CSIQ [1] dataset, was selected as the sunset with the large dark foreground of the tree is challenging for many enhancement algorithms. The images produced by RICE and BOIEM, shown in Fig. 4.4(f) and Fig. 4.4(g) respectively, exhibited similar problems with poor contrast. The image produced by ROHIM, shown in Fig. 4.4(h), had increased brightness, but contrast remained poor. The SECE, RSECE and SMIRANK output images, shown in Fig. 4.4(c) - Fig. 4.4(e) respectively, had colour that remained dull and lifeless. The proposed method optimised by EMEG, QRCM, BIQME and RIQMC, each produced similarly visually pleasing outputs, shown in Fig. 4.4(i) - Fig. 4.4(l) respectively, with vivid colour and appropriate enhancement over the entire image and image quality better than the original, as shown in Fig. 4.4(a).

(a) Original **(b)** Input **(c)** SECE **(d)** RSECE

(e) SMIRANK **(f)** RICE **(g)** BOIEM **(h)** ROHIM

(i) MGC-EMEG **(j)** MGC-QRCM **(k)** MGC-BIQME **(l)** MGC-RIQMC

Figure 4.4 : The enhancement results for the proposed optimised enhancement method and the other benchmarking algorithms using the *family* image from the CSIQ dataset. (a) The original image. (b) The contrast reduced input image. The enhanced output by (c) SECE, (d) RSECE, (e) SMIRANK, (f) RICE, (g) BOIEM, (h) ROHIM and the proposed (i) MGC-EMEG, (j) MGC-QRCM, (k) MGC-BIQME and (l) MGC-RIQMC.

The contrast reduced *girl in red* and *painted face* images, from the TID2013 [42] dataset, were chosen as it is difficult for enhancement algorithms to produce natural enhancement in the human face. Like in the previous example, the images produced by RICE and BOIEM, shown in Fig. 4.5(f) - Fig. 4.5(g) and Fig. 4.6(f) - Fig. 4.6(g) respectively, exhibited under-enhancement with overall poor contrast. The images produced by ROHIM, shown in Fig. 4.5(h) and Fig. 4.6(h), had over-saturated colour, resulting in outputs with unnatural appearance. The SECE, RSECE and SMIRANK output images, shown in Fig. 4.5(c) - Fig. 4.5(e) respectively, were over-enhanced with the girl's eyes being too dark in the *girl in red* image. For the *painted face* outputs of these methods, shown in Fig 4.6(c) - Fig. 4.6(e) respectively, the colour appears washed out and dull. The outputs produced by the proposed method optimised by EMEG, QRCM, BIQME and RIQMC, shown in Fig. 4.5(i) - Fig. 4.5(l) and Fig. 4.6(i) - Fig. 4.6(l) respectively, all displayed adequate and naturally appearing enhancement.

The *pyramid* image, from the RGBNIR [2] dataset, was used to see how the enhancement algorithms performed on natural scenery. The images produced by RICE and BOIEM, in Fig. 4.7(e) - Fig. 4.7(f) respectively, failed to provide adequate enhancement. SECE and SMIRANK produced outputs, shown in Fig. 4.7(b) and Fig. 4.7(d) respectively, that were over-enhanced, which can be seen by the extremes of dark and light in the sky. RSECE, shown in Fig. 4.7(c), also produced an output that was over-enhanced, but this is more noticeable in the sand and the pyramid itself where there are a loss of details. The ROHIM output image, shown in Fig. 4.7(g), was over-saturated, resulting in unnatural colour. The proposed method

(a) Original **(b)** Input **(c)** SECE **(d)** RSECE

(e) SMIRANK **(f)** RICE **(g)** BOIEM **(h)** ROHIM

(i) MGC-EMEG **(j)** MGC-QRCM **(k)** MGC-BIQME **(l)** MGC-RIQMC

Figure 4.5 : The enhancement results for the proposed optimised enhancement method and the other benchmarking algorithms using the *girl in red* image from the TID2013 dataset. (a) The original image. (b) The contrast reduced input image. The enhanced output by (c) SECE, (d) RSECE, (e) SMIRANK, (f) RICE, (g) BOIEM, (h) ROHIM and the proposed (i) MGC-EMEG, (j) MGC-QRCM, (k) MGC-BIQME and (l) MGC-RIQMC.

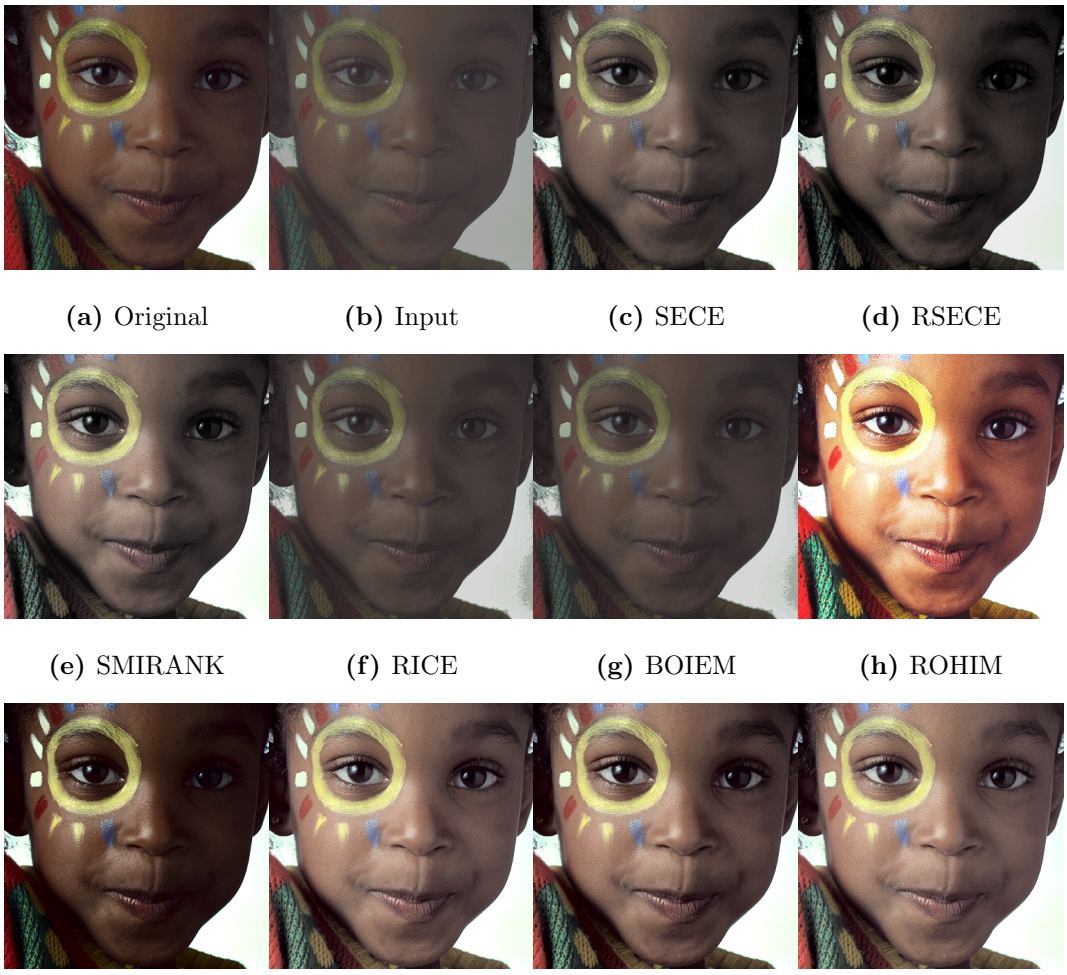

(a) Original **(b)** Input **(c)** SECE **(d)** RSECE

(e) SMIRANK **(f)** RICE **(g)** BOIEM **(h)** ROHIM

(i) MGC-EMEG **(j)** MGC-QRCM **(k)** MGC-BIQME **(l)** MGC-RIQMC

Figure 4.6 : The enhancement results for the proposed optimised enhancement method and the other benchmarking algorithms using the *painted face* image from the TID2013 dataset. (a) The original image. (b) The contrast reduced input image. The enhanced output by (c) SECE, (d) RSECE, (e) SMIRANK, (f) RICE, (g) BOIEM, (h) ROHIM and the proposed (i) MGC-EMEG, (j) MGC-QRCM, (k) MGC-BIQME and (l) MGC-RIQMC.

optimised by EMEG, QRCM, BIQME, and RIQMC, produced visually pleasing images with vivid colour that reveals more details in the pyramid itself, shown in Fig. 4.7(h) - Fig. 4.7(k) respectively.

4.4 Conclusion

By applying a binary search in conjunction with the proposed MGC to find the optimum intersection point in order to maximise an IQM, an image with superior enhancement to other benchmarking algorithms can be obtained. Moreover, by adjusting the γ value in conjunction with the optimisation based on an IQM, a wide range of the degree of enhancement can be set by a user in order to achieve a desirable outcome.

As the proposed method is optimised by maximising an IQM, its output reflects what attributes of image quality were targeted by that particular IQM. Hence, the proposed method can also be used to assess how well an IQM correlates with visual perception.

From the experimental results, it has been confirmed that EMEG, QRCM, BIQME and RIQMC all correlated well with visual perception and outperformed all the other benchmarking algorithms quantitatively. Furthermore, the proposed method, when optimising BIQME and RIQMC, outperformed the BOIEM and ROHIM which also optimise enhancement based on BIQME and RIQMC respectively. In other words, the proposed optimisation method was better at maximising those IQMs then the other benchmarking optimisation methods. Moreover, when a new IQM which gives more accurate assessment on image quality is developed, our pro-

(a) Input **(b)** SECE **(c)** RSECE

(d) SMIRANK **(e)** RICE **(f)** BOIEM **(g)** ROHIM

(h) MGC-EMEG **(i)** MGC-QRCM **(j)** MGC-BIQME **(k)** MGC-RIQMC

Figure 4.7 : The enhancement results for the proposed optimised enhancement method and the other benchmarking algorithms using the *pyramid* image from the RGBNIR dataset. (a) The input image. The enhanced output by (b) SECE, (c) RSECE, (d) SMIRANK, (e) RICE, (f) BOIEM, (g) ROHIM and the proposed (h) MGC-EMEG, (i) MGC-QRCM, (j) MGC-BIQME and (k) MGC-RIQMC.

posed method will also be improved by optimising this new IQM for better image enhancement.

Chapter 5

Adaptive Detail Enhancement with Optimised Background Enhancement

5.1 Introduction

When enhancing the contrast of an image, it is often the case that details are lost in bright or dark regions of an image, due to the re-mapping of intensity values. To retain those details, some enhancement methods also apply detail enhancement in conjunction with global contrast enhancement to improve an output image. However, as both details and noise contain high frequency components, many detail enhancement methods are unable to differentiate between the two and will often enhance the noise along with details.

Halo effects are another common problem often associated with detail enhancement. They are caused by the high-pass filtering of input images and result in either overshooting or a ringing effect at edges. This manifests in an output image as a contrasting light or dark boundary produced alongside an edge.

Both the spatial entropy-based contrast enhancement (SECE) [3] and the residual spatial entropy-based contrast enhancement (RSECE) [24] methods apply detail enhancement by increasing the weight to the high frequency components in the frequency domain using the discrete cosine transform (DCT), after which they are referred to as SECEDCT and RSECEDCT respectively. In both algorithms, detail

enhancement is applied after global contrast enhancement and if the details are already lost in the initial global contrast enhancement, then detail enhancement will have minimal effect. Furthermore, the noise level will be raised and halo effects may be produced when the weights to the high frequency components are increased, resulting in output images with worse signal-to-noise ratio and halo effects at edges.

In this chapter, an adaptive detail enhancement method is proposed that reduces enhancement adaptively in homogeneous regions where there are no details to be enhanced. By reducing enhancement in those homogeneous regions with minimal details, the enhancement of noise can be avoided and the signal-to-noise ratio can be improved in the output image. Moreover, by separating the edges from the details prior to performing enhancement using an edge-preserving filter, the proposed method will enhance only the details and not the edges, so that halo effects at edges can be avoided.

5.2 Method

5.2.1 Background and Detail Separation

To extract the background of an image, the conventional method is by filtering the original image by a Gaussian low-pass filter to remove high frequency components and therefore the details. The details are then extracted by taking the difference between the original image and the extracted background [46]. However, the Gaussian low-pass filter is unable to preserve edges, which means this conventional method for detail separation will include edges in the extracted details and subsequent detail enhancement will cause some degree of halo effects at edges. It

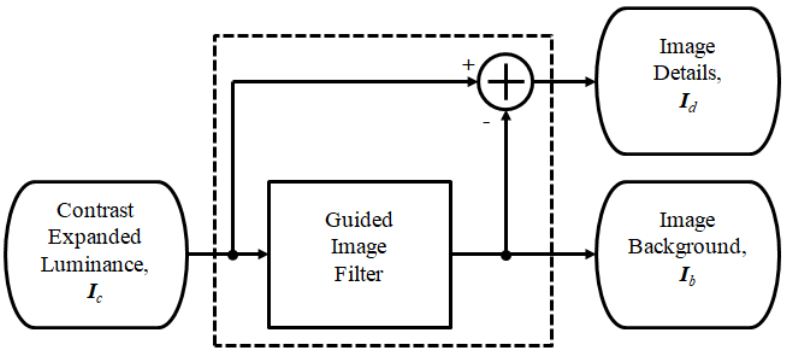

Figure 5.1 : Flowchart for background and detail separation using a guided image filter.

is therefore necessary to exclude edges in the extracted details for enhancement to avoid halo effects. The bilateral filter [47] is known to smooth out details while preserving sharp edges of an image, which makes it a popular choice for separating image background and details [48]. However, bilateral filters may suffer from "gradient reversal" artifacts [49, 48]. Therefore, a number of different filters have been proposed to separate the image background and details.

An edge-preserving smoothing operator, based on the weighted least squares optimisation framework, was proposed in [50] for multi-scale detail and background separation. A Gaussian image pyramid filter was proposed in [51] to separate details level-by-level from coarse to fine from the image background. A global filter computed from image affinities was proposed in [52] to perform multi-scale detail and background separation and by defining details as oscillations between local minima and maxima, the filter proposed in [53] can smooth high contrast details while preserving salient edges. One common problem with all of these methods, is that a precise setting of parameters is required for each image in order to avoid artifacts.

Hence, the guided image filter (GIF) [49], which has similar properties to the bilateral filter, but does not suffer from the "gradient reversal" problem, is applied in the proposed method so that the difference between its output and the original image will extract the details without any edges to avoid halo effects, as shown in Fig. 5.1.

Let $\boldsymbol{X}$ be an original image in RGB colour space with an intensity range of $[0,\ L-1]$ where L is 256 for an 8-bit image and $\boldsymbol{X}_c$ be the output processed by the contrast expansion method described in Chapter 2. Let $\boldsymbol{I}_c$ be the luminance component of $\boldsymbol{X}_c$ and $\boldsymbol{I}_b$ be the image background, which is the GIF output with $\boldsymbol{I}_c$ as the input. Hence, the image details, $\boldsymbol{I}_d$, without containing any edges, can be extracted by the following:

$$\boldsymbol{I}_d = \boldsymbol{I}_c - \boldsymbol{I}_b. \tag{5.1}$$

The background is then enhanced separately from the details by the optimised image enhancement method presented in the previous chapter to give the enhanced background, $\widetilde{\boldsymbol{I}}_b$.

5.2.2 MAD Based Adaptive Detail Enhancement

A novel median of absolute deviation from the median (MAD) [28] based adaptive method [36] is proposed to enhance only the details to a desirable degree which can be set by a user. As details and noise both contain high frequency components, it is difficult to differentiate between the two in the frequency domain. However, details are always associated with edges while noise is not. In this application, the MAD

operator is used to determine the existence of edges. In homogeneous regions, there are no edges and therefore high frequency components are considered as noise. In all other regions they are considered as details. As there are no details for enhancement in homogeneous regions of an image, hence, in order to suppress the enhancement of noise to improve the signal-to-noise ratio, no enhancement should be applied in those regions. An adaptive weight to control the degree of enhancement is proposed so that a desirable degree of enhancement will be applied to regions with details while maintaining minimal enhancement in homogeneous regions. The adaptive weight applied to $\boldsymbol{I}_d$ is as follows:

$$\tilde{I}_d(i,j) = w(i,j) I_d(i,j), \tag{5.2}$$

where $\tilde{\boldsymbol{I}}_d$ is the enhanced details and $w(i,j)$ is the adaptive weight for detail enhancement at the location (i,j) given as follows:

$$w(i,j) = \begin{cases} w_s + \frac{(1-w_s)}{1+(R\times MAD(i,j))^2} & S1 = A \\ w_s & S1 = B \end{cases}, \tag{5.3}$$

where $S1 = A$ when the adaptive algorithm is "ON" and at $S1 = B$ when it is "OFF", w_s is the user set weight for detail enhancement, $MAD(i,j)$ is the MAD [28] within a 3x3 filter window centred at (i,j) in the image background, $\boldsymbol{I}_b$, with an intensity range of $[0,\ L-1]$ and R is a normalised scaler for the MAD given by the following:

$$R = \frac{256}{L}. \tag{5.4}$$

For 8-bit luminance component, $L = 256$ and $R = 1$.

The MAD is used as a robust estimator for the standard deviation. In homogeneous regions of the image background, $\boldsymbol{I}_b$, the MAD value will tend to zero

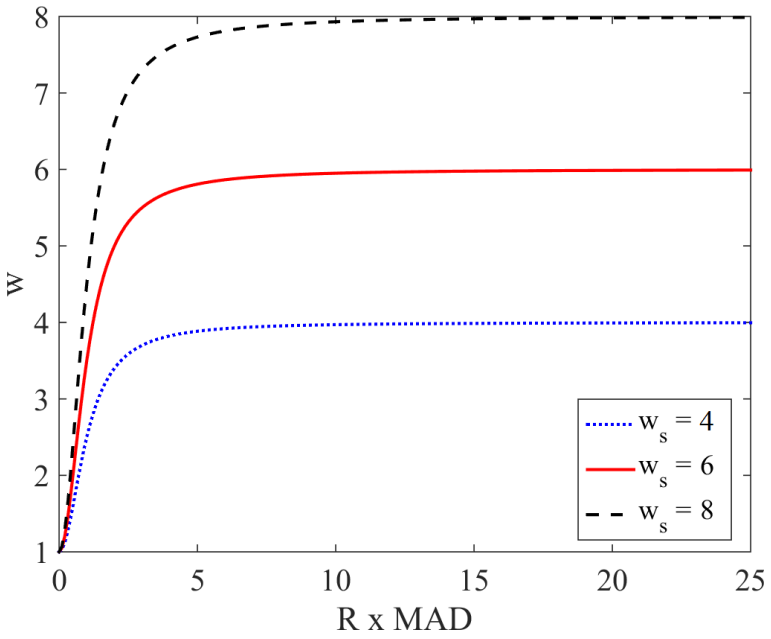

Figure 5.2 : The adaptive weight, w, verses $(RxMAD)$ for various user set weights, w_s.

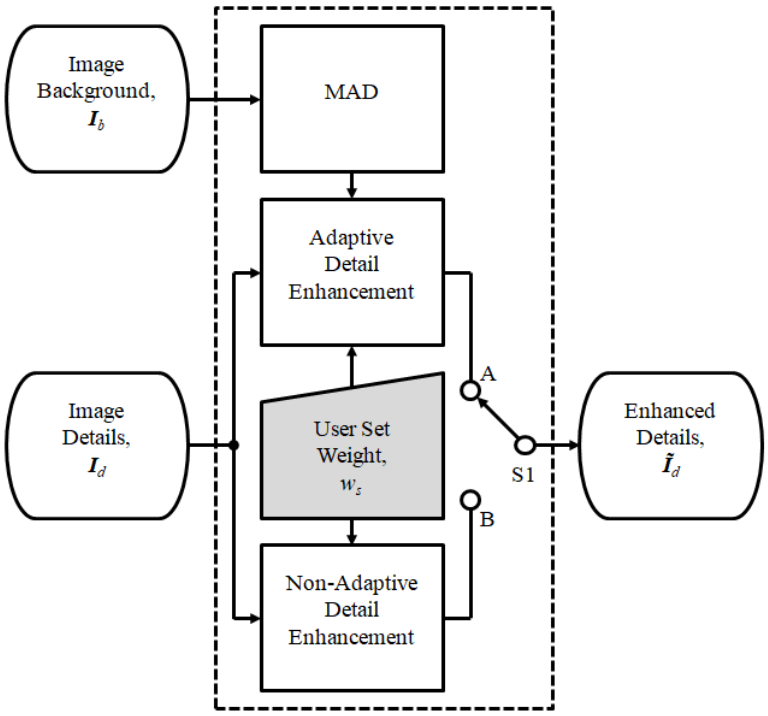

Figure 5.3 : Flowchart for the proposed detail enhancement method, $S1$ is at A when the adaptive algorithm is "ON" and $S1$ is at B when it is "OFF".

and therefore the adaptive weight, $w(i,j)$, will tend to unity. In this case, no enhancement will be applied regardless of the value of w_s and hence, there will be no enhancement of noise in those regions for the improvement of the signal-to-noise ratio. In other non-homogeneous regions, the MAD value will be large and the adaptive weight will be approaching the user set weight, w_s. Increasing w_s above unity will increase the degree of detail enhancement in non-homogeneous regions and vice versa. Fig. 5.2 gives the curves for the adaptive weight, $w(i,j)$ versus $(R \times MAD)$ for different user set weights, w_s by (5.3). The solid red line, which shows the adaptive weight curve when $S1$ at A (i.e. the adaptive algorithm is "ON") and $w_s = 6$, is the default value used for all the 807 test images in our experimental results. When $(R \times MAD)$ tends to zero in homogeneous regions, $w(i,j)$ tends to unity which is the weight for no enhancement. When $(R \times MAD)$ gets larger in non-homogeneous regions, $w(i,j)$ approaches the user set weight quickly, to produce uniform enhancement in all non-homogeneous regions. Fig. 5.3 gives the block diagram for our proposed MAD based adaptive detail enhancement method. The default position for switch, $S1$, is A, at which adaptive detail enhancement is turned on. However, if the user wishes to enhance weak details in homogeneous regions at the expense of poorer signal-to-noise ratio, the adaptive equation for detail enhancement can be turned off by switching $S1$ to B and the detail enhancement weight, $w(i,j)$, will be a constant value equal to the user set weight, w_s for all regions of the image.

The final enhanced image, $\boldsymbol{Y}$, is obtained by combining the enhanced background, $\widetilde{\boldsymbol{I}}_b$, with the enhanced details, $\widetilde{\boldsymbol{I}}_d$, as follows:

$$\boldsymbol{Y} = \tilde{\boldsymbol{I}}_b + \tilde{\boldsymbol{I}}_d. \tag{5.5}$$

After combining the enhanced background, $\tilde{\boldsymbol{I}}_b$, with the enhanced details, $\tilde{\boldsymbol{I}}_d$, some intensity values may be outside the range [0,L-1]. As scaling the details back to the range of [0,L-1] would reduce the strength of those details already within that range, clipping is therefore applied for values outside the range in order to preserve the strength of detail enhancement as follows:

$$Y(i,j) = \begin{cases} 0 & Y(i,j) < 0 \\ (L-1) & Y(i,j) > (L-1) \\ Y(i,j) & otherwise \end{cases}, \tag{5.6}$$

Refer to Fig. 5.4 for our proposed overall enhancement method.

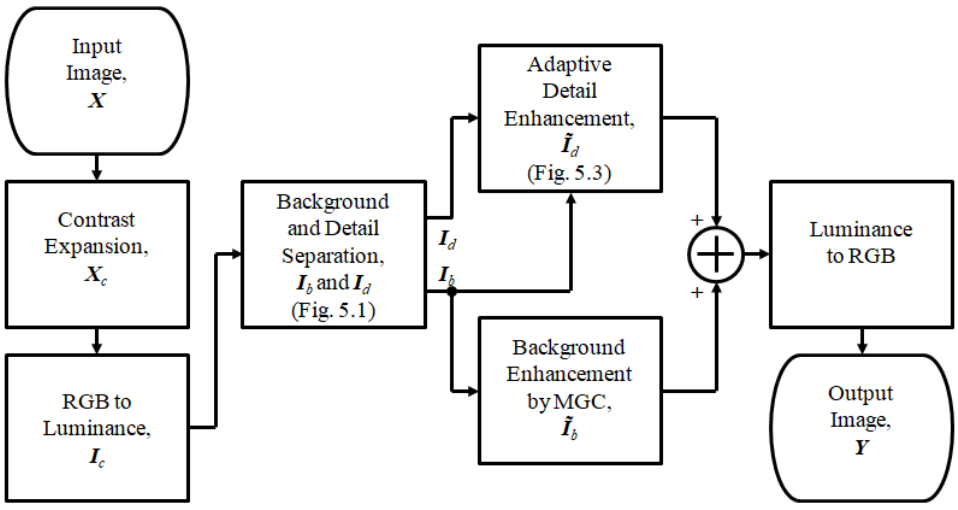

Figure 5.4 : Flowchart for the overall image enhancement method with the proposed adaptive detail enhancement.

5.3 Results

A total of 807 test images from the NIRRGB [2], CSIQ [1] and TID2013 [42] datasets were used for quantitative evaluations and some were selected for visual assessment.

The proposed method is compared with four benchmarking algorithms, namely, BOIEM [19], ROHIM [20], SECEDCT [3] and RSECEDCT [24]. To assess the effect adaptive detail enhancement has on improving the optimised enhancement method from the previous chapter, it is also compared with the proposed MGC-QRCM and MGC-BIQME enhancement methods (i.e. MGC enhancement optimised by QRCM and BIQME respectively). These are the methods used to enhance the background of the proposed adaptive detail enhancement method. Default parameter settings for all algorithms are used. In the proposed method, the user set weight for detail enhancement, $w_s = 6$, was used for all the experimental results except Fig. 5.5 which shows the effect of enhancement with various values of w_s. For background enhancement, $\gamma = 2.2$, was used for all of the experimental results except Fig. 5.5, Fig. 5.6 and Fig. 5.7, where only the effect of detail enhancement was explored. The proposed enhancement methods are labelled as ADE-QRCM and ADE-BIQME to represent adaptive detail enhancement with background enhancement optimised by QRCM and BIQME respectively.

5.3.1 Quantitative Results

Three IQMs, namely, the quality-aware relative contrast measure (QRCM) [8], the blind image quality measure of enhanced images (BIQME) [19] and the no-

reference image quality metric for contrast distortion (NIQMC) [54] were used for the quantitative comparison. QRCM is a combination of the relative contrast enhancement between the input and output image, and any distortions that result from enhancement, BIQME combines contrast, sharpness, brightness, colourfulness and naturalness into one quality score using a regression module. As the proposed method optimises the background enhancement based on QRCM and BIQME, NIQMC which combines both local and global information together to produce a score based on the concept of information maximisation, was used as an impartial IQM.

In Table 5.1-5.3, the p-values [8] for each of the benchmarking algorithms, namely, BOIEM (i.e. M1), ROHIM (i.e. M2), SECEDCT (i.e. M3), RSECEDCT (i.e. M4), MGC-QRCM (i.e. M5) and MGC-BIQME (i.e. M6) were found for all 807 test images to statistically determine which algorithm provided the best enhancement. The p-values [8] based on QRCM in Table 5.1, represent the proportion of enhanced test images when $\{QRCM_A > QRCM_B\}$ where $QRCM_A$ and $QRCM_B$ are values produced by algorithms A and B, for a test image respectively. Table 5.2 and 5.3 contains the p-values which are based on BIQME and NIQMC respectively.

In Table 5.1, the proposed methods, ADE-QRCM (i.e. Row M7) and ADE-BIQME (i.e. Row M9), when the adaptive algorithm was "ON" (i.e. $S1$ at A) obtained p-values higher than 0.82 for all of the 807 test images when compared with the other benchmarking algorithms. When the adaptive algorithm was "OFF" (i.e. $S1$ at B), the proposed methods, ADE-QRCM (i.e. Row M8) and ADE-BIQME (i.e. Row M10) obtained p-values higher than 0.94 for all of the 807 test

images when compared with the other benchmarking algorithms. In other words, the proposed algorithm statistically outscored all the ten benchmarking algorithms for all the 807 test images in the three datasets quantitatively regardless of the position of switch, $S1$. The better score for the proposed method when $S1$ at A (i.e. the adaptive algorithm is "OFF"), is because QRCM is based on the image gradient and a higher degree of enhancement in the homogeneous regions will give a higher score as a result. On the other hand, the output image when $S1$ at B (i.e. the adaptive algorithm is "ON") gives a cleaner image in homogeneous regions, as shown in the visual assessment results in the following section 5.3.2.

Table 5.1 : The p-values for $QRCM_A > QRCM_B$ where M1:BOIEM, M2:ROHIM, M3:SECEDCT, M4:RSECEDCT, M5:MGC-QRCM, M6:MGC-BIQME, M7:ADE-QRCM ($S1$ at A), M8:ADE-QRCM ($S1$ at B), M9:ADE-BIQME ($S1$ at A) and M10:ADE-BIQME ($S1$ at B).

	M1	M2	M3	M4	M5	M6	M7	M8	M9	M10
M1	-	0.285	0.004	0.002	0.025	0.087	0.000	0.000	0.007	0.005
M2	0.715	-	0.048	0.033	0.162	0.279	0.014	0.005	0.032	0.020
M3	0.996	0.952	-	0.169	0.958	0.985	0.033	0.000	0.177	0.057
M4	0.998	0.967	0.831	-	0.929	0.958	0.139	0.007	0.346	0.079
M5	0.975	0.836	0.042	0.071	-	0.963	0.007	0.007	0.052	0.031
M6	0.913	0.719	0.015	0.042	0.007	-	0.000	0.000	0.009	0.007
M7	1.000	0.986	0.967	0.860	0.993	1.000	-	0.010	0.861	0.196
M8	1.000	0.995	1.000	0.993	0.993	1.000	0.990	-	1.000	0.848
M9	0.993	0.968	0.823	0.653	0.948	0.991	0.102	0.000	-	0.002
M10	0.995	0.980	0.943	0.921	0.969	0.993	0.804	0.112	0.995	-

For the comparison of our proposed method with the other six benchmarking algorithms using BIQME, the p-values in Table 5.2 show that the proposed method at either position of the switch (i.e. Row M7 - M10) outperformed all of the other

benchmarking algorithms with p-values over 0.65.

Table 5.2 : The p-values for $BIQME_A > BIQME_B$ where M1:BOIEM, M2:ROHIM, M3:SECEDCT, M4:RSECEDCT, M5:MGC-QRCM, M6:MGC-BIQME, M7:ADE-QRCM ($S1$ at A), M8:ADE-QRCM ($S1$ at B), M9:ADE-BIQME ($S1$ at A) and M10:ADE-BIQME ($S1$ at B).

	M1	M2	M3	M4	M5	M6	M7	M8	M9	M10
M1	-	0.243	0.384	0.321	0.124	0.043	0.093	0.147	0.043	0.081
M2	0.755	-	0.719	0.690	0.437	0.275	0.304	0.342	0.156	0.198
M3	0.613	0.279	-	0.392	0.173	0.051	0.093	0.145	0.029	0.073
M4	0.677	0.310	0.603	-	0.222	0.084	0.108	0.149	0.040	0.073
M5	0.875	0.563	0.827	0.778	-	0.022	0.129	0.323	0.062	0.161
M6	0.957	0.725	0.948	0.914	0.957	-	0.457	0.568	0.121	0.310
M7	0.907	0.694	0.907	0.892	0.869	0.539	-	0.627	0.136	0.347
M8	0.853	0.658	0.854	0.850	0.673	0.432	0.368	-	0.166	0.164
M9	0.955	0.843	0.970	0.960	0.938	0.876	0.833	0.830	-	0.670
M10	0.918	0.802	0.926	0.927	0.839	0.689	0.649	0.808	0.323	-

For the comparison using NIQMC, as shown in Table 5.3, the proposed method again outperformed the other benchmarking algorithms with p-values over 0.59.

Table 5.4 gives the average processing time per test image in seconds in MATLAB using an 8th generation Intel® Core™ i7 Q840 processor at 1.87GHz for the benchmarking algorithms and the proposed method with the adaptive algorithm both "ON" and "OFF" (i.e. $S1$ at A and $S1$ at B). The MATLAB code for the benchmarking algorithms in this chapter were provided by their respective authors. Table 5.4 shows that the difference in processing times of the proposed method with the adaptive algorithm "ON" or 'OFF" is insignificant. For SECEDCT and RESECDCT, performing detail enhancement using the DCT is more computationally efficient than the proposed method, however, the visual assessment results in

Table 5.3 : The p-values for $NIQMC_A > NIQMC_B$ where M1:BOIEM, M2:ROHIM, M3:SECEDCT, M4:RSECEDCT, M5:MGC-QRCM, M6:MGC-BIQME, M7:ADE-QRCM ($S1$ at A), M8:ADE-QRCM ($S1$ at B), M9:ADE-BIQME ($S1$ at A) and M10:ADE-BIQME ($S1$ at B).

	M1	M2	M3	M4	M5	M6	M7	M8	M9	M10
M1	-	0.295	0.088	0.089	0.154	0.145	0.138	0.110	0.131	0.113
M2	0.705	-	0.456	0.442	0.428	0.418	0.359	0.291	0.340	0.283
M3	0.912	0.544	-	0.362	0.446	0.455	0.322	0.261	0.333	0.259
M4	0.911	0.558	0.638	-	0.533	0.525	0.408	0.322	0.399	0.292
M5	0.846	0.572	0.554	0.467	-	0.504	0.221	0.138	0.289	0.186
M6	0.855	0.582	0.545	0.475	0.481	-	0.332	0.263	0.196	0.129
M7	0.862	0.641	0.678	0.592	0.778	0.668	-	0.089	0.477	0.295
M8	0.890	0.709	0.739	0.678	0.862	0.737	0.911	-	0.649	0.470
M9	0.869	0.660	0.667	0.601	0.710	0.804	0.499	0.351	-	0.098
M10	0.887	0.717	0.741	0.708	0.814	0.871	0.704	0.507	0.901	-

the following section 5.3.2, show that the quality of detail enhancement is much better in the proposed method. In the proposed ADE-QRCM and ADE-BIQME methods, background enhancement was performed by the MGC-QRCM and MGC-BIQME methods proposed in the previous chapter respectively. The difference in processing time between these proposed methods, as given in Table 5.4, is due to the background and detail separation and the adaptive detail enhancement.

5.3.2 Visual Assessment

To assess how various values of the user set weight change the degree of detail, w_s was set to the values of 1, 6 and 12, as shown in Fig. 5.5(b) - Fig. 5.5(d), respectively. The γ value was set to 1 so that no enhancement was applied to the background and only the effect of detail enhancement can be observed. This

Table 5.4 : The average processing time in seconds for an image in each of the three datasets for the proposed adaptive detail enhancement method and the other benchmarking algorithms.

Method	Average Processing Time (s)		
	RGBNIR	CSIQ	TID2013
BOIEM	4.23	2.77	2.88
ROHIM	24.26	9.37	7.09
SECEDCT	3.13	1.06	0.84
RSECEDCT	1.69	0.61	0.57
MGC-QRCM	3.74	1.50	1.27
MGC-BIQME	29.44	17.27	17.03
ADE-QRCM ($S1$ at A)	8.48	3.18	2.38
ADE-QRCM ($S1$ at B)	8.51	3.17	2.39
ADE-BIQME ($S1$ at A)	34.89	18.41	15.61
ADE-BIQME ($S1$ at B)	34.94	18.39	15.57

shows that the proposed method allows the user to have control over a wide range of the degree of detail enhancement while most enhancement methods have no or limited control over the degree of detail enhancement. In general, $w_s = 6$, provides a good degree of detail enhancement and hence, it was set as the default value in our experimental results for comparison with other benchmarking algorithms.

To examine the effects of background and detail separation using different window sizes of the GIF, window sizes of 3x3, 5x5 and 7x7 were applied and the output images are shown in Fig. 5.6(b) - Fig. 5.6(d), respectively. The γ value was again set to 1 to produce the images in Fig. 5.6, so that there was no enhancement to the background and only the effect of detail enhancement can be observed. A window size of 3x3 will include only finer details which can often make the output image appear noisy, while window sizes larger than 7x7 will include more coarse details

(a) **(b)**

(c) **(d)**

Figure 5.5 : Results of the proposed method using a different user set weight, w_s, on (a) the *lake* image from the CSIQ dataset [1] for (b) $w_s = 1$, (c) $w_s = 6$, (d) $w_s = 12$. $\gamma = 1$ so no enhancement was applied to the background.

which can have an unnatural appearance. Therefore a window size of 5x5 was set as the default value to produce balanced outputs for all of the experimental results.

To examine the effect the GIF smoothing parameter has on detail enhancement, the *building* image, which has a combination of sharp edges at various angles and small details, as shown in Fig. 5.7(a), from the RGBNIR dataset [2], was used as the input. A smoothing parameter value of (L-1)/8, (L-1)/2 and (L-1)/0.5 was applied and the output images are shown in Fig. 5.7(b) - Fig. 5.7(d) respectively. The γ value was set to 1 in each case so that only the effect the GIF has on detail enhancement can be observed. When larger values are used for the GIF smoothing parameter, such as (L-1)/0.5, more edges are blurred in the GIF output which means they are included as details, this in turn produces more coarse detail enhancement and strong halo effects in the output image, as shown in Fig. 5.7(d). When small values are used for the GIF smoothing parameter then fewer edges are blurred in the GIF output and finer detail without halo effects is produced in the output image, as shown in Fig. 5.7(b). As a result, a smoothing parameter of (L-1)/2 was used as the default value for all of the experimental results, as it gives adequate detail enhancement without halo effects, as shown in Fig. 5.7(c).

To examine the difference of the halo effects after detail enhancement between the conventional method using a Gaussian lowpass filter and a GIF for background and detail separation, the *test pattern* image with sharp edges at various angles, as shown in Fig. 5.8(a), from the TID2013 dataset [42], was used as the input. The enhanced output produced by the conventional Gaussian lowpass filter, as shown in Fig. 5.8(b), displayed strong halo effects at the proximity of the sharp edges

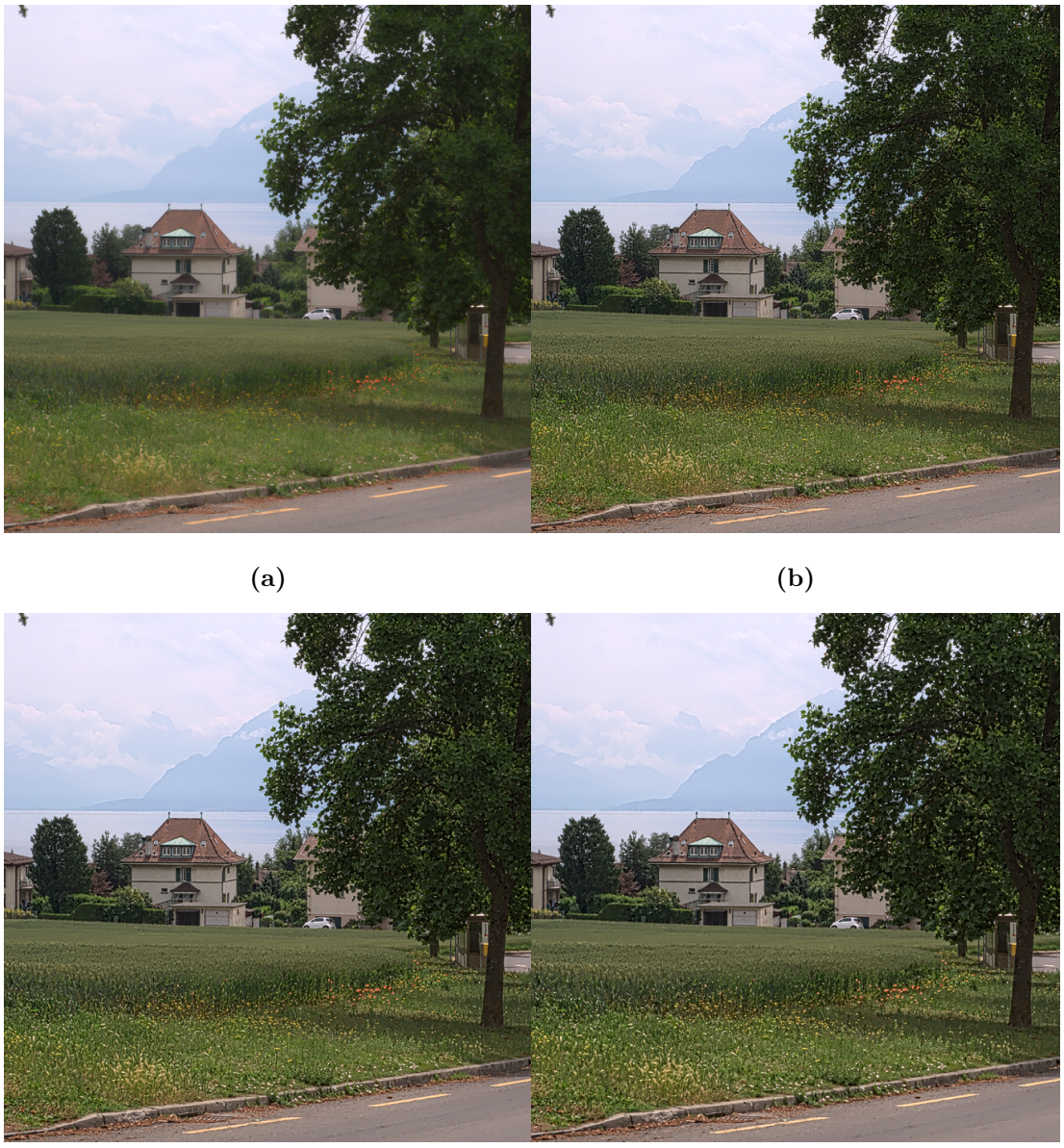

(a) **(b)**

(c) **(d)**

Figure 5.6 : Results of the proposed method using different guided image filter window sizes on (a) the *country* image from the RGBNIR dataset [2] with (b) [3x3] window size, (c) [5x5] window size, (d) [7x7] window size. $\gamma = 1$ so no enhancement was applied to the background.

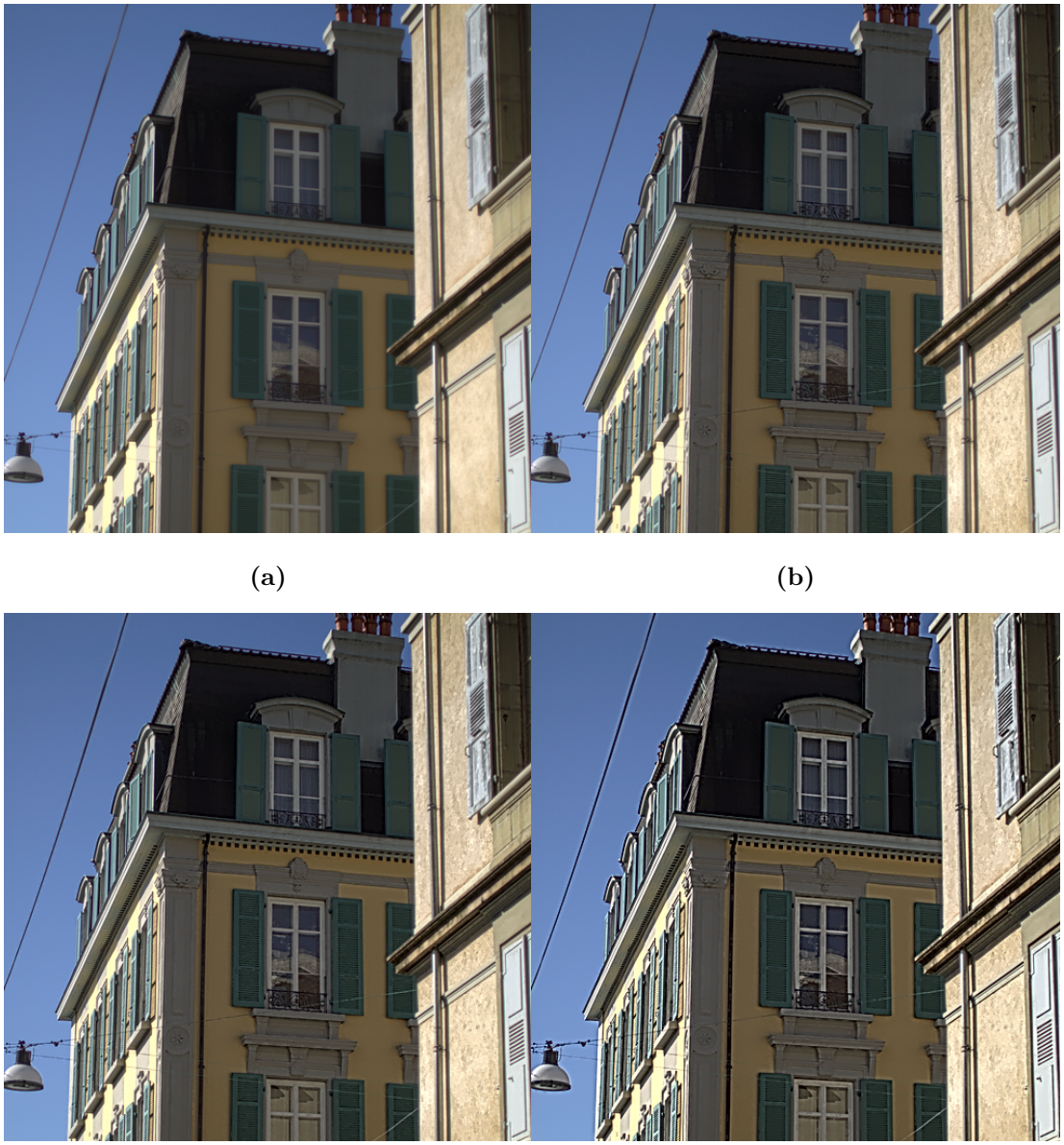

(a) **(b)**

(c) **(d)**

Figure 5.7 : Results of the proposed method using different values for guided image filter smoothing parameter on (a) the *building* image from the RGBNIR dataset [2] with (b) a smoothing parameter value of $(L\text{-}1)/8$, (c) a smoothing parameter value of $(L\text{-}1)/2$, (d) a smoothing parameter value of $(L\text{-}1)/0.5$. $\gamma = 1$ so no enhancement was applied to the background.

particularly along the rims of the circles and all the characters, while the enhanced output using a GIF, as shown in Fig. 5.8(c), showed no sign of halo effects at all.

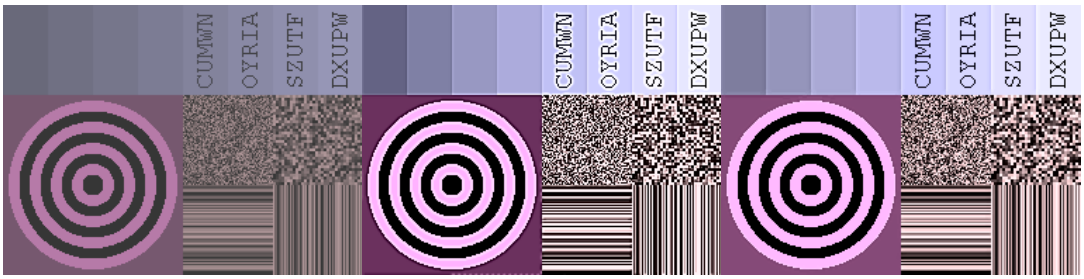

(a) **(b)** **(c)**

Figure 5.8 : Results of the proposed method using different filter types for background and detail separation on (a) the contrast reduced input image *test pattern* from the TID2013 dataset with (b) a Gaussian low pass filter and (c) a GIF.

To examine the proposed adaptive detail enhancement algorithm in the suppression of noise in homogeneous regions, the switch $S1$ was set at position A and B to produce the outputs shown in Fig. 5.9(d) and Fig. 5.9(c), respectively. When comparing the outputs with the original image, as shown in Fig. 5.9(b), which is a cropped region of Fig. 5.9(a), the noise level in the homogeneous region of Fig. 5.9(c) when the adaptive detail enhancement was turned off (i.e. when $S1$ at B) was much higher than that in Fig. 5.9(d) when the adaptive detail enhancement was turned on (i.e. $S1$ at A). On the other hand, the enhancement in non-homogeneous regions was similar in both Fig. 5.9(c) and Fig. 5.9(d).

The contrast reduced *foxy* image from the CSIQ [1] datase, was selected as the fox and surrounding foliage contain lots of details to be enhanced. The image produced by BOIEM, shown in Fig. 5.10(c) was under-enhanced with poor contrast

while the image produced by ROHIM, shown in Fig. 5.10(d) was brighter, but still had poor contrast. The SECEDCT and RSECEDCT output images, shown in Fig. 5.10(e) and Fig. 5.10(f) respectively, both have dull colour. The proposed MGC-QRCM and MGC-BIQME methods from the previous chapter, shown in Fig. 5.10(g) and Fig. 5.10(h) respectively, give good enhancement with vivid colour. The outputs produced by the proposed method, shown in Fig. 5.10(i) and Fig. 5.10(j) respectively, both give the same level of global enhancement as the MGC-QRCM and MGC-BIQME methods because they are applied for background enhancement, but they reveal more details in the image, particularly in the fox's fur.

The contrast reduced *girl in red* and *painted face* images from the TID2013 [42] dataset, were again used to assess the quality of detail enhancement in the human face. The images produced by BOIEM, shown in Fig. 5.11(c) and Fig. 5.12(c) respectively, exhibited under-enhancement with overall poor contrast. The images produced by ROHIM, shown in Fig. 5.11(d) and Fig. 5.12(d), over-saturated the colour resulting in outputs with unnatural appearance and also a loss of details in the brighter areas of both girls faces. The SECEDCT and RSECEDCT output images, shown in Fig. 5.11(e) - Fig. 5.11(f) respectively, are both dull in colour and over-enhanced around the girl's eyes. For the outputs of these methods, shown in Fig 5.12(f) - Fig. 5.12(f) respectively, they are both over-enhanced where the left side of the girls cheek is too dark. The outputs produced by the proposed method, shown in Fig. 5.11(i) - Fig. 5.11(j) and Fig. 5.12(i) - Fig. 5.12(j) respectively, both give the same adequate enhancement as the proposed MGC-QRCM and MGC-BIQME methods from the previous chapter, shown in Fig. 5.11(g) - Fig. 5.11(h) and Fig.

5.12(g) - Fig. 5.12(h) respectively, but with stronger details in the *girl in reds* eyes and hair and around the paint in the *painted face* image.

The *pyramid* image from the RGBNIR [2] dataset, was used again as it has the homogeneous region of the sky as well as the details of the pyramid and city which are difficult for detail enhancement algorithms to produce natural enhancement. A section of the original image was used to clearly show the enhancement results. The image produced by BOIEM, in Fig. 5.13(c), has overall poor contrast like the input. The image given by ROHIM, shown in Fig. 5.13(d), was over-saturated resulting in unnatural colour and also has noise in the sky. SECEDCT and RSECEDCT produced outputs, shown in Fig. 5.13(e) and Fig. 5.13(f) respectively, that were very noisy in the sky. The proposed method enhanced the details in the pyramid and the city while also suppressing the noise in the homogeneous region of the sky to give more natural detail enhancement as shown in Fig. 5.13(i) and Fig. 5.13(j) respectively.

The *bike* image from the RGBNIR [2] dataset, was used because it has edges which may cause halo effects for some detail enhancement algorithms. A section of the original image was used to clearly show edges at which halo effects may occur. The image produced by BOIEM, in Fig. 5.14(c), has only minor enhancement. The image given by ROHIM, shown in Fig. 5.14(d), was over-enhanced with a loss of details in the brighter regions. SECEDCT and RSECEDCT produced outputs, shown in Fig. 5.14(e) and Fig. 5.14(f) respectively, that had halo effects at edges, as seen by the dark outlines around the orange area. The proposed method enhanced the details without any halo effect as shown in Fig. 5.14(i) and Fig. 5.14(j) respectively.

5.4 Conclusion

A novel image enhancement method, by enhancing the background and details using individual novel enhancement techniques has been proposed in this chapter. By excluding edges in detail enhancement through a guided image filter (GIF), halo effects at edges have been avoided. The proposed adaptive detail enhancement method was also proven to be able to maintain low noise level in homogeneous regions by suppressing the enhancement of noise in those regions. It has been shown that the proposed method outperformed the other benchmarking algorithms both quantitatively and visually without the usual adverse problems of other enhancement methods in terms of over-enhancement and noise in different regions and halo effects at edges.

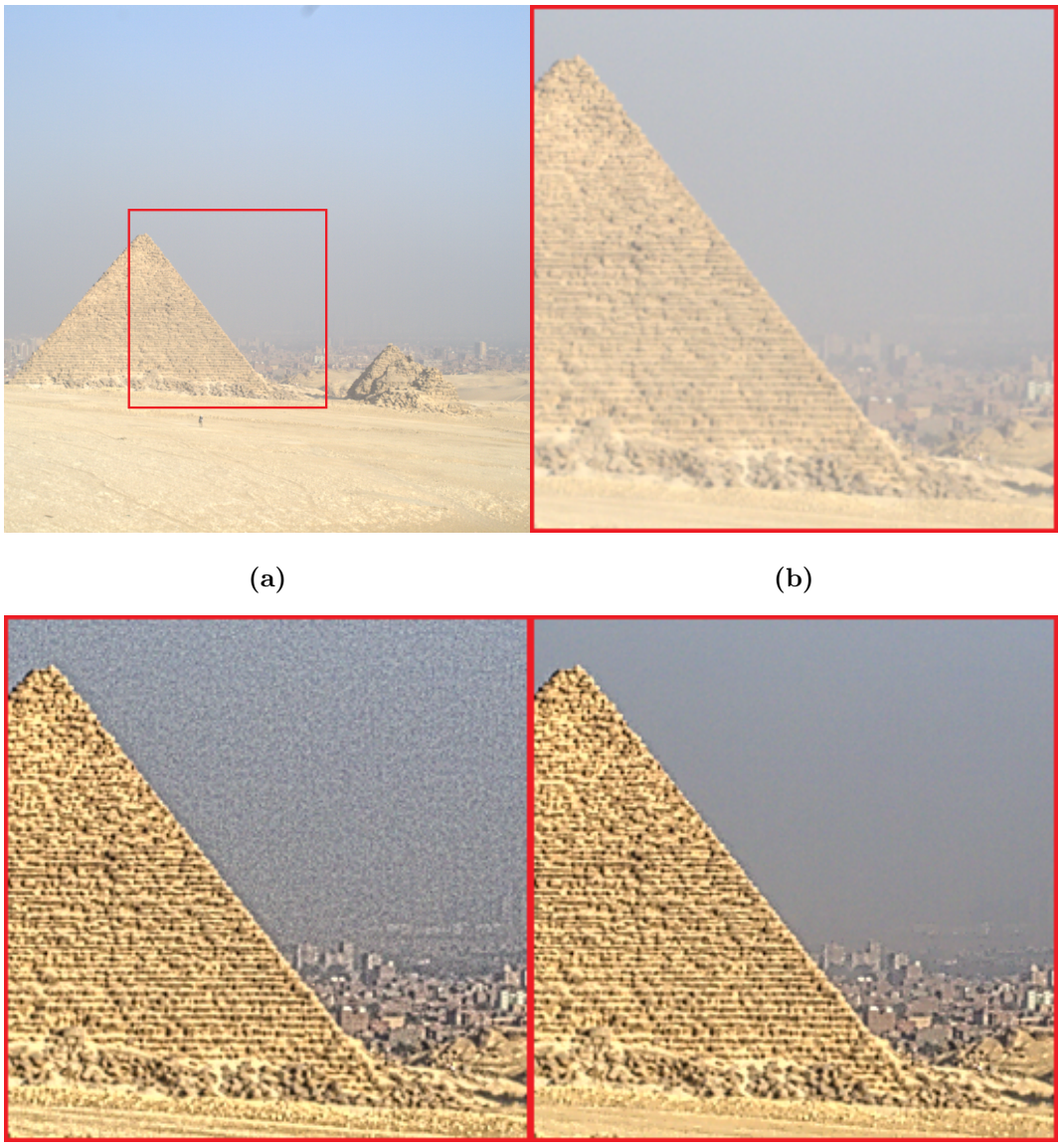

(a) **(b)**

(c) **(d)**

Figure 5.9 : Results of the proposed method using different detail enhancement on (a) the *pyramid* image from the RGBNIR dataset. (b) The zoomed-in area of the input, (c) the proposed method with a constant enhancement weight, $w_s = 6$ ($S1$ at B (i.e. the adaptive algorithm is "OFF")) and (c) the proposed method with adaptive enhancement, $w_s = 6$ ($S1$ at A (i.e. the adaptive algorithm is "ON")).

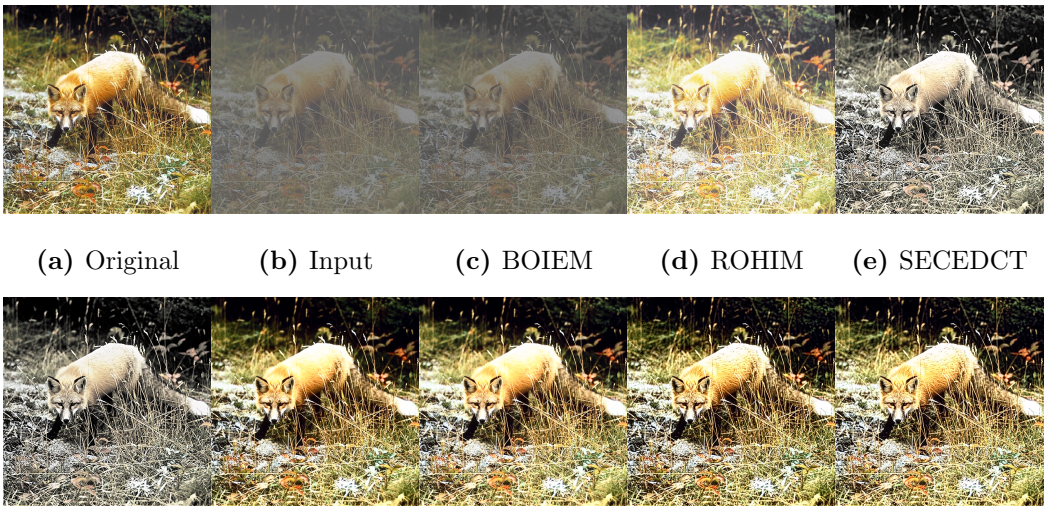

(a) Original **(b)** Input **(c)** BOIEM **(d)** ROHIM **(e)** SECEDCT

(f) RSECEDCT **(g)** MGC-QRCM **(h)** MGC-BIQME **(i)** ADE-QRCM **(j)** ADE-BIQME

Figure 5.10 : The enhancement results for the proposed adaptive detail enhancement method and the other benchmarking algorithms using the *foxy* image from the CSIQ dataset. (a) The original image. (b) The contrast reduced input image. The enhanced output by (c) BOIEM, (d) ROHIM, (e) SECEDCT, (f) RSECEDCT, (g) MGC-QRCM, (h) MGC-BIQME and the proposed (i) ADE-QRCM and (j) ADE-BIQME.

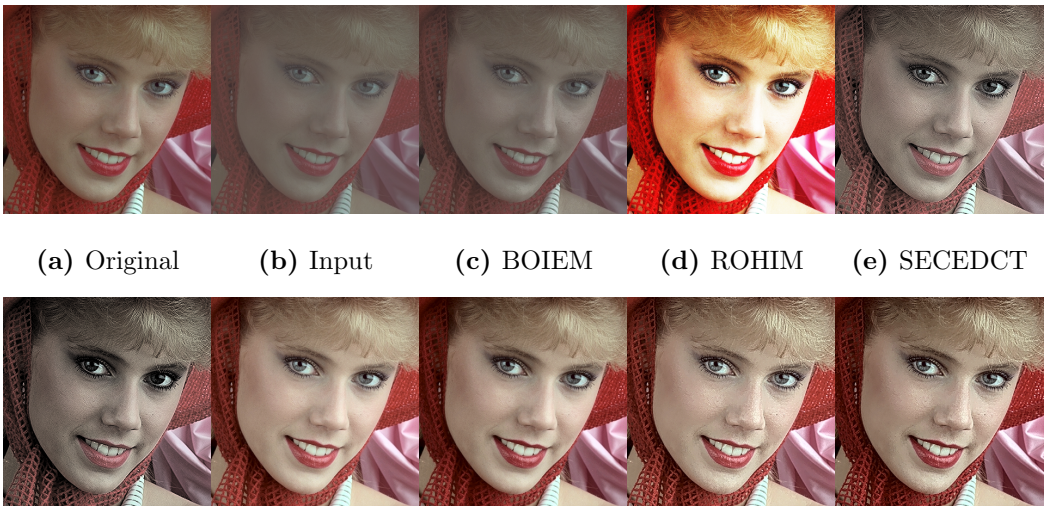

(a) Original **(b)** Input **(c)** BOIEM **(d)** ROHIM **(e)** SECEDCT

(f) RSECEDCT **(g)** MGC-QRCM **(h)** MGC-BIQME **(i)** ADE-QRCM **(j)** ADE-BIQME

Figure 5.11 : The enhancement results for the proposed adaptive detail enhancement method and the other benchmarking algorithms using the *girl in red* image from the TID2013 dataset. (a) The original image. (b) The contrast reduced input image. The enhanced output by (c) BOIEM, (d) ROHIM, (e) SECEDCT, (f) RSECEDCT, (g) MGC-QRCM, (h) MGC-BIQME and the proposed (i) ADE-QRCM and (j) ADE-BIQME.

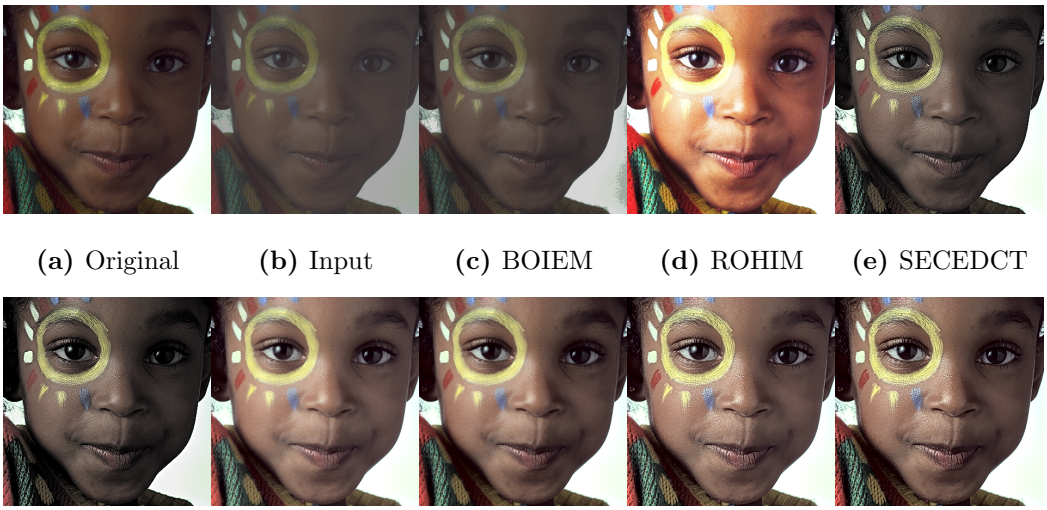

(a) Original **(b)** Input **(c)** BOIEM **(d)** ROHIM **(e)** SECEDCT

(f) RSECEDCT **(g)** MGC-QRCM **(h)** MGC-BIQME **(i)** ADE-QRCM **(j)** ADE-BIQME

Figure 5.12 : The enhancement results for the proposed adaptive detail enhancement method and the other benchmarking algorithms using the *painted face* image from the TID2013 dataset. (a) The original image. (b) The contrast reduced input image. The enhanced output by (c) BOIEM, (d) ROHIM, (e) SECEDCT, (f) RSECEDCT, (g) MGC-QRCM, (h) MGC-BIQME and the proposed (i) ADE-QRCM and (j) ADE-BIQME.

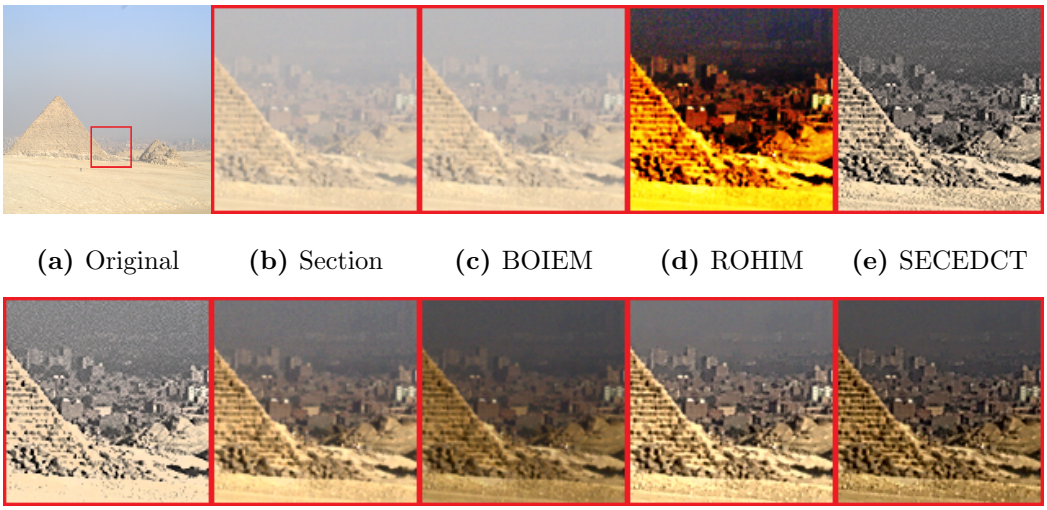

(a) Original **(b)** Section **(c)** BOIEM **(d)** ROHIM **(e)** SECEDCT

(f) RSECEDCT **(g)** MGC-QRCM **(h)** MGC-BIQME **(i)** ADE-QRCM **(j)** ADE-BIQME

Figure 5.13 : The enhancement results for the proposed adaptive detail enhancement method and the other benchmarking algorithms using the *pyramid* image from the RGB-NIR dataset. (a) The input image. (b) The zoomed-in area of the input. The enhanced output by (c) BOIEM, (d) ROHIM, (e) SECEDCT, (f) RSECEDCT, (g) MGC-QRCM, (h) MGC-BIQME and the proposed (i) ADE-QRCM and (j) ADE-BIQME.

(a) Original **(b)** Section **(c)** BOIEM **(d)** ROHIM **(e)** SECEDCT

(f) RSECEDCT **(g)** MGC-QRCM **(h)** MGC-BIQME **(i)** ADE-QRCM **(j)** ADE-BIQME

Figure 5.14 : The enhancement results for the proposed adaptive detail enhancement method and the other benchmarking algorithms using the *bike* image from the RGBNIR dataset. (a) The input image. (b) The zoomed-in area of the input. The enhanced output by (c) BOIEM, (d) ROHIM, (e) SECEDCT, (f) RSECEDCT, (g) MGC-QRCM, (h) MGC-BIQME and the proposed (i) ADE-QRCM and (j) ADE-BIQME.

Chapter 6

Applications

6.1 Introduction

The image enhancement methods presented in this thesis can be used in many different applications that range from being applied directly for image and video enhancement, to being applied as a pre-processing step to improve an input for further processing. Two different applications are explored in this chapter, the first is image expansion and the second is enhancement prior to colour filter array (CFA) demosaicking.

Current image expansion methods are often unable to preserve sharp edges and may produce jagged edges and halo effects. A method is presented in this chapter, that uses the proposed MGC applied adaptively to an expanded image, so that the sharpness of edges can be recovered.

Enhancement is usually performed after CFA demosaicking as image enhancement algorithms are typically developed for full colour images. However, enhancing an image prior to demosaicking, particularly for images with a narrow intensity range, may reduce interpolation errors by increasing the intensity range before interpolation. Therefore, a method is presented to apply the proposed image enhancement techniques prior to CFA demosaicking.

6.2 Improved Image Expansion

Image expansion methods can be separated into two groups, learning based methods and interpolation based methods. Learning based methods are known as super-resolution methods [55, 56, 57] as they require extra details in the output image. These methods demand external information in the form of training sets with pairs of high and low resolution images. However, once trained these methods may not adapt well to different classes of images [56]. Furthermore, the complexity of these methods can limit their practical performance [57] for real-time processing.

Interpolation based methods can expand an image using only a single image input and require no extra information. They expand an image by estimating missing pixels using the values of known neighbours. Traditional interpolation methods used to expand an image, such as the bilinear and bicubic [58] methods are unable to preserve sharp edges. Many other interpolation-based methods including new edge directed interpolation (NEDI) [59] its variants, modified edge directed interpolation (MEDI) [60], improved new edge directed interpolation (INEDI) [61], edge-guided image interpolation (EGII) [62] and real-time artifact free image upscaling (RTIU) [63], directional cubic convolution interpolation (DCCI) [64], adaptive distance-based edge preserving interpolation (ADEPI) [65] and trilateral filter regression interpolation (TRFI) [66] are only able to expand an image by powers of two, which limits their practical application. Furthermore, these methods are often unable to preserve sharp edges. To resolve this problem, some interpolation-based methods, namely, improved Canny edge based image expansion (Zhang) [67] and

adaptive interpolation based on local gradient features (Hwang) [68], attempt to use the image gradient, or an edge detection method, to adaptively alter the sharpness of a blurred edge in the expanded image. However, these methods may produce halo effects with jagged edges.

The MGC [45] described in Chapter 3 can be applied to image expansion to preserve the sharpness of edges. By taking the absolute difference between the nearest neighbour interpolation method and another interpolation algorithm and using this to adaptively adjust the γ value of the MGC the sharpness of the original edge can be regained.

6.2.1 Improved Image Expansion Method

Refer to Fig. 6.1 for the flowchart of the overall proposed image expansion algorithm. In order to retain the sharpness of an edge and prevent jagged edges, the absolute difference between the original image expanded by the nearest neighbour method and another interpolation algorithm with a different degree of edge preservation capability is used to produce an edge residual image. The edge residual image will have a larger magnitude corresponding to the degree of sharpness of an edge and is then used to adaptively regain the sharpness of the edges in the expanded image.

As there is no requirement for preserving sharp edges by the other interpolation algorithm, its smoothing capabilities are of higher priority. In this application, bicubic [58] interpolation is chosen due to its good performance in expanding smooth regions and its computational efficiency.

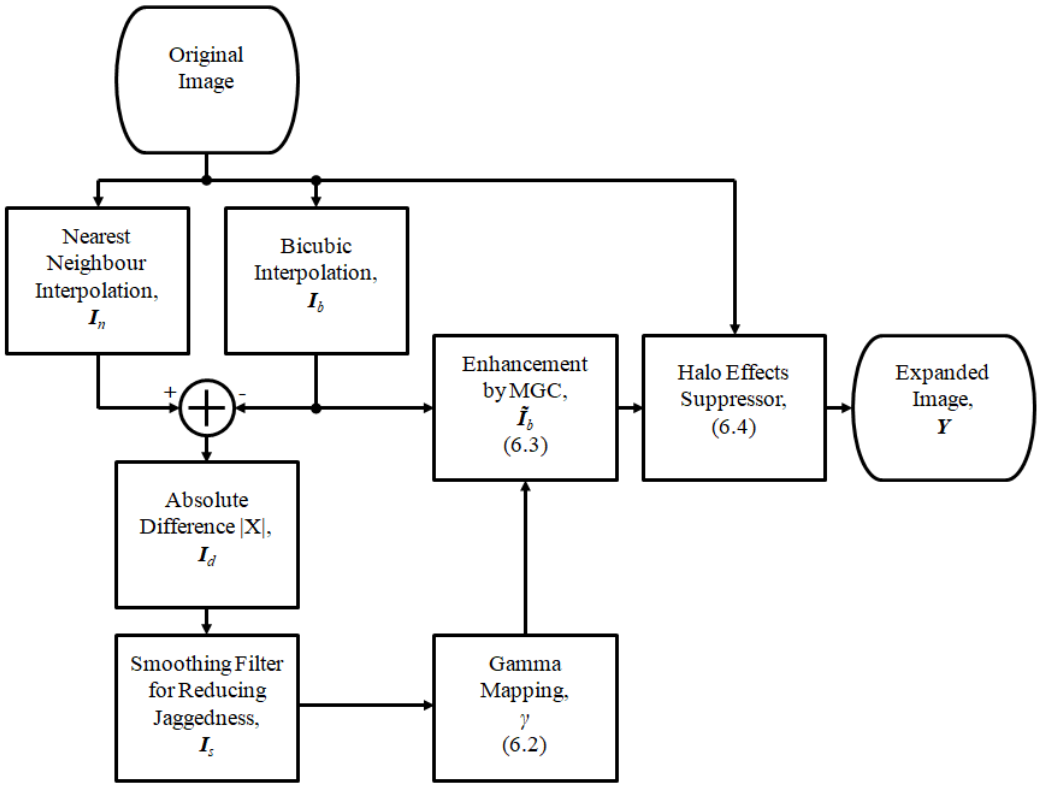

Figure 6.1 : Flowchart for the proposed image expansion method.

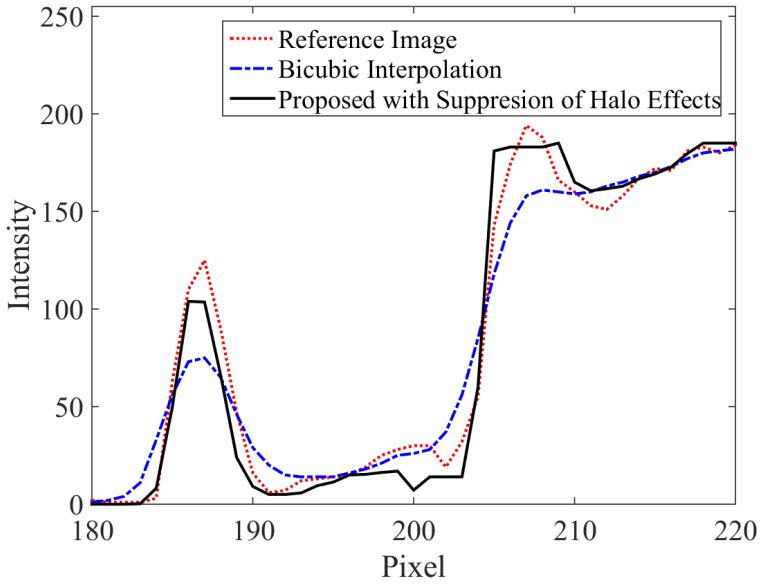

Figure 6.2 : A cross section of the expanded *zebra* image output in Fig. 6.4.

Let $I_n(i,j)$ and $I_b(i,j)$ be the luminance outputs expanded by the nearest neighbour and bicubic interpolation methods respectively where (i,j) are the pixel locations, and $I_d(i,j)$ be the edge residual image which is the absolute difference of these two interpolations as follows:

$$I_d(i,j) = |I_b(i,j) - I_n(i,j)| . \tag{6.1}$$

For smooth regions, $I_d(i,j)$ will be small and no further processing will be required for the expanded image. For regions with sharp edges, $I_d(i,j)$ will be large and a corresponding larger gamma adjustment will then be applied to regain the sharpness of the edges.

Due to the jagged edges produced by the nearest neighbour interpolation method, the edge residual image has to be smoothed to remove jaggedness in the residual image. A moving average filter with a window of size NxN is used to produce a smoothed residual image, $I_s(i,j)$, without jaggedness where $N = (2\lfloor m \rceil - 1)$, $\lfloor m \rceil$ is the nearest integer function of m and m is the scaling factor, where m is any positive real number and not necessarily an integer.

In order to regain the sharpness of an edge, the MGC can be used as it both increases and decreases intensities above and below an intersection point which is the mid-point of an edge. The intersection point for each pixel location, $P(i,j)$, should be set to the mid-intensity level of any possible edge centred at that pixel location and this mid-intensity value is defined as the mean intensity value of all the pixels within a window of size NxN centred at (i,j) in the bicubic expanded image,

I_b.

A γ value of unity corresponds to no enhancement and the degree of enhancement increases with γ. Therefore, the smoothed edge residual image, I_s, must then be mapped accordingly so that a value of 0 in it will map to a $\gamma(i,j)$ value of unity, where $\gamma(i,j)$ is the input parameter to our proposed MGC algorithm. One mapping function that will meet this requirement is the exponential function. As the γ value produced by the mapping function must also be large to adequately regain the original sharpness of the edge, the exponential function has been found to be suitable for our application as follows:

$$\gamma(i,j) = e^{\frac{I_s(i,j)}{k}}, \tag{6.2}$$

where k is a scaling factor that controls the strength of enhancement and $k = 10$ is adequate for reproducing strong edges without over-enhancing weak edges.

The enhanced expanded image output, $\tilde{\boldsymbol{I}}_b$, is the result of applying the MGC to the bicubic interpolation output, I_b, as follows:

$$\tilde{I}_b(i,j) = \begin{cases} \frac{I_b(i,j)^{\gamma(i,j)}}{P(i,j)^{\gamma(i,j)-1}}, & I_b(i,j) < P(i,j) \\ 255 - \frac{(255-I_b(i,j))^{\gamma(i,j)}}{(255-P(i,j))^{\gamma(i,j)-1}}, & I_b(i,j) > P(i,j) \\ I_b(i,j), & otherwise \end{cases} . \tag{6.3}$$

In order to avoid halo effects resulting from over-enhancement of strong edges, the maximum intensity value, $I_{max}(r,s)$, and minimum intensity value, $I_{min}(r,s)$, of pixels inside the window of size 3x3 centred at (r,s) in the original image is determined and any enhanced pixel value, $\tilde{\boldsymbol{I}}_b(i,j)$, outside this range will be clipped

to produce $Y(i,j)$ as follows:

$$Y(i,j) = \begin{cases} I_{min}(r,s), & \tilde{I}_b(i,j) < I_{min}(r,s) \\ I_{max}(r,s), & \tilde{I}_b(i,j) > I_{max}(r,s) \\ \tilde{I}_b(i,j), & otherwise \end{cases}, \tag{6.4}$$

where $r = \lfloor \frac{i}{m} \rceil$ and $s = \lfloor \frac{j}{m} \rceil$. Refer to Fig. 6.2 as an example at the location of a sharp edge of the cross section of a real image without any overshooting. As overshooting will manifest itself as halo effects in the expanded image, this shows that the proposed method is able to regain the sharpness of an edge in the expanded image without halo effects.

6.2.2 Improved Image Expansion Results

Five standard image datasets, namely, Set5 [69], Set14 [70], BSD100 [71], Urban100 [72] and Sun-Hays80 [73], were used to produce the experimental results. To assess the proposed method quantitatively, three image quality measures (IQMs), namely, structural similarity (SSIM) [25], feature similarity (FSIM) [74] and expected measure of enhancement by gradient (EMEG) [3], were used. SSIM will show how close the expanded images resemble the input images. FSIM uses phase congruency to show how the features in the input images are enlarged faithfully in the expanded images and EMEG is based on the gradient of the expanded image to assess how well the edges are preserved in the expanded images. For comparison, four computationally efficient benchmarking algorithms, namely, bilinear, bicubic [58], Hwang [68] and Zhang [67], were used.

For quantitative assessment as shown in Table 6.1, 6.2 and 6.3 using SSIM, FSIM

and EMEG respectively with various scaling factors, m and the best results for each image set were shown in bold. In general, the performance of the benchmarking algorithms reduces with the scaling factor, m, but the proposed method was still able to outperform them in most cases. For SSIM and FSIM, as shown in Table 6.1 and Table 6.2, the proposed method outperformed the other benchmarking algorithms for most of the test image sets, especially for large scaling factors, m. For EMEG, as shown in Table 6.3 respectively, the proposed method outperforms all the benchmarking algorithms for the all five test images datasets and various scaling factors.

Table 6.1 : The average SSIM values for each image expansion method applied to each dataset with different scaling factors, m.

Dataset	m	Bilinear	Bicubic	Hwang	Zhang	Proposed
Set5	2	0.901	**0.921**	0.911	0.894	0.917
	3	0.837	0.856	0.853	0.839	**0.861**
	4	0.769	0.794	0.786	0.772	**0.807**
Set14	2	0.903	0.929	0.904	0.897	**0.933**
	3	0.820	0.840	0.827	0.823	**0.851**
	4	0.744	0.772	0.753	0.750	**0.785**
BSD100	2	0.803	0.838	0.805	0.791	**0.855**
	3	0.706	0.728	0.712	0.699	**0.748**
	4	0.629	0.652	0.635	0.621	**0.671**
Urban100	2	0.853	0.890	0.856	0.853	**0.901**
	4	0.870	0.897	0.873	0.876	**0.913**
Sun-Hays80	8	0.755	0.782	0.760	0.757	**0.800**
Average	-	0.799	0.825	0.806	0.798	**0.837**

For visual assessment, four test images, namely, *lena* of size 256x256, *zebra* of size 195x130, *butterfly* of size 64x64 and *hillside* of size 120x80, were used as the inputs as shown in Fig. 6.3(a), Fig. 6.4(a), Fig. 6.5(a) and Fig. 6.6(a) respectively. To

Table 6.2 : The average FSIM values for each image expansion method applied to each dataset with different scaling factors, m.

Dataset	m	Bilinear	Bicubic	Hwang	Zhang	Proposed
Set5	2	0.928	**0.943**	0.941	0.927	0.940
	3	0.879	0.891	0.895	0.882	**0.897**
	4	0.831	0.847	0.847	0.834	**0.858**
Set14	2	0.938	**0.956**	0.943	0.935	0.953
	3	0.886	0.901	0.897	0.889	**0.908**
	4	0.829	0.850	0.842	0.835	**0.860**
BSD100	2	0.873	0.901	0.876	0.880	**0.908**
	3	0.804	0.824	0.811	0.815	**0.829**
	4	0.741	0.765	0.747	0.755	**0.771**
Urban100	2	0.888	0.914	0.900	0.890	**0.917**
	4	0.919	0.940	0.929	0.924	**0.946**
Sun-Hays80	8	0.835	0.857	0.842	0.839	**0.861**
Average	-	0.862	0.882	0.872	0.867	**0.887**

Table 6.3 : The average EMEG values for each image expansion method applied to each dataset with different scaling factors, m.

Dataset	m	Bilinear	Bicubic	Hwang	Zhang	Proposed
Set5	2	0.136	0.160	0.189	0.201	**0.295**
	3	0.118	0.129	0.155	0.174	**0.296**
	4	0.088	0.104	0.124	0.137	**0.270**
Set14	2	0.147	0.175	0.198	0.207	**0.304**
	3	0.122	0.134	0.159	0.175	**0.285**
	4	0.089	0.105	0.124	0.136	**0.253**
BSD100	2	0.125	0.151	0.161	0.174	**0.238**
	3	0.103	0.112	0.129	0.146	**0.217**
	4	0.072	0.086	0.094	0.112	**0.188**
Urban100	2	0.175	0.214	0.229	0.230	**0.385**
	4	0.111	0.134	0.158	0.158	**0.348**
Sun-Hays80	8	0.038	0.047	0.064	0.058	**0.146**
Average	-	0.110	0.129	0.149	0.159	**0.269**

reveal clearly the problems due to different scaling factors, $m = 2, 3, 4, 4.5$ for each dimension was used to expand Fig. 6.3(a), Fig. 6.4(a), Fig. 6.5(a) and Fig. 6.6(a) respectively. In particular, a scaling factor of 4.5 was used to expand Fig. 6.6(a) to show that the proposed method can perform effectively using non-integer scaling factors. The corresponding expanded images produced by the five benchmarking algorithms and the proposed method were shown in Fig. 6.3(c)-(h), Fig. 6.4(c)-(h), Fig. 6.5(c)-(h) and Fig. 6.6(c)-(h) respectively.

For the nearest neighbour method, pixelization and jagged edges were obvious in the output image, even though it can preserve vertical and horizontal edges very well. For the bilinear and bicubic methods, both perform well in the smooth regions, but smear sharp edges. For Hwang's method, it produces jagged edges and for Zhang's method, it cannot preserve sharp edges very well and the edges in its output looks slightly blurred. For the output images produced by the proposed method, as shown in Fig. 6.3(h), Fig. 6.4(h), Fig. 6.5(h) and Fig. 6.6(h), it is obvious that the proposed method was able to regain the sharpness of the edges without jaggedness.

6.2.3 Improved Image Expansion Conclusion

In the proposed method, the MGC is used with an adaptive γ value, based on the absolute differences of two interpolation methods with different degrees of edge preservation, to regain the sharpness of the edges as well as reducing jaggedness and prevent blurring of edges in the expanded images. The proposed mapping function was able to regain the sharpness of the edges by mapping the whole smoothed edge residual image to the γ values of the modified gamma curve for every pixel in

(a) Input **(b)** Reference

(c) Nearest **(d)** Bilinear

(e) Bicubic **(f)** Hwang

(g) Zang **(h)** Proposed

Figure 6.3 : The image expansion results for the proposed method and the other benchmarking algorithms using the *lena* image from the Set14 dataset. (a) The input image. (b) The original image of the same size as the outputs. The outputs were expanded by a scaling factor of $m = 2$ using (c) Nearest Neighbour, (d) Bilinear, (e) Bicubic, (f) Hwang, (g) Zhang and (h) the proposed method.

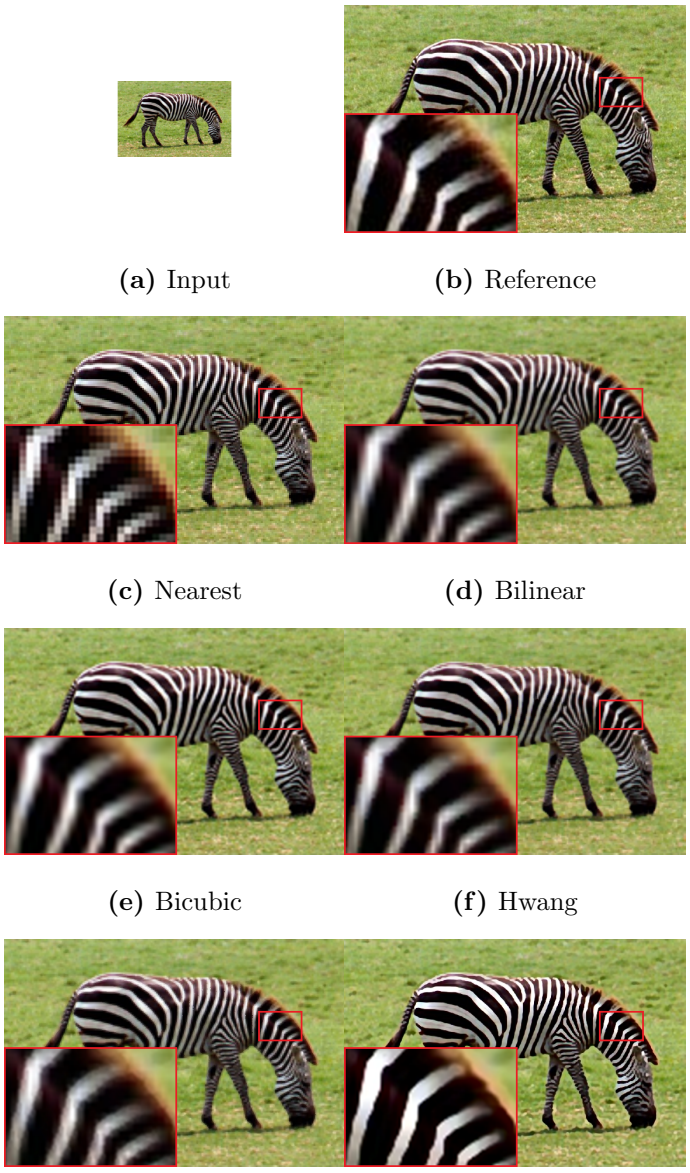

(a) Input **(b)** Reference

(c) Nearest **(d)** Bilinear

(e) Bicubic **(f)** Hwang

(g) Zang **(h)** Proposed

Figure 6.4 : The image expansion results for the proposed method and the other benchmarking algorithms using the *zebra* image from the Set14 dataset. (a) The input image. (b) The original image of the same size as the outputs. The outputs were expanded by a scaling factor of $m = 3$ using (c) Nearest Neighbour, (d) Bilinear, (e) Bicubic, (f) Hwang, (g) Zhang and (h) the proposed method.

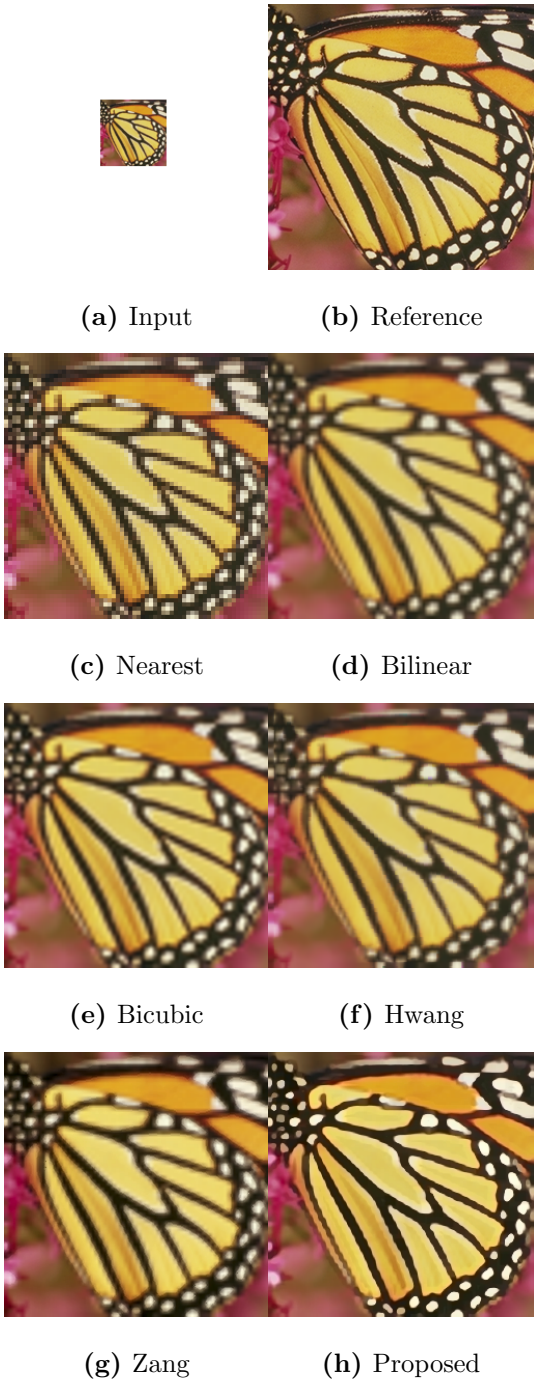

(a) Input **(b)** Reference

(c) Nearest **(d)** Bilinear

(e) Bicubic **(f)** Hwang

(g) Zang **(h)** Proposed

Figure 6.5 : The image expansion results for the proposed method and the other benchmarking algorithms using the *butterfly* image from the Set5 dataset. (a) The input image. (b) The original image of the same size as the outputs. The outputs were expanded by a scaling factor of $m = 4$ using (c) Nearest Neighbour, (d) Bilinear, (e) Bicubic, (f) Hwang, (g) Zhang and (h) the proposed method.

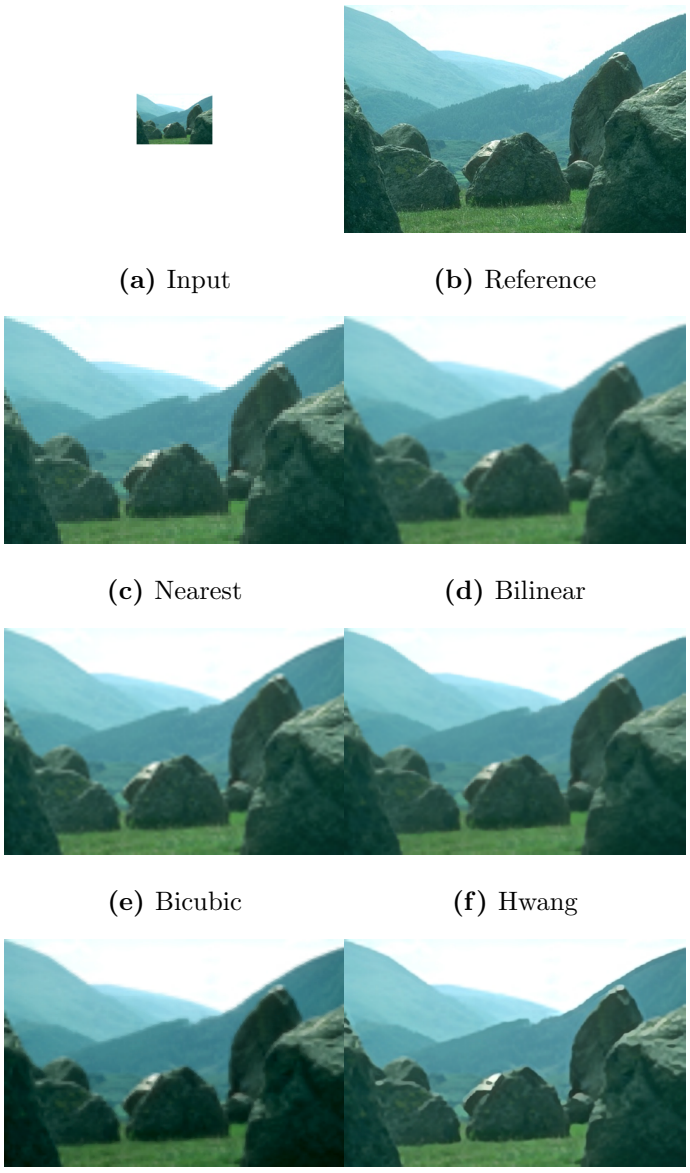

(a) Input **(b)** Reference

(c) Nearest **(d)** Bilinear

(e) Bicubic **(f)** Hwang

(g) Zang **(h)** Proposed

Figure 6.6 : The image expansion results for the proposed method and the other benchmarking algorithms using the *hillside* image from the BSD100 dataset. (a) The input image. (b) The original image of the same size as the outputs. The outputs were expanded by a scaling factor of $m = 4.5$ using (c) Nearest Neighbour, (d) Bilinear, (e) Bicubic, (f) Hwang, (g) Zhang and (h) the proposed method.

the expanded image. The sharpness of the edge was correctly recovered by setting the intersection point of the modified gamma curve to the mid-intensity value of the corresponding edge. Halo effects, due to the over-enhancement of strong edges, were also suppressed by limiting the intensity value of a pixel to a value within the intensity range inside a filter window centred at the corresponding location in the original image. Quantitative and visual results show that the proposed method outperformed other benchmarking techniques producing sharp expanded output images without edge jaggedness nor halo effects for a wide range of test input images.

6.3 Image Enhancement Prior to Colour Filter Array Demosaicking

For colour images captured by single-image sensors, enhancement is usually performed after CFA demosaicking because most image enhancement algorithms are developed for full colour images. As enhancement prior to demosaicking will produce a different result from enhancement after demosaicking, it will be more desirable to enhance an image prior to demosaicking particularly for images with a narrow intensity range. One reason is that demosaicking is the interpolation of missing colours, and interpolation within a narrow intensity range with only a few discrete intensity levels may lead to large interpolation errors. On the other hand, if enhancement is performed prior to demosaicking to widen the range of intensity, the above-mentioned interpolation errors could be reduced. The image enhancement algorithm [38] proposed in this thesis can be adapted so that they can be applied to CFA images prior to demosaicking. Results indicate that enhancement prior to

demosaicking can produce more visually pleasing images than those performed after demosaicking.

6.3.1 Enhancement Prior to CFA Demosaicking Method

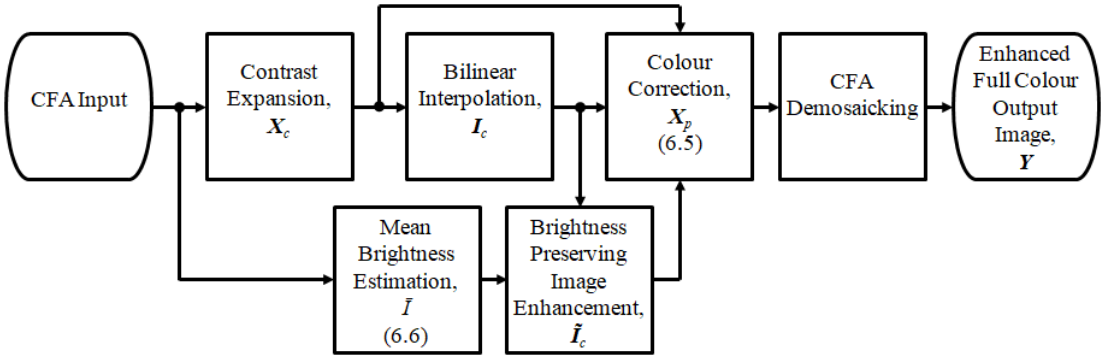

Figure 6.7 : Flowchart for the proposed enhancement prior to demosaicking method

As existing enhancement methods were developed for enhancing full-colour images, the image enhancement with brightness preservation by successive approximation method [38] described in Chapter 3 is proposed for enhancing CFA images prior to demosaicking. This is because it is desirable to preserve the mean brightness of an image in some applications, particularly for video enhancement to avoid flickering, or if the input is too bright or too dark, the brightness of the image can be adjusted whilst avoiding clipping of the intensity values. In order to recover the vivid colour from a poor contrast image, the contrast expansion method [38, 36, 37] described in Chapter 2, is first applied to the CFA input images.

In general, contrast enhancement is applied to the luminance component of the image. If enhancement is applied to the individual RGB colour planes of the image instead, the resultant full colour of the image may deviate from the original colour.

In the CFA domain, the luminance component of a full image is not available. In order to avoid colour deviation when enhancing the CFA image, enhancement is applied to the CFA image, $X_c(m,n)$, using the ratio of the luminance component before and after enhancement at location (m,n) to enhance the corresponding colour pixels in order to maintain the original colour as follows:

$$X_p(m,n) = \frac{\tilde{I}_c(m,n)}{I_c(m,n)} X_c(m,n), \tag{6.5}$$

where $X_c(m,n)$ and $X_p(m,n)$ are the respective input and enhanced pixel values of the corresponding colour, i.e. R, G or B, at location (m,n) in the CFA image and $I_c(m,n)$ and $\tilde{I}_c(m,n)$ are the luminance components before and after enhancement.

This requires the luminance component I_c to be estimated from the CFA image first. In the proposed method, as shown in Fig. 6.7, the luminance component L_i is estimated using a computationally efficient Bilinear interpolation method after contrast expansion. As the ratio of the luminance of a smeared edge before enhancement to the luminance of a smeared edge after enhancement will have a similar ratio as the luminance of a sharp edge before enhancement to the luminance of a sharp edge after enhancement, the edge preserving property of this estimated luminance is not crucial. It has been shown in the experimental results that using Bilinear interpolation to estimate the luminance component has no adverse effects on preserving the edges of the output image.

The luminance of the interpolated output I_c is then enhanced by the proposed STSA method described in Chapter 3 to produce the enhanced luminance compo-

nent $\tilde{I}_c(m,n)$ at pixel location (m,n).

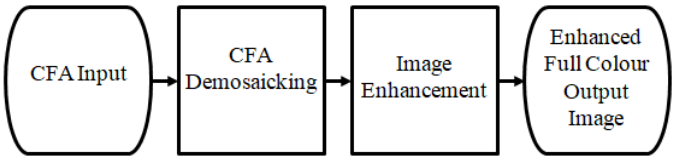

Figure 6.8 : Flowchart for standard enhancement after demosaicking

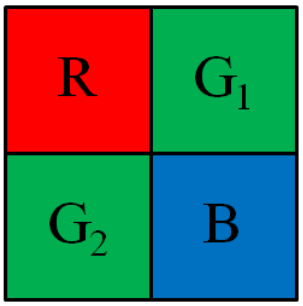

Figure 6.9 : The 2x2 Bayer pattern

For comparison of the mean brightness, $\bar{I}$, of the original image with the mean brightness of the enhanced image in successive approximation for each iteration, $\bar{I}$ must be estimated from the original CFA image. To do this, a luminance value I_l is first estimated from each 2x2 Bayer pattern group of the CFA image as shown in Fig.6.9, using [11]:

$$I_l = 0.2989R + 0.5870\left(\frac{G_1 + G_2}{2}\right) + 0.1140B \tag{6.6}$$

The mean brightness $\bar{I}$ is then the average of all the luminance values I_l of the whole CFA image.

6.3.2 Enhancement Prior to CFA Demosaicking Results

For performance evaluation of the proposed method, the complete set of the CSIQ [1] test image dataset was used. As recently developed algorithms were all designed for enhancing full-colour images, they are not directly applicable for CFA images. No algorithms for enhancement of CFA images prior to demosaicking were therefore included for benchmarking. In the experimental results, benchmarking algorithms for enhancement after demosaicking, including RSWHE [17], RICE [9], AGCWD [33], SECE [3] and RSECE [24], were used for the comparison with the proposed enhancement method prior to demosaicking. Refer to Fig. 6.8 for the procedure of the benchmarking algorithms in producing the enhanced full-colour image output.

Table 6.4 gives the average IQM values, namely, BIQME [19], EMEG [3] and NIQMC [54], of the output enhanced images produced by the benchmarking and the proposed methods and the best values for each IQM are highlighted in bold. The proposed method produced the highest average score for each IQM, outperforming the other benchmarking algorithms for all the three IQMs.

In order to confirm that the interpolation algorithm for the estimation of the luminance component, $I_c(m, n)$, does not have a strong effect on the performance of the proposed method in its edge-preserving capability, a number of different interpolation methods, namely, nearest neighbour, bilinear, bicubic and high-order interpolation (HOI) [75], were evaluated as shown in Table 6.5. HOI [75] is an edge-preserving interpolation technique while bilinear and bicubic will blur sharp edges.

However, the values as shown in Table 6.5 have minimal variations within the same IQM. From the results in Table 6.5, Bilinear interpolation gave the best balance between performance and computational efficiency.

Table 6.4 : The average values for different IQMs for the CSIQ dataset.

Enhancement Methods	Image Quality Measure (IQM)		
	BIQME	EMEG	NIQMC
RSWHE	0.499	0.233	4.254
RICE	0.499	0.240	4.236
AGCWD	0.485	0.257	4.222
SECE	0.568	0.320	5.139
RSECE	0.572	0.347	5.204
Proposed Method	**0.602**	**0.358**	**5.339**

Table 6.5 : The average values for different IQMs using different interpolation methods for the CSIQ dataset.

IQM	Interpolation Methods			
	Nearest Neighbour	Bilinear	Bicubic	HOI
BIQME	0.598	0.602	0.600	0.602
EMEG	0.340	0.358	0.340	0.381
NIQMC	5.338	5.339	5.343	5.342

For visual assessment, four images of different types from the CSIQ [1] test image dataset, namely, the *child swimming* in Fig. 6.10, the *butter flower* in Fig. 6.11, the *turtle* in Fig. 6.12 and the *trolley* in Fig. 6.13, were used for the comparison of the proposed method with the other benchmarking algorithms. In these figures, (a) gives the original image as a reference, (b) is the CFA input to the proposed method, (c) is a demosaicked image of (b) and is the input to the benchmarking algorithms for enhancement after demosaicking. The outputs of the benchmarking

algorithms, namely RSWHE, RICE, AGCWD, SECE and RSECE, were shown in (d), (e), (f), (g) and (h) respectively and (i) is the output of the proposed method. As shown in Fig. 6.10 - Fig. 6.13 (d) - (f), the RSWHE, RICE and AGCWD methods all produced under-enhanced image outputs with poor contrast. For the SECE and RSECE methods, as shown in Fig. 6.10 - Fig. 6.13 (g) - (h), the contrast of the outputs was improved, but the colour still remains dull and washed out. The proposed method, which performs enhancement prior to demosaicking, as shown in Fig. 6.10 - Fig. 6.13(i), produced output images with much better contrast and vivid colour.

6.3.3 Enhancement Prior to CFA Demosaicking Conclusion

The enhancement methods presented in this thesis can be applied for enhancing images in the CFA domain. It has been shown quantitatively and visually that enhancing prior to demosaicking produces more desirable results, and the proposed method is particularly beneficial for enhancing images with a narrow intensity range. Using an estimated luminance component for enhancement as a reference, the output colour in the enhanced images can be faithfully reproduced with little deviation from the original colour. As the proposed method can preserve the mean brightness of enhanced images, it is also suitable for video enhancement without causing any flickering.

6.4 Conclusion

In this chapter, two different applications have been explored which utilise some of the image enhancement methods presented in this thesis. To recover the sharp-

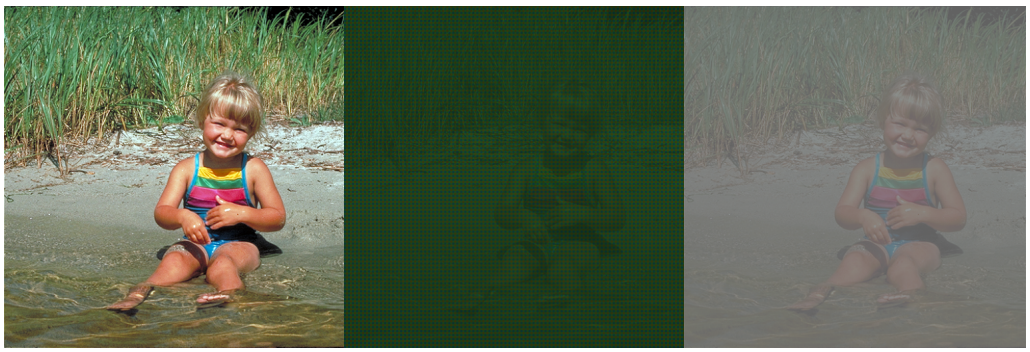

(a) Original **(b)** CFA Input **(c)** Demosaicked CFA

(d) RSWHE **(e)** RICE **(f)** AGCWD

(g) SECE **(h)** RSECE **(i)** Proposed

Figure 6.10 : The enhancement results for the proposed enhancement prior to demosaicking method and the other benchmarking algorithms using the *child swimming* image from the CSIQ dataset. (a) The original image. (b) The CFA input. (c) The demosaicked CFA of (b). The enhanced output by (d) RSWHE, (e) RICE, (f) AGCWD, (g) SECE, (h) RSECE and (i) the proposed method (enhancement prior to demosaicking).

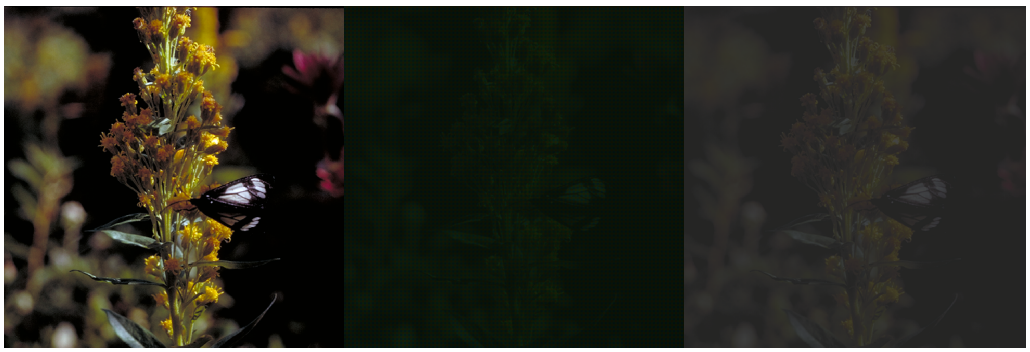

(a) Original **(b)** CFA Input **(c)** Demosaicked CFA

(d) RSWHE **(e)** RICE **(f)** AGCWD

(g) SECE **(h)** RSECE **(i)** Proposed

Figure 6.11 : The enhancement results for the proposed enhancement prior to demosaicking method and the other benchmarking algorithms using the *butter flower* image from the CSIQ dataset. (a) The original image. (b) The CFA input. (c) The demosaicked CFA of (b). The enhanced output by (d) RSWHE, (e) RICE, (f) AGCWD, (g) SECE, (h) RSECE and (i) the proposed method (enhancement prior to demosaicking).

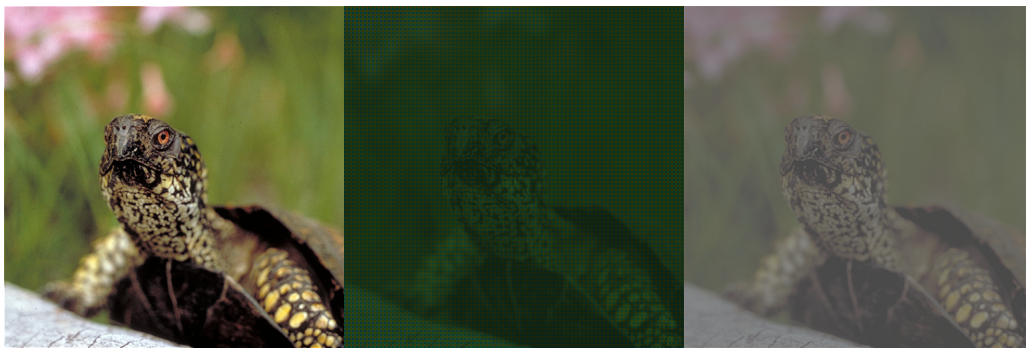

(a) Original **(b)** CFA Input **(c)** Demosaicked CFA

(d) RSWHE **(e)** RICE **(f)** AGCWD

(g) SECE **(h)** RSECE **(i)** Proposed

Figure 6.12 : The enhancement results for the proposed enhancement prior to demosaicking method and the other benchmarking algorithms using the *turtle* image from the CSIQ dataset. (a) The original image. (b) The CFA input. (c) The demosaicked CFA of (b). The enhanced output by (d) RSWHE, (e) RICE, (f) AGCWD, (g) SECE, (h) RSECE and (i) the proposed method (enhancement prior to demosaicking).

(a) Original **(b)** CFA Input **(c)** Demosaicked CFA

(d) RSWHE **(e)** RICE **(f)** AGCWD

(g) SECE **(h)** RSECE **(i)** Proposed

Figure 6.13 : The enhancement results for the proposed enhancement prior to demosaicking method and the other benchmarking algorithms using the *trolley* image from the CSIQ dataset. (a) The original image. (b) The CFA input. (c) The demosaicked CFA of (b). The enhanced output by (d) RSWHE, (e) RICE, (f) AGCWD, (g) SECE, (h) RSECE and (i) the proposed method (enhancement prior to demosaicking).

ness of edges in an expanded image, the proposed MGC described in Chapter 3 is applied with an adaptive γ value, based on the difference between two interpolation algorithms. Results show that the proposed method of image expansion with the MGC outperforms other benchmarking algorithms both quantitatively and visually, with outputs that have clearly sharper edges free from jaggedness and halo effects.

When applying the ratio equation given by 6.5, the proposed image enhancement methods presented in this thesis can also be applied to CFA images prior to demosaicking. This can reduce interpolation errors for input images with poor contrast, as the intensity range is expanded prior to demosaicking. When using the proposed STSA method described in Chapter 3 to enhance images prior to demosaicking, the results show that better output images can be produced then when applying enhancement after demosaicking.

Aside from the two examples given in this chapter, there are many other applications for which the proposed image enhancement methods may be incorporated into to improve the outcomes. These include applications on devices such as mobile phones, digital cameras including security and surveillance cameras, digital TVs, DVD and Bluray players, and many other audio-visual devices.

Chapter 7

Conclusion

A number of novel image enhancement methods have been presented in this thesis. They have been shown to outperform the benchmarking techniques, without suffering from the existing problems that many contemporary techniques do. These new methods make several specific contributions to the area of image enhancement and its applications.

To avoid the over-enhancement problems that plague many histogram equalisation based enhancement methods, a multi-level histogram shape segmentation method which groups together regions of intensities with a similar frequency of occurrence was proposed in this thesis. By detecting abrupt changes in the slope of a histogram, the proposed method can appropriately segment the histogram. Then when equalisation is applied, intensity values can only by re-mapped within the same segment, preventing over-enhancement from occurring. Results based on the 807 test images show that the proposed method outperformed the other benchmarking equalisation based techniques, especially in terms of the visual quality of output images.

The proposed image enhancement method with brightness preservation can provide any degree of enhancement whilst simultaneously preserving the brightness of an image. This is achieved by using successive approximation to locate the position

of the intersection point of an S-shaped curve, such that the brightness of the input image is maintained. The results showed that both proposed methods, namely STSA and MGCSA, had an average mean or median brightness error of 0. Furthermore, the proposed MGCSA method was able to preserve the mean or median brightness with an error of ± 2 for all of the 807 test images, none of the other benchmarking algorithms were able to preserve the brightness with the same accuracy. Moreover, the proposed method's ability to independently adjust the degree of enhancement whilst still preserving brightness is a feature no other benchmarking algorithm can boast. This method can also be used to adjust the brightness of an image, without causing clipping of the intensity values, so that details of the image are not lost. It is especially suitable for video enhancement, with the ability to adjust the brightness of a video while maintaining the brightness transition from frame to frame, so that flickering will not occur.

Image enhancement can be optimised by taking advantage of recently developed IQMs which have a better correlation with visual perception. It has been shown that for each tested IQM, there exists a global maximum which will produce an optimally enhanced output image according to that IQM. The IQM value is used as the feedback in a binary search to locate the intersection point of an S-shaped curve such that the IQM value is maximised. When compared with other optimisation methods, it was shown that the proposed method consistently produced higher IQM values for the 807 test images. Furthermore, as this method optimises enhancement based on an IQM, it can also be used to assess how well IQMs correlate with visual perception. As future IQMs improve the correlation with visual perception, they

can also be used with this method to give even better quality outputs. Moreover, a different feedback can be used within the binary search, depending on the application, so that enhancement can be optimised for that specific application to improve its outcomes.

To apply extra enhancement to image details that may otherwise be lost in contrast enhancement, an adaptive MAD based detail enhancement method was proposed. By separating the background and details of an image, the proposed method can improve image quality whilst avoiding halo effects and suppressing noise in homogeneous regions. Results show that the proposed adaptive detail enhancement, applied in conjunction with background enhancement, had a superior performance to the proposed optimised enhancement methods. Furthermore, the adaptive MAD based method was shown to outperform the benchmarking algorithms visually with less noise in homogeneous regions and without halo effects at edges.

The image enhancement methods presented in this thesis have also been shown to have many other applications. The proposed MGC was shown to be able to regain the sharpness of edges for improving image expansion when applied with an adaptive γ value. When the proposed enhancement methods are applied prior to CFA demosaicking, it was shown that they can reduce interpolation errors for images with poor contrast, giving better quality enhancement then benchmarking algorithms applied after demosaicking. Apart from the two applications presented in this thesis, the research findings have many other applications, including mobile phones, digital cameras including security and surveillance cameras, digital TVs, DVD and Bluray players, and many other audio-visual devices.

Chapter 8

Future Extensions

The image enhancement methods presented in this thesis have been shown to outperform other benchmarking algorithms when implemented in software. In particular, the proposed image enhancement method with brightness preservation by successive approximation is especially suitable for video enhancement. However, for video enhancement, it would be desirable to apply the enhancement method in real-time. Future extension of the enhancement methods presented in this thesis is the implementation of the proposed algorithms on field-programmable gate arrays (FPGAs), for real time processing. This will increase the impact these methods can have in hardware such as mobile phones, digital cameras, including security and surveillance cameras, digital TVs and more.

Another method that would benefit from the real time implementation on FPGAs is the proposed image expansion method. This could be applied in devices with a camera, such as mobile phones and security and surveillance cameras, to improve the quality of digital zooming.

The proposed optimised enhancement method has been shown to be able to optimise an image based on a particular IQM, giving better results than other benchmarking optimised enhancement methods. However, as already stated in the conclusion, different feedback can be used in place of the IQM value in the binary

search to optimise the image based on certain criteria.

Bibliography

[1] E. C. Larson and D. M. Chandler, "Most apparent distortion: full-reference image quality assessment and the role of strategy," *Journal of Electronic Imaging*, vol. 19, pp. 19 – 19 – 21, January 2010.

[2] M. Brown and S. Ssstrunk, "Multi-spectral sift for scene category recognition," in *CVPR 2011*, June 2011, pp. 177–184.

[3] T. Celik, "Spatial entropy-based global and local image contrast enhancement," *IEEE Transactions on Image Processing*, vol. 23, no. 12, pp. 5298–5308, December 2014.

[4] D. Tohl, J. S. J. Li, and C. M. Bull, "Pre-processing techniques to improve the efficiency of video identification for the pygmy bluetongue lizard," in *Proceedings of the 10th International Conference on Computer Vision Theory and Applications - Volume 1: VISAPP, (VISIGRAPP 2015)*, INSTICC. SciTePress, 2015, pp. 623–629.

[5] D. Tohl, J. S. J. Li, L. Shamiminoori, and C. M. Bull, "Image asymmetry measurement for the study of endangered pygmy bluetongue lizard," in *2013 28th International Conference on Image and Vision Computing New Zealand (IVCNZ 2013)*, November 2013, pp. 76–81.

[6] L. Shamiminoori and C. Bull, "Can we use head scale symmetry in endangered

pygmy bluetongue lizards (tiliqua adelaidensis) to alert managers to population condition?" *Herpetological Conservation and Biology*, vol. 11, pp. 188–198, April 2016.

[7] J. S. J. Li, D. Tohl, S. Randhawa, L. Shamimi, and C. M. Bull, "Non-invasive lizard identification using signature curves," in *TENCON 2009 - 2009 IEEE Region 10 Conference*, January 2009, pp. 1–5.

[8] T. Celik, "Spatial mutual information and pagerank-based contrast enhancement and quality-aware relative contrast measure," *IEEE Transactions on Image Processing*, vol. 25, no. 10, pp. 4719–4728, October 2016.

[9] K. Gu, G. Zhai, X. Yang, W. Zhang, and C. W. Chen, "Automatic contrast enhancement technology with saliency preservation," *IEEE Transactions on Circuits and Systems for Video Technology*, vol. 25, no. 9, pp. 1480–1494, September 2015.

[10] Q. Wang and R. K. Ward, "Fast image/video contrast enhancement based on weighted thresholded histogram equalization," *IEEE Transactions on Consumer Electronics*, vol. 53, no. 2, pp. 757–764, May 2007.

[11] R. C. Gonzalez and R. E. Woods, *Digital Image Processing*, 3rd ed. New Jersey: Prentice Hall, 2008.

[12] Y. T. Kim, "Contrast enhancement using brightness preserving bi-histogram equalization," *IEEE Transactions on Consumer Electronics*, vol. 43, no. 1, pp. 1–8, February 1997.

[13] Y. Wang, Q. C., and B. Zhang, "Image enhancement based on equal area dualistic sub-image histogram equalization method," *IEEE Transactions on Consumer Electronics*, vol. 45, no. 1, pp. 68–75, February 1999.

[14] S. D. Chen and A. R. Ramli, "Minimum mean brightness error bi-histogram equalization in contrast enhancement," *IEEE Transactions on Consumer Electronics*, vol. 49, no. 4, pp. 1310–1319, November 2003.

[15] K. Sim, C. Tso, and Y. Tan, "Recursive sub-image histogram equalization applied to gray scale images," *Pattern Recognition Letters*, vol. 28, no. 10, pp. 1209 – 1221, 2007.

[16] S. D. Chen and A. R. Ramli, "Contrast enhancement using recursive mean-separate histogram equalization for scalable brightness preservation," *IEEE Transactions on Consumer Electronics*, vol. 49, no. 4, pp. 1301–1309, November 2003.

[17] M. Kim and M. G. Chung, "Recursively separated and weighted histogram equalization for brightness preservation and contrast enhancement," *IEEE Transactions on Consumer Electronics*, vol. 54, no. 3, pp. 1389–1397, August 2008.

[18] K. Gu, G. Zhai, M. Liu, X. Min, X. Yang, and W. Zhang, "Brightness preserving video contrast enhancement using s-shaped transfer function," in *2013 Visual Communications and Image Processing (VCIP)*, November 2013, pp. 1–6.

[19] K. Gu, D. Tao, J. F. Qiao, and W. Lin, "Learning a no-reference quality assess-

ment model of enhanced images with big data," *IEEE Transactions on Neural Networks and Learning Systems*, vol. 29, no. 4, pp. 1301–1313, April 2018.

[20] K. Gu, G. Zhai, W. Lin, and M. Liu, "The analysis of image contrast: From quality assessment to automatic enhancement," *IEEE Transactions on Cybernetics*, vol. 46, no. 1, pp. 284–297, January 2016.

[21] Z. Wang and A. C. Bovik, "A universal image quality index," *IEEE Signal Processing Letters*, vol. 9, no. 3, pp. 81–84, March 2002.

[22] H. R. Sheikh and A. C. Bovik, "Image information and visual quality," *IEEE Transactions on Image Processing*, vol. 15, no. 2, pp. 430–444, February 2006.

[23] W. Xue, L. Zhang, X. Mou, and A. C. Bovik, "Gradient magnitude similarity deviation: A highly efficient perceptual image quality index," *IEEE Transactions on Image Processing*, vol. 23, no. 2, pp. 684–695, February 2014.

[24] T. Celik and H. C. Li, "Residual spatial entropy-based image contrast enhancement and gradient-based relative contrast measurement," *Journal of Modern Optics*, vol. 63, no. 16, pp. 1600–1617, September 2016.

[25] Z. Wang, A. C. Bovik, H. R. Sheikh, and E. P. Simoncelli, "Image quality assessment: from error visibility to structural similarity," *IEEE Transactions on Image Processing*, vol. 13, no. 4, pp. 600–612, April 2004.

[26] S. Agaian, K. P. Lentz, and A. M. Grigoryan, "A new measure of image enhancement," in *IASTED International Conference on Signal Processing & Communication*, 2000, pp. 1–7.

[27] K. Panetta, C. Gao, and S. Agaian, "No reference color image contrast and quality measures," *IEEE Transactions on Consumer Electronics*, vol. 59, no. 3, pp. 643–651, August 2013.

[28] Y. Lee and S. Kassam, "Generalized median filtering and related nonlinear filtering techniques," *IEEE Transactions on Acoustics, Speech, and Signal Processing*, vol. 33, no. 3, pp. 672–683, June 1985.

[29] A. Rosenfeld and A. C. Kak, *Digital Picture Processing.* New York: Academic Press, 1976.

[30] S. E. Umbaugh, *Computer Vision and Image Processing.* New Jersey: Prentice Hall, 1998.

[31] K. R. Castleman, *Digital Image Processing.* New Jersey: Prentice Hall, 1996.

[32] M. H. Kabir, M. Abdullah-Al-Wadud, and O. Chae, "Brightness preserving image contrast enhancement using weighted mixture of global and local transformation functions," *Int. Arab J. Inf. Technol.*, vol. 7, no. 4, pp. 403–410, October 2010.

[33] S. Huang, F. Cheng, and Y. Chiu, "Efficient contrast enhancement using adaptive gamma correction with weighting distribution," *IEEE Transactions on Image Processing*, vol. 22, no. 3, pp. 1032–1041, March 2013.

[34] J. Baby and V. Karunakaran, "Bi-level weighted histogram equalization with adaptive gamma correction," *International Journal of Computational Engineering Research*, vol. 4, no. 3, pp. 25–30, March 2014.

[35] S. Srinivasan and N. Balram, "Adaptive contrast enhancement using local region stretching," in *The 9th Asian Symposium on Information Display*, October 2006, pp. 8–12.

[36] D. Tohl and J. S. J. Li, "Contrast enhancement by multi-level histogram shape segmentation with adaptive detail enhancement for noise suppression," *Signal Processing: Image Communication*, vol. 71, pp. 45–55, February 2019.

[37] D. Tohl, J. S. J. Li, S. Randhawa, and N. Pickering, "Image enhancement prior to color filter array demosaicking," in *IEEE Region 10 Conference (TENCON 2018)*, October 2018, pp. 1279–1283.

[38] D. Tohl and J. S. J. Li, "Image enhancement by s-shaped curves using successive approximation for preserving brightness," *IEEE Signal Processing Letters*, vol. 24, no. 8, pp. 1247–1251, August 2017.

[39] M. W. Schwarz, W. B. Cowan, and J. C. Beatty, "An experimental comparison of rgb, yiq, lab, hsv, and opponent color models," *ACM Trans. Graph.*, vol. 6, no. 2, pp. 123–158, April 1987. [Online]. Available: http://doi.acm.org/10.1145/31336.31338

[40] J. Bednar and T. Watt, "Alpha-trimmed means and their relationship to median filters," *IEEE Transactions on Acoustics, Speech, and Signal Processing*, vol. 32, no. 1, pp. 145–153, February 1984.

[41] A. W. Bowman and A. Azzalini, *Applied Smoothing Techniques for Data Analysis*. New York: Oxford University Press Inc., 1997.

[42] N. Ponomarenko, L. Jin, O. Ieremeiev, V. Lukin, K. Egiazarian, J. Astola, B. Vozel, K. Chehdi, M. Carli, F. Battisti, and C.-C. J. Kuo, "Image database tid2013: Peculiarities, results and perspectives," *Signal Processing: Image Communication*, vol. 30, pp. 57–77, 2015.

[43] K. Gu, G. Zhai, S. Wang, M. Liu, J. Zhoi, and W. Lin, "A general histogram modification framework for efficient contrast enhancement," in *2015 IEEE International Symposium on Circuits and Systems (ISCAS)*, May 2015, pp. 2816–2819.

[44] C. A. Poynton, "Smpte tutorial: gamma and its disguises: The nonlinear mappings of intensity in perception, crts, film, and video," *SMPTE Journal*, vol. 102, no. 12, pp. 1099–1108, December 1993.

[45] D. Tohl and J. S. J. Li, "Improved image expansion for preserving sharpness without jagged edges," in *IEEE Region 10 Conference (TENCON 2018)*, October 2018, pp. 1269–1274.

[46] T. Luft, C. Colditz, and O. Deussen, "Image enhancement by unsharp masking the depth buffer," in *International Conference on Computer Graphics and Interactive Techniques (SIGGRAPH)*, 2006, pp. 1206–1213.

[47] C. Tomasi and R. Manduchi, "Bilateral filtering for gray and color images," in *Sixth International Conference on Computer Vision (IEEE Cat. No.98CH36271)*, January 1998, pp. 839–846.

[48] Z. Li and J. Zheng, "Edge-preserving decomposition-based single image haze

removal," *IEEE Transactions on Image Processing*, vol. 24, no. 12, pp. 5432–5441, December 2015.

[49] K. He, J. Sun, and X. Tang, "Guided image filtering," *IEEE Transactions on Pattern Analysis and Machine Intelligence*, vol. 35, no. 6, pp. 1397–1409, June 2013.

[50] Z. Farbman, R. Fattal, D. Lischinski, and R. Szeliski, "Edge-preserving decompositions for multi-scale tone and detail manipulation," *ACM Trans. Graph.*, vol. 27, no. 3, pp. 67:1–67:10, August 2008. [Online]. Available: http://doi.acm.org/10.1145/1360612.1360666

[51] X. Li, Y. Gu, S. Hu, and R. R. Martin, "Mixed-domain edge-aware image manipulation," *IEEE Transactions on Image Processing*, vol. 22, no. 5, pp. 1915–1925, May 2013.

[52] H. Talebi and P. Milanfar, "Nonlocal image editing," *IEEE Transactions on Image Processing*, vol. 23, no. 10, pp. 4460–4473, October 2014.

[53] K. Subr, C. Soler, and F. Durand, "Edge-preserving multiscale image decomposition based on local extrema," *ACM Trans. Graph.*, vol. 28, no. 5, pp. 147:1–147:9, December 2009. [Online]. Available: http://doi.acm.org/10.1145/1618452.1618493

[54] K. Gu, W. Lin, G. Zhai, X. Yang, W. Zhang, and C. W. Chen, "No-reference quality metric of contrast-distorted images based on information maximization," *IEEE Transactions on Cybernetics*, vol. 47, no. 12, pp. 4559–4565, De-

cember 2017.

[55] C. Dong, C. C. Loy, K. He, and X. Tang, "Image super-resolution using deep convolutional networks," *IEEE Transactions on Pattern Analysis and Machine Intelligence*, vol. 38, no. 2, pp. 295–307, February 2016.

[56] M. Bevilacqua, A. Roumy, C. Guillemot, and M. L. A. Morel, "Single-image super-resolution via linear mapping of interpolated self-examples," *IEEE Transactions on Image Processing*, vol. 23, no. 12, pp. 5334–5347, December 2014.

[57] R. Timofte, V. D. Smet, and L. V. Gool, "A+: Adjusted anchored neighborhood regression for fast super-resolution," in *2014 12th Asian Conference on Computer Vision (ACCV 2014)*, November 2014, pp. 1–5.

[58] H. Hou and H. Andrews, "Cubic splines for image interpolation and digital filtering," *IEEE Transactions on Acoustics, Speech, and Signal Processing*, vol. 26, no. 6, pp. 508–517, December 1978.

[59] X. Li and M. T. Orchard, "New edge-directed interpolation," *IEEE Transactions on Image Processing*, vol. 10, no. 10, pp. 1521–1527, October 2001.

[60] W.-S. Tam, C.-W. Kok, and W.-C. Siu, "A modified edge directed interpolation for images," in *2009 17th European Signal Processing Conference*, August 2009, pp. 283–287.

[61] N. Asuni and A. Giachetti, "Accuracy improvements and artifacts removal in edge based image interpolation," in *VISAPP*, 2008.

[62] L. Zhang and X. Wu, "An edge-guided image interpolation algorithm via directional filtering and data fusion," *IEEE Transactions on Image Processing*, vol. 15, no. 8, pp. 2226–2238, August 2006.

[63] A. Giachetti and N. Asuni, "Real-time artifact-free image upscaling," *IEEE Transactions on Image Processing*, vol. 20, no. 10, pp. 2760–2768, October 2011.

[64] D. Zhou, X. Shen, and W. Dong, "Image zooming using directional cubic convolution interpolation," *IET Image Processing*, vol. 6, no. 6, pp. 627–634, August 2012.

[65] A. K. Jha, A. Kumar, G. Schaefer, and M. A. R. Ahad, "An adaptive distance-based edge preserving interpolation algorithm for natural images," in *2015 International Conference on Informatics, Electronics Vision (ICIEV)*, June 2015, pp. 1–5.

[66] T. Chang, K. Lee, G. Chen, S. Chiu, and J. Yang, "Super resolution using trilateral filter regression interpolation," in *2017 IEEE 2nd International Conference on Signal and Image Processing (ICSIP)*, August 2017, pp. 86–89.

[67] S. Zhang and H. Shi, "An improvement of the canny edge based image expansion algorithm," in *2017 10th International Congress on Image and Signal Processing, BioMedical Engineering and Informatics (CISP-BMEI)*, October 2017, pp. 1–5.

[68] J. W. Hwang and H. S. Lee, "Adaptive image interpolation based on local

gradient features," *IEEE Signal Processing Letters*, vol. 11, no. 3, pp. 359–362, March 2004.

[69] M. Bevilacqua, A. Roumy, C. Guillemot, and M. A. Morel, "Low-complexity single-image super-resolution based on nonnegative neighbor embedding," in *Proceedings of the British Machine Vision Conference*. BMVA Press, 2012, pp. 135.1–135.10.

[70] R. Zeyde, M. Elad, and M. Protter, "On single image scale-up using sparse-representations," in *Curves and Surfaces*, J.-D. Boissonnat, P. Chenin, A. Cohen, C. Gout, T. Lyche, M.-L. Mazure, and L. Schumaker, Eds. Berlin, Heidelberg: Springer Berlin Heidelberg, 2012, pp. 711–730.

[71] D. Martin, C. Fowlkes, D. Tal, and J. Malik, "A database of human segmented natural images and its application to evaluating segmentation algorithms and measuring ecological statistics," in *Proceedings Eighth IEEE International Conference on Computer Vision. ICCV 2001*, vol. 2, 2001, pp. 416–423 vol.2.

[72] J. B. Huang, A. Singh, and N. Ahuja, "Single image super-resolution from transformed self-exemplars," in *2015 IEEE Conference on Computer Vision and Pattern Recognition (CVPR)*, June 2015, pp. 5197–5206.

[73] L. Sun and J. Hays, "Super-resolution from internet-scale scene matching," in *2012 IEEE International Conference on Computational Photography (ICCP)*, April 2012, pp. 1–12.

[74] L. Zhang, L. Zhang, X. Mou, and D. Zhang, "Fsim: A feature similarity index

for image quality assessment," *IEEE Transactions on Image Processing*, vol. 20, no. 8, pp. 2378–2386, August 2011.

[75] J. S. J. Li and S. Randhawa, "Color filter array demosaicking using high-order interpolation techniques with a weighted median filter for sharp color edge preservation," *IEEE Transactions on Image Processing*, vol. 18, no. 9, pp. 1946–1957, September 2009.